

POLITECNICO DI TORINO

Master of Science in Automotive Engineering

Master Thesis

**Development of a Numerical Platform to Support the  
Optimization of the PHOENICE Highly Efficient  
Spark Ignition Engine**



**Supervisors:**

Prof. Federico Millo

Prof. Luciano Rolando

Mr. Giuseppe Castellano

**Candidate:**

Giovanni Brussolo

Academic year 2022/2023



## Abstract

The “Fit for 55” package, which the European Parliament approved on June 2022 to achieve a Net Zero CO<sub>2</sub> Emissions by 2050, will ban Internal Combustion Engines (ICEs) within 2035, leading to a dramatic increase in the number of Battery Electric Vehicles (BEV).

Nevertheless, the combined use of innovative ICE technologies and powertrain hybridization can still play a crucial role in the reduction of the carbon footprint of the transport sector. In such a framework, this thesis supports, through numerical simulations, the optimization of the PHOENICE (PHEV towards zero Emissions & ultimate ICE efficiency) engine concept, which aims at achieving a gross indicated efficiency of 47% through the use of highly diluted combustion (EGR + Air), new charge motion, Miller cycle with high compression ratio and electrified turbocharger.

Indeed, the calibration of such a complex system cannot rely only on experimental tests and requires a reliable numerical platform to find the set of operating parameters capable of maximizing its performance.

Therefore, in this research work, a digital engine twin was created in the GT-Suite environment, paying particular attention to the capability of the combustion model to reproduce the burn rate in highly diluted conditions correctly. The model includes all the features of the actual engine whose sub-models were calibrated with experimental data. The model was then used to optimize the valve lift for different operating points.

Finally, the robustness of the proposed virtual test rig was proved by comparing the simulation results against an initial set of experimental tests performed at the IFPEN laboratories on the first engine prototype over different Air-to-Fuel (A/F) ratios and Exhaust Gas Recirculating system (EGR) levels.



## Sommario

Il pacchetto “Fit for 55”, approvato dal Parlamento Europeo nel Giugno 2022 ai fini di raggiungere emissioni nette di CO<sub>2</sub> pari a zero entro il 2050, bannerà i motori a combustione interna (ICEs) entro il 2035, portando ad un drastico aumento del numero di veicoli elettrici (BEV).

Ciò nonostante, l'utilizzo congiunto di tecnologie innovative nei motori a combustione e l'ibridizzazione del powertrain possono ancora svolgere un ruolo cruciale nella riduzione dell'impronta ecologica del settore dei trasporti. In questo frangente, questo progetto di tesi supporta, tramite simulazione numerica, l'ottimizzazione del motore PHOENICE (PHev tOwards zero EmissionNs & ultimate ICE efficiency), il quale punta a raggiungere un rendimento termico indicato pari a 47% grazie all'utilizzo di una combustione molto diluita (EGR + Aria), di un innovativo moto della carica di aspirazione, del ciclo di Miller ad alto rapporto di compressione e di un turbocompressore elettrico.

La calibrazione di un modello così complesso non può basarsi solo su risultati sperimentali, è necessario far uso di un'affidabile piattaforma numerica per trovare i parametri operativi in grado di massimizzare le performance.

Per questo motivo, in questo progetto di ricerca, è stato creato un gemello digitale in GT-Suite del motore, ponendo particolare attenzione alla capacità del modello di combustione di riprodurre correttamente i burn rate in ambiente magro. Il modello include tutte le feature del motore reale, i quali sotto-assiemi sono stati calibrati tramite dati sperimentali. Il modello è stato poi utilizzato per ottimizzare le alzate valvola per diversi punti operativi.

In conclusione, la robustezza del banco prova virtuale è stata confermata comparando i risultati delle simulazioni a quelli di un set di test preliminari, condotti, per differenti rapporti aria-benzina (A/F) e percentuali di EGR, nei laboratori di IFPEN sul primo prototipo motore.



## **Acknowledgments**

First and foremost, I want to thank everyone in the e3 PoliTO research group, who, ever since I joined their laboratory, made me feel welcome and were always available to provide support whenever needed. Words cannot express my gratitude to Professor Millo, Professor Rolando, and Mr. Giuseppe Castellano for giving me the opportunity to work on such an exciting and involving topic. All of this was only possible with their help and technical guidance.

I am also deeply grateful for all the friends I've met during my career. I will forever remember the time spent together, from the ever-present dinners and night's out to watching Formula 1 together.

I would also like to take a moment to acknowledge the deep support that my family, girlfriend, and relatives provided me during my five-year journey in Politecnico. They were and still are my rock.

Lastly, I thank myself for achieving this milestone and persevering through the tough times. After all these years, there are still no "Sorci Verdi" to be found.



# Table of Contents

<b>ABSTRACT</b> .....	<b>II</b>
<b>SOMMARIO</b> .....	<b>IV</b>
<b>ACKNOWLEDGMENTS</b> .....	<b>VI</b>
<b>TABLE OF CONTENTS</b> .....	<b>VIII</b>
<b>LIST OF FIGURES</b> .....	<b>X</b>
<b>LIST OF TABLES</b> .....	<b>XIV</b>
<b>LIST OF ACRONYMS</b> .....	<b>XV</b>
<b>1 INTRODUCTION</b> .....	<b>1</b>
1.1 PHOENICE PROJECT .....	1
1.2 STATE OF THE ART: SPARK IGNITION INTERNAL COMBUSTION ENGINE EFFICIENCY .....	3
1.3 BASELINE ENGINE: GLOBAL SMALL ENGINE (GSE) .....	5
1.4 PHOENICE ENGINE CONCEPT .....	6
1.4.1 <i>Garrett E-Turbo</i> .....	7
1.4.2 <i>Low-Pressure EGR</i> .....	9
1.4.3 <i>Dual Diluted Combustion and Swumble™</i> .....	10
1.4.4 <i>Water Charge Air Cooler</i> .....	12
1.4.5 <i>Exhaust Line</i> .....	13
1.4.6 <i>Waste Heat Recovery System (WHRS)</i> .....	15
1.5 USED SOFTWARE.....	16
<b>2 MODEL DEVELOPMENT</b> .....	<b>17</b>
2.1 CAD DISCRETIZATION .....	17
2.1.1 <i>Discretization Work Procedure</i> .....	18
2.1.2 <i>Low-Pressure Intake Line</i> .....	19
2.1.3 <i>Intake Manifold</i> .....	22
2.1.4 <i>Exhaust Line</i> .....	24
2.1.5 <i>EGR Loop</i> .....	27
2.1.6 <i>Intake and Exhaust Conduits</i> .....	29
2.2 ENGINE MODEL UPDATES .....	31
2.2.1 <i>Garrett E-Turbo &amp; Efficiency Map</i> .....	31
2.2.2 <i>Intake Valves Flow and Turbulence Coefficients</i> .....	33
2.2.3 <i>Combustion Chamber Geometry</i> .....	37
2.3 COMPLETE MODEL ASSEMBLY .....	38
<b>3 MODEL CALIBRATION</b> .....	<b>39</b>
3.1 AFTERTREATMENT BRICKS CALIBRATION .....	39
3.1.1 <i>Calibration Procedure</i> .....	39
3.1.2 <i>EHC + TWC<sub>1</sub></i> .....	43
3.1.3 <i>TWC<sub>2</sub></i> .....	47
3.1.4 <i>GPF</i> .....	49
3.1.5 <i>NO-Ox</i> .....	51
3.1.6 <i>SCR<sub>1</sub> &amp; SCR<sub>2</sub></i> .....	53
3.2 HEAT EXCHANGERS PRESSURE DROP CALIBRATION .....	55
3.2.1 <i>Calibration Procedure</i> .....	55
3.2.2 <i>EGR Cooler Calibration</i> .....	56
3.2.3 <i>Water Charge Air Cooler Calibration</i> .....	58
<b>4 PRELIMINARY ENGINE CALIBRATION</b> .....	<b>62</b>
4.1 INTAKE CHARGE TEMPERATURE SENSITIVITY ANALYSIS .....	62
4.2 MAXIMUM E-TURBO ROTATIONAL SPEED SENSITIVITY ANALYSIS .....	64
4.2.1 <i>Acceptable Performance Scenario</i> .....	64

4.2.2	<i>Maximum Performance Scenario</i> .....	67
4.3	INTAKE VALVES STRATEGY OPTIMIZATION.....	69
4.3.1	<i>Methodology and Boundary Conditions</i> .....	69
4.3.2	<i>Results Analysis – Baseline Configuration</i> .....	71
4.3.3	<i>Experimental Validation</i> .....	73
4.3.4	<i>Effects of Garrett E-Turbo – Hybrid Configuration</i> .....	74
4.3.5	<i>Effects of PHOENICE Exhaust Line – PHOENICE Configuration</i> .....	76
<b>5</b>	<b>MODEL CORRELATION AGAINST EXPERIMENTAL DATA</b> .....	<b>78</b>
5.1	EXPERIMENTAL TEST BENCH DESCRIPTION.....	78
5.2	CYLINDER PRESSURE ONLY ANALYSIS.....	80
5.3	CORRELATION MODEL AND RESULTS.....	83
5.4	SITURB COMBUSTION MODEL TUNING.....	88
<b>6</b>	<b>CONCLUSIONS</b> .....	<b>93</b>
<b>7</b>	<b>REFERENCES</b> .....	<b>94</b>

# List of Figures

Figure 1-1 - PHEV C-SUV for PHOENICE demonstrator vehicle .....	1
Figure 1-2 – PHOENICE Hybrid Architecture .....	2
Figure 1-3 - PHOENICE Logo .....	2
Figure 1-4 – Ideal cycle vs. EIVC and LIVC Miller cycles .....	4
Figure 1-5 – Baseline Stellantis GSE-T4 Engine.....	5
Figure 1-6 – PHOENICE GSE-T4 Tuning .....	6
Figure 1-7 – E-Turbo Performance tested on a Mercedes A-Class prototype. ....	7
Figure 1-8 - Compressor Maps: Baseline vs. PHOENICE .....	7
Figure 1-9 – Turbine Maps: Baseline vs. PHOENICE .....	8
Figure 1-10 - WG Turbocharger (left) vs. VNT Turbocharger <sup>[11]</sup> (right).....	8
Figure 1-11 – PHOENICE Low Pressure EGR Line.....	9
Figure 1-12 – Swirl vs. Tumble vs. Squish <sup>[12,13]</sup> .....	10
Figure 1-13 – Burning velocity as a function of the equivalence ratio $\phi$ <sup>[14]</sup> .....	10
Figure 1-14 – Swumble™ Intake Air Charge Motion <sup>[15]</sup> .....	11
Figure 1-15 – Performance of Swumble™ concept in lean conditions <sup>[17]</sup> .....	11
Figure 1-16 – PHOENICE WCAC CAD Render .....	12
Figure 1-17 – Engine-out emissions function of $\phi$ (left) TWC efficiency function of $\alpha$ (right) <sup>[14]</sup> ..	13
Figure 1-18 – PHOENICE EATS Layout.....	14
Figure 1-19 – Exhaust Heat Recovery System (EHRS) vs. Thermo-Electric Generator (TEG) <sup>[18]</sup> ..	15
Figure 1-20 – Working principle of the Seebeck effect <sup>[19]</sup> .....	15
Figure 1-21 – Used Software icons.....	16
Figure 2-1 - Flow lines discretization procedure flowchart.....	18
Figure 2-2 – Low-Pressure Intake Line CAD geometry: before clean-up (left) and after (right) .....	19
Figure 2-3 – Low-Pressure Intake Line Airbox holes.....	19
Figure 2-4 – Low-Pressure Intake Line Final Cleaned-up Geometry.....	20
Figure 2-5 - Low-Pressure Intake Line GEM3D Discretization.....	20
Figure 2-6 – Low-Pressure Intake Line GT-POWER sub-assembly model.....	21
Figure 2-7 – High-Pressure Intake Line CAD geometry: before clean-up (left) and after (right).....	22
Figure 2-8 – High-Pressure Intake Line Final Cleaned-up Geometry .....	22
Figure 2-9 - High-Pressure Intake Line GEM3D Discretization .....	23
Figure 2-10 – High- Pressure Intake Line GT-POWER sub-assembly model .....	23
Figure 2-11 – Exhaust Line CAD geometry: before clean-up (left) and after (right).....	24
Figure 2-12 – Exhaust Line Final Cleaned-up Geometry .....	25
Figure 2-13 – Exhaust Line GEM3D Discretization .....	25
Figure 2-14 – Exhaust Line GT-POWER sub-assembly model .....	26
Figure 2-15 – EGR Loop CAD geometry: before clean-up (left) and after (right) .....	27
Figure 2-16 – EGR Loop Final Cleaned-up Geometry.....	27
Figure 2-17 – EGR Loop GEM3D Discretization .....	28
Figure 2-18 – EGR Loop GT-POWER sub-assembly model .....	28
Figure 2-19 – Conduits CAD geometry .....	29
Figure 2-20 – Conduits GEM3D Discretization .....	29
Figure 2-21 – Conduits GT-POWER sub-assembly model.....	30
Figure 2-22 – Baseline GSE-T4 Turbocharger model (above) vs. PHOENICE E-Turbo (bottom) ..	31
Figure 2-23 – Compressor and Turbine Maps: GSE-T4 vs. PHOENICE .....	32
Figure 2-24 – MotorGeneratorMap GT-POWER Template.....	32
Figure 2-25 – Electric Motor Efficiency Map as a Function of Torque and Rotational Speed .....	32
Figure 2-26 – Intake Valves Forward Discharge Coefficient PHOENICE vs. GSE-T4 .....	34
Figure 2-27 – Intake Valves Tumble Coefficient PHOENICE vs. GSE-T4.....	35

Figure 2-28 – CD and Ct Coefficients: GSE-T4 vs. IFPEN GSE-T4 vs. IFPEN PHOENICE .....	36
Figure 2-29 – PHOENICE new piston design with CR 13.6.....	37
Figure 2-30 – PHOENICE new cylinder head design .....	37
Figure 2-31 – Updated PHOENICE Engine GT-POWER Model .....	38
Figure 3-1 – Crossflow brick (left) vs. Throughflow brick (right) .....	39
Figure 3-2 – Crossflow brick cross-section (left) vs. Throughflow brick cross-section (right) .....	39
Figure 3-3 – CatalystBrick vs. ParticulateFilter GT-POWER templates.....	39
Figure 3-4 – Visual representation of the ATS bricks testing conditions.....	40
Figure 3-5 – Exhaust Mass Flow Rate as a function of Time.....	40
Figure 3-6 – Individual Brick Model .....	41
Figure 3-7 – Short cone discretization: actual system (left) equivalent discretized system (right) ...	41
Figure 3-8 – Pulsated MFR at Turbine Outlet .....	42
Figure 3-9 – Ideal Pressure Drop vs. Mass Flow Rate Quadratic Trend .....	42
Figure 3-10 – EATS Bricks Calibration procedure flowchart .....	42
Figure 3-11 – Visual representation of the EHC-TWC <sub>1</sub> ATS brick testing conditions.....	43
Figure 3-12 – EHC+TWC <sub>1</sub> 1D CFD GT-POWER individual brick model.....	43
Figure 3-13 – EHC+TWC <sub>1</sub> optimized P <sub>drop</sub> .....	44
Figure 3-14 – Physical effect of C <sub>D</sub> and FM on pressure drop .....	44
Figure 3-15 – EHC+TWC <sub>1</sub> manually calibrated P <sub>drop</sub> .....	45
Figure 3-16 – Updated TWC <sub>1</sub> 1D CFD GT-POWER individual brick model .....	45
Figure 3-17 – Updated TWC <sub>1</sub> optimized P <sub>drop</sub> .....	46
Figure 3-18 – Updated TWC <sub>1</sub> manually calibrated P <sub>drop</sub> .....	46
Figure 3-19 – Visual representation of the TWC <sub>2</sub> ATS brick testing conditions .....	47
Figure 3-20 – TWC <sub>2</sub> 1D CFD GT-POWER individual brick model.....	47
Figure 3-21 – TWC <sub>2</sub> optimized P <sub>drop</sub> .....	48
Figure 3-22 – TWC <sub>2</sub> manually calibrated P <sub>drop</sub> .....	48
Figure 3-23 – Visual representation of the GPF ATS brick testing conditions .....	49
Figure 3-24 – GPF 1D CFD GT-POWER individual brick model.....	49
Figure 3-25 – GPF optimized P <sub>drop</sub> .....	50
Figure 3-26 – GPF manually calibrated P <sub>drop</sub> .....	50
Figure 3-27 – Virtual representation of the NO-Ox ATS brick testing conditions.....	51
Figure 3-28 – NO-Ox 1D CFD GT-POWER individual brick model .....	51
Figure 3-29 – NO-Ox optimized P <sub>drop</sub> .....	52
Figure 3-30 – NO-Ox manually calibrated P <sub>drop</sub> .....	52
Figure 3-31 – Visual representation of the SCR <sub>1</sub> ATS brick testing conditions .....	53
Figure 3-32 – SCR <sub>1</sub> 1D CFD GT-POWER individual brick model .....	53
Figure 3-33 – SCR <sub>1</sub> optimized P <sub>drop</sub> .....	54
Figure 3-34 – SCR <sub>1</sub> manually calibrated P <sub>drop</sub> .....	54
Figure 3-35 – Coolers’ Calibration Procedure Flowchart.....	55
Figure 3-36 – EGRC Experimental Test set-up .....	56
Figure 3-37 – EGRC 1D CFD GT-POWER test bench digital twin .....	56
Figure 3-38 – EGRC optimized P <sub>drop</sub> .....	57
Figure 3-39 – EGRC manually calibrated P <sub>drop</sub> .....	57
Figure 3-40 – Visual representation of the WCAC test bench set-up.....	58
Figure 3-41 – WCAC 3D-CFD Simulation model set-up.....	58
Figure 3-42 – WCAC 1D CFD GT-POWER Calibration Model .....	59
Figure 3-43 – WCAC optimized P <sub>drop</sub> .....	60
Figure 3-44 – WCAC manually optimized P <sub>drop</sub> .....	60
Figure 3-45 – WCAC Outlet Temperature Sensitivity Analysis .....	61
Figure 4-1 – PHOENICE Engine Performance for Different WCAC Outlet Temperatures – MEP.....	62

Figure 4-2 – PHOENICE Engine Performance for Different WCAC Outlet Temperatures – Combustion Efficiency .....	63
Figure 4-3 – PHOENICE Engine Performance for Different WCAC Outlet Temperatures – Volumetric Efficiency.....	63
Figure 4-4 – PHOENICE Engine Performance for Different Maximum Turbocharger Speeds– MEP .....	64
Figure 4-5 – PHOENICE Engine Performance for Different Maximum Turbocharger Speeds – Combustion Efficiency .....	65
Figure 4-6 – PHOENICE Engine Performance for Different Maximum Turbocharger Speeds – Volumetric Efficiency.....	65
Figure 4-7 – PHOENICE Engine Performance for Different Maximum Turbocharger Speeds – Compressor Maps .....	66
Figure 4-8 – PHOENICE Engine Performance for Different Maximum Turbocharger Speeds– uncapped BMEP MEP .....	67
Figure 4-9 – PHOENICE Engine Performance for Different Maximum Turbocharger Speeds – uncapped BMEP Combustion Efficiency .....	67
Figure 4-10 – PHOENICE Engine Performance for Different Maximum Turbocharger Speeds – uncapped BMEP Volumetric Efficiency.....	68
Figure 4-11 – PHOENICE Engine Performance for Different Maximum Turbocharger Speeds – max BMEP Compressor Maps.....	68
Figure 4-12 – VVA DoE Different Engine Configurations.....	69
Figure 4-13 – VVA DoE Sub-assemblies’ differences.....	69
Figure 4-14 – Exhaust Back Pressure: GSE-T4 vs. PHOENICE .....	70
Figure 4-15 – Investigated eIVO – eIVC DoE Area.....	70
Figure 4-16 – VVA DoE 3000 RPM x 7 bar BMEP – BMEP, BTE and MFB50.....	71
Figure 4-17 – VVA DoE 3000 RPM x 7 bar BMEP – PMEP and Volumetric Efficiency .....	72
Figure 4-18 – VVA DoE 3000 RPM x 7 bar BMEP – Residuals, Backpressure and Throttling .....	72
Figure 4-19 – PHOENICE Engine prototype at IFPEN test facility <sup>[22]</sup> .....	73
Figure 4-20 – 3000 RPM x 7 bar BMEP Experimental Results: BTE Improvements .....	73
Figure 4-21 – VVA DoE 3000 RPM x 7 bar BMEP: E-Turbo Effect – BMEP, BTE and MFB50 ..	74
Figure 4-22 – VVA DoE 3000 RPM x 13 bar BMEP: E-Turbo Effect – BMEP .....	74
Figure 4-23 – VVA DoE 3000 RPM x 7 bar BMEP: E-Turbo Effect – Residuals, Backpressure and Throttling .....	75
Figure 4-24 – VVA DoE 3000 RPM x 7 bar BMEP: Exhaust Line Effect – BMEP, BTE and MFB50 .....	76
Figure 4-25 – VVA DoE 3000 RPM x 13 bar BMEP: Exhaust Line Effect – BMEP .....	76
Figure 4-26 – VVA DoE 3000 RPM x 7 bar BMEP: Exhaust Line Effect – Residuals, Backpressure and Throttling.....	77
Figure 5-1 – Schematic of the PHOENICE Engine prototype at IFPEN test facility <sup>[22]</sup> .....	78
Figure 5-2 – IFPEN Test Bench Sensors Layout.....	79
Figure 5-3 – GT-POWER 1D CFD Cylinder Pressure Only Analysis (CPOA) model.....	80
Figure 5-4 – CPOA Simulation Results .....	81
Figure 5-5 – CPOA generate burn profile.....	82
Figure 5-6 – CPOA Combustion main parameters .....	82
Figure 5-7 – Import of Experimental data from excel in GT-POWER case set-up.....	83
Figure 5-8 – Main model controllers’ sub-assembly .....	83
Figure 5-9 – Correlation model controllers’ sub-assembly .....	84
Figure 5-10 – Example of model-based EGR Valve Controller oscillating .....	84
Figure 5-11 – Correlation Model pressure evolution vs. Experimental measurements.....	85
Figure 5-12 – Correlation Model temperature evolution vs. Experimental measurements .....	85
Figure 5-13 – Correlation Model operating parameters vs. Experimental measurements.....	86

Figure 5-14 – Correlation Model combustion parameters vs. Experimental measurements .....	86
Figure 5-15 – Correlation Model performances vs. Experimental measurements .....	87
Figure 5-16 – Polynomial curve fit of the optimal DEM.....	89
Figure 5-17 – SITurb pressure evolution vs. Experimental measurements and CPOA.....	90
Figure 5-18 – SITurb temperature evolution vs. Experimental measurements and CPOA.....	91
Figure 5-19 – SITurb combustion parameters vs. Experimental measurements and CPOA.....	91
Figure 5-20 – SITurb performances vs. Experimental measurements and CPOA .....	92

## List of Tables

Table 1-1 – GSE T3 and GSE-T4 Engine Specifications .....	5
Table 1-2 – Comparison between baseline and PHOENICE EATS components volume .....	13
Table 2-1 – Principal 1D GT-POWER Templates.....	17
Table 3-1 – EHC+TWC <sub>1</sub> main geometrical characteristics .....	43
Table 3-2 – EHC+TWC <sub>1</sub> Initial Conditions.....	43
Table 3-3 – Updated TWC <sub>1</sub> main geometrical characteristics.....	45
Table 3-4 – TWC <sub>2</sub> main geometrical characteristics .....	47
Table 3-5 – TWC <sub>2</sub> Initial Conditions.....	47
Table 3-6 – GPF main geometrical characteristics .....	49
Table 3-7 – GPF Initial Conditions.....	49
Table 3-8 – NO-Ox main geometrical characteristics .....	51
Table 3-9 – NO-Ox Initial Conditions .....	51
Table 3-10 – SCR <sub>1</sub> main geometrical characteristics.....	53
Table 3-11 – SCR <sub>1</sub> Initial Conditions .....	53
Table 3-12 – EGRC Initial Conditions .....	56
Table 3-13 – WCAC Initial Conditions .....	59
Table 4-1 – VVA DoE Key Operating Points.....	70
Table 5-1 – IFPEN DDCA Assessment: EGR and Lambda Sweep Combinations.....	79
Table 5-2 – Optimal DEM for each of the 18 Cases.....	89

## List of Acronyms

<b>AFR</b>	-	Air-Fuel Ratio
<b>BDC</b>	-	Bottom Dead Centre
<b>BEV</b>	-	Battery Electric Vehicle
<b>BMEP</b>	-	Brake Mean Effective Pressure
<b>BSFC</b>	-	Brake-Specific Fuel Consumption
<b>BTE</b>	-	Brake Thermal Efficiency
<b>CAD</b>	-	Computer-Aided Design
<b>CC</b>	-	Closed Coupled
<b>CFD</b>	-	Computational Fluid Dynamics
<b>CI</b>	-	Compression-Ignition
<b>CPSI</b>	-	Cell Per Square Inch
<b>DC</b>	-	Discharge Coefficient
<b>DDCA</b>	-	Dual Dilution Combustion Approach
<b>DEM</b>	-	Dilution Effect Multiplier
<b>DHE</b>	-	Dedicated Hybrid Engine
<b>DHE</b>	-	Dedicated Hybrid Engine
<b>DI</b>	-	Direct Ignition
<b>DOC</b>	-	Diesel Oxidation Catalyst
<b>DoE</b>	-	Design of Experiment
<b>DPF</b>	-	Diesel Particulate Filter
<b>EGR</b>	-	Exhaust Gas Recirculation
<b>EGRC</b>	-	Exhaust Gas Recirculation Cooler
<b>EHC</b>	-	Electrically Heated Catalyst
<b>EHRS</b>	-	Exhaust gas-to-coolant Heat Recovery System
<b>eIVC</b>	-	Electric IVC
<b>EIVC</b>	-	Early Intake Valve Closure
<b>eIVO</b>	-	Electric IVO
<b>EU</b>	-	European Union
<b>FL</b>	-	Forward Losses
<b>FM</b>	-	Friction Multiplier
<b>GDI</b>	-	Gasoline Direct Injection
<b>GPF</b>	-	Gasoline Particulate Filter
<b>GSE</b>	-	Global Small Engine
<b>ICE</b>	-	Internal Combustion Engine
<b>IVC</b>	-	Intake Valve Closure
<b>IVO</b>	-	Intake Valve Opening
<b>LDV</b>	-	Light Duty Vehicle
<b>LIVC</b>	-	Late Intake Valve Closure
<b>LNT</b>	-	Lean NO <sub>x</sub> Trap
<b>MEP</b>	-	Mean Effective Pressure
<b>MFB50</b>	-	Mass Fraction Burned 50%
<b>MFR</b>	-	Mass Flow Rate
<b>P2X</b>	-	Power to X
<b>PFI</b>	-	Port Fuel Injection
<b>PGM</b>	-	Platinum-Group Metal
<b>PHEV</b>	-	Plug-in Hybrid Electric Vehicle
<b>PM</b>	-	Particle Matter
<b>PM</b>	-	Particulate Matter

<b>PMEP</b>	-	Pumping Mean Effective Pressure
<b>S&amp;S</b>	-	Start & Stop
<b>SCR</b>	-	Selective Catalytic Reduction
<b>SI</b>	-	Spark Ignition
<b>SOI</b>	-	Start of Injection
<b>TDC</b>	-	Top Dead Centre
<b>TDCf</b>	-	Top Dead Centre Firing
<b>TEG</b>	-	Thermoelectric Generator
<b>TKE</b>	-	Turbulence Kinetic Energy
<b>TPA</b>	-	Three Pressure Analysis
<b>TWC</b>	-	Three Way Catalyst
<b>UF</b>	-	Under Floor
<b>VNT</b>	-	Variable Nozzle Turbine
<b>VVA</b>	-	Variable Valve Actuator
<b>VVT</b>	-	Variable Valve Timing
<b>WCAC</b>	-	Water Charge Air Cooler
<b>WG</b>	-	Waste Gate
<b>WHRS</b>	-	Waste Heat Recovery Systems



# 1 Introduction

## 1.1 PHOENICE Project

The European "Fit for 55" proposal states that tank-to-wheel CO<sub>2</sub> emissions from Light Duty Vehicles (LDV) should be reduced by at least 55% by 2030 and 90% by 2050 compared to 1990 levels <sup>[1]</sup>. This drastic reduction in emissions is necessary to keep the rate of global warming at or below +1.5°C/year relative to the pre-industrial era. On top of that, the future Euro 7 pollutant law is anticipated to cut the pollution limitations even further and include new species, such as NH<sub>3</sub>, N<sub>2</sub>O, CH<sub>2</sub>O, and CH<sub>4</sub> <sup>[2]</sup>. Moreover, compliance factors are projected to close the gap between laboratory testing and Real Driving Emission (RDE) <sup>[3]</sup>.

As these reductions do not comply with Internal Combustion Engines (ICEs), in 2021, the European Commission declared that all LDVs fit with a thermal powertrain will be banned starting from 2035. Although this ban will lead to net-zero tank-to-wheel emissions, many raise the question of looking at the whole picture, including the well-to-tank emissions.

The combined use of all currently available technologies should be done to decrease the amount of greenhouse gases that are released into the atmosphere. Less energy-intensive architectures provide a balance between emissions, ownership costs, and practicality with respect to Battery Electric Vehicles (BEV).

As a matter of fact, in such a context, hybrid electric powertrains are considered the primary short-term solution to lower fuel consumption and exhaust emissions. Theoretically, with a Plug-in Hybrid Electric Vehicle (PHEV), it is possible to maximize the potential of both the electric and the thermal part, reaching zero emissions in city driving conditions and near zero emissions where the internal combustion engine must take over. Making the most out of this architecture is, therefore, crucial.

In this framework, as part of the Horizon 2020 (H2020) project, PHEV tOwards zero EmissioNs & ultimate ICE efficiency, PHOENICE for short, aims to create a C-class PHEV (P1/P4) SUV vehicle demonstrator whose fuel consumption and pollutant emissions will be minimized for real-world driving conditions without compromising performance and drivability <sup>[4]</sup>.

Due to the importance of this market niche in the European market, the PHOENICE vehicle demonstrator will be built on a mass-produced C-Class plug-in hybrid car (*Figure 1-1*). The technologies used, however, are not tied to any particular application.



Figure 1-1 - PHEV C-SUV for PHOENICE demonstrator vehicle

As seen in *Figure 1-2*, the hybrid architecture consists of a modern gasoline engine that drives the front axle using a six-speed automatic transmission (AT) and two electric motors, one of which is in the P0 position and acts as both the starter and alternator and the other of which is in the P4 position to enable the electric all-wheel drive (AWD) operation. While braking, both motors can regenerate energy.

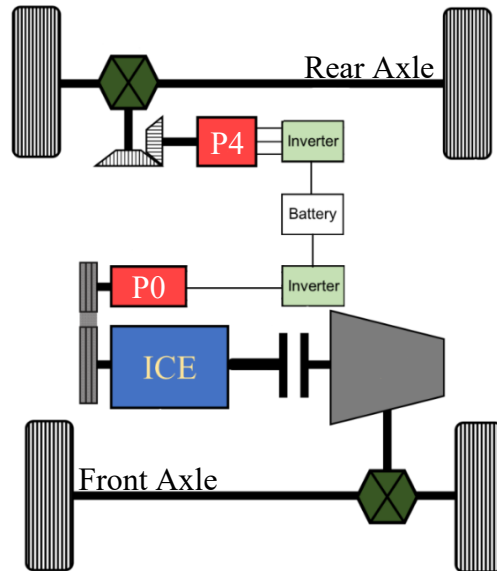


Figure 1-2 – PHOENICE Hybrid Architecture

To achieve the target indicated efficiency of 47%, the base vehicle requires optimization of a highly efficient gasoline engine, relying on dual diluted combustion, innovative in-cylinder charge motion and ignition technologies, high-pressure injection, and an electrified Turbocharger. Moreover, an ad hoc after-treatment system will simultaneously attain the desired near-zero pollutant emissions in transitory settings. A Gasoline Particulate Filter (GPF), an Electrically Heated Catalyst (EHC), two Three Way Catalysts (TWCs), and a Selective Catalyst Reduction system (SCR) will all function simultaneously as part of the after-treatment system to reduce both controlled and unregulated pollutants. Other systems, such as energy recovery systems and a water charge air cooler, will also be added to increase engine efficiency.

This project will facilitate the transition of the European automotive sector to more eco-friendly mobility in the medium term, both in terms of air quality and Green House Gases (GHG). Moreover, alcohol-based fuels produced by P2X processes will be considered to improve CO<sub>2</sub> reduction further. The vehicle demonstrator will hone design abilities for engines and after-treatment systems, focusing on the offered solutions' cost-to-performance ratios.

PHOENICE is funded by the European Community and is coordinated by the French energy research organization IFPEN. Several other companies also participate in the project, such as Centro Ricerche Fiat CRF, FEV Europe, Johnson Matthey, Marelli Europe, Garrett Motion, In Extenso Innovation Croissance, and Politecnico di Torino.



Figure 1-3 - PHOENICE Logo

## 1.2 State of the art: Spark Ignition Internal Combustion Engine Efficiency

For more than a century, gasoline internal combustion engines have been the primary power source for transportation. However, despite their widespread use, these engines have many efficiency limitations. Most gasoline spark-ignited engines today operate on stoichiometric air-fuel ratios ( $\lambda = 1$ ) as the laminar burning speed of this mixture enables complete oxidation of the hydrocarbon molecules that make up the fuel. Moreover, the traditional gasoline after-treatment system must operate under stoichiometric conditions to obtain the best conversion efficiency. Unfortunately, due to their structure and mode of operation, these engines are often only capable of 42% efficiency at most. The high temperatures attained during combustion, with the consequent energy loss at the exhaust and the low volume of intake air at low loads, impose, under stoichiometric operation, high thermal losses at medium to high loads and substantial pumping losses at low loads.

As electric motors handle the low-load portion of the driving cycles, low-load losses do not affect PHEVs; nevertheless, coolant and energy losses must be adequately addressed. For these reasons, the ultra-lean burn may be a viable option to reach efficiency above 45%. Increased air dilution will reduce the combustion temperature by absorbing some heat without reacting while also reducing the likelihood of abnormal combustion. A higher resistance to knock allows the compression ratio to be increased, with the consequent increase in engine efficiency. However, it is crucial to remember that under these circumstances, high-complexity systems are required for the ignition and turbocharging processes, which may not be compatible with the PHOENICE TRL 7 target (i.e., project EAGLE<sup>[5]</sup>).

The engine concept selected for PHOENICE will combine the strengths of air dilution with those of EGR. This kind of combustion, called the Dual Dilution Combustion Approach (DDCA), represents the best trade-off regarding efficiency, pollutant emissions, cost, and complexity. The maximum target dilution rate (EGR + air) is 1.7, with air being the main component and EGR being limited to at most 15%, with the only goal of reducing NO<sub>x</sub> emission. Indeed, the repartition between EGR and air will be optimized for each operating point on the engine map.

Several technologies will aid combustion to ensure the feasibility of such a lean burn. The main contributions will come from a high-pressure injection system (350 bar) and the innovative intake charge air motion Swumble™<sup>[6,7]</sup>, which proved to be able to increase the Turbulence Kinetic Energy (TKE) at Top Dead Centre (TDC) by more than 50%.

On the other hand, an extensive dilution calls for a lot of intake air. For this reason, the vehicle demonstrator will be equipped with an electrified turbocharger<sup>[8]</sup>. An E-Turbo also enables energy regeneration through exhaust gas enthalpy and enhanced transient performance, with the e-motor boosting the turbo shaft speed, uncoupling it from the exhaust flow.

On top of that, the engine will employ Variable Valve Actuation systems (VVA) to enable the exploitation of the more efficient Miller Cycle <sup>[9,10]</sup> and minimize pumping losses at part load thanks to un-throttled operation.

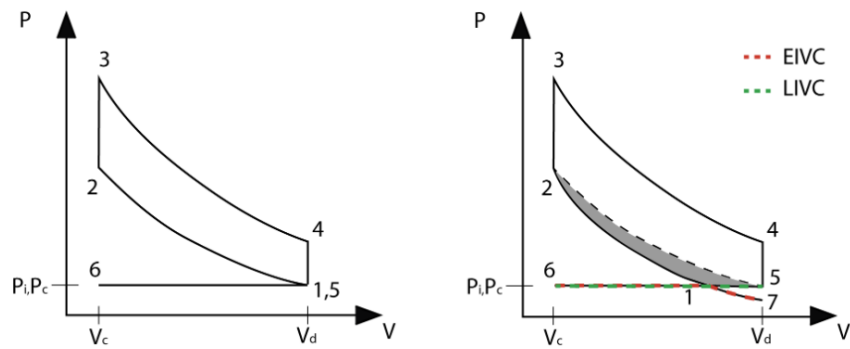


Figure 1-4 – Ideal cycle vs. EIVC and LIVC Miller cycles

Indeed, the goal is to optimize the trade-off between efficiency and pollutant emissions across the whole engine map by using air and EGR as needed, based on the engine operating conditions. Air dilution seeks to significantly improve efficiency, while EGR will focus on reducing  $\text{NO}_x$  and Particle Matter (PM) emissions.

### 1.3 Baseline Engine: Global Small Engine (GSE)

The Global Small Engine (GSE) was created in 2016 by Fiat, subsequently renamed to Stellantis, to replace the outdated MultiAir and TwinAir lines of engines. The GSE is a modular 3- or 4-cylinder engine initially developed as a normally aspirated engine for the Brazilian market before being launched, in 2018, as a turbocharged variant for the European and North American markets. An engine block that can be produced with several cylinder layouts, in this case, 3 and 4, while maintaining the same unitary displacement and internal components is referred to as a modular engine. Because two engines can be produced on the same production line and their shared components can be swapped out for one another, this manufacturing process has various benefits, including lower costs and greater availability of Original Equipment Manufacturer (OEM) replacements.



Figure 1-5 – Baseline Stellantis GSE-T4 Engine

The base engine used in PHOENICE is the GSE-T4, the GDI 4-cylinder turbo version employed in various lines such as the Jeep Compass, Jeep Renegade, and Fiat 500X.

The engine features the latest iteration of the MultiAir, the Fiat-developed variable valve timing system which enables independent lift control of each intake valve, a wastegate turbocharger, a long stroke designed engine with a compression ratio of 10.5, a high-pressure Direct Injection system (DI) up to 200 bar and an exhaust manifold integrated into the cylinder head. The engine can reach 132 kW of peak power, and on top of that, it is assisted by a P1/P4 hybrid configuration, adding 44 more kW to the whole powertrain. The vehicle can employ AWD through the ICE on the front wheels and the P4 electric motor on the rear wheels. *Table 1-1* summarizes the primary engine data.

		T3	T4
Bore x Stroke	mm	70 x 86,5	
Displacement	cc	999	1332
Compression Ratio	[-]	10,5:1	
Fuel injection system	[-] @ bar	GDI @ 200	
Max Power	kW @ rpm	88 @ 6000	132 @ 5750
Max Torque	Nm @ rpm	190 @ 1750	270 @ 1800

Table 1-1 – GSE T3 and GSE-T4 Engine Specifications

## 1.4 PHOENICE Engine Concept

PHOENICE's primary objective is to use engine tuning and modification to increase the overall braking thermal efficiency of a production engine to 47% to hasten the transition to carbon neutrality without drastically altering the end-user experience. The engine should, however, be kept as close to the baseline version as possible to reduce costs and make the transition easier for the manufacturer. Only the most essential elements should be added or replaced.

The main differences with respect to the Stellantis-developed engine can be summarized in four major components:

- An innovative e-turbocharged engine specifically designed for hybrid architecture.
- A Waste Heat Recovery System.
- A complete Aftertreatment system compliant with Euro 7 legislation.
- A complete control strategy.

These main differences are shown in *Figure 1-6* and will now be briefly discussed alongside the other changes.

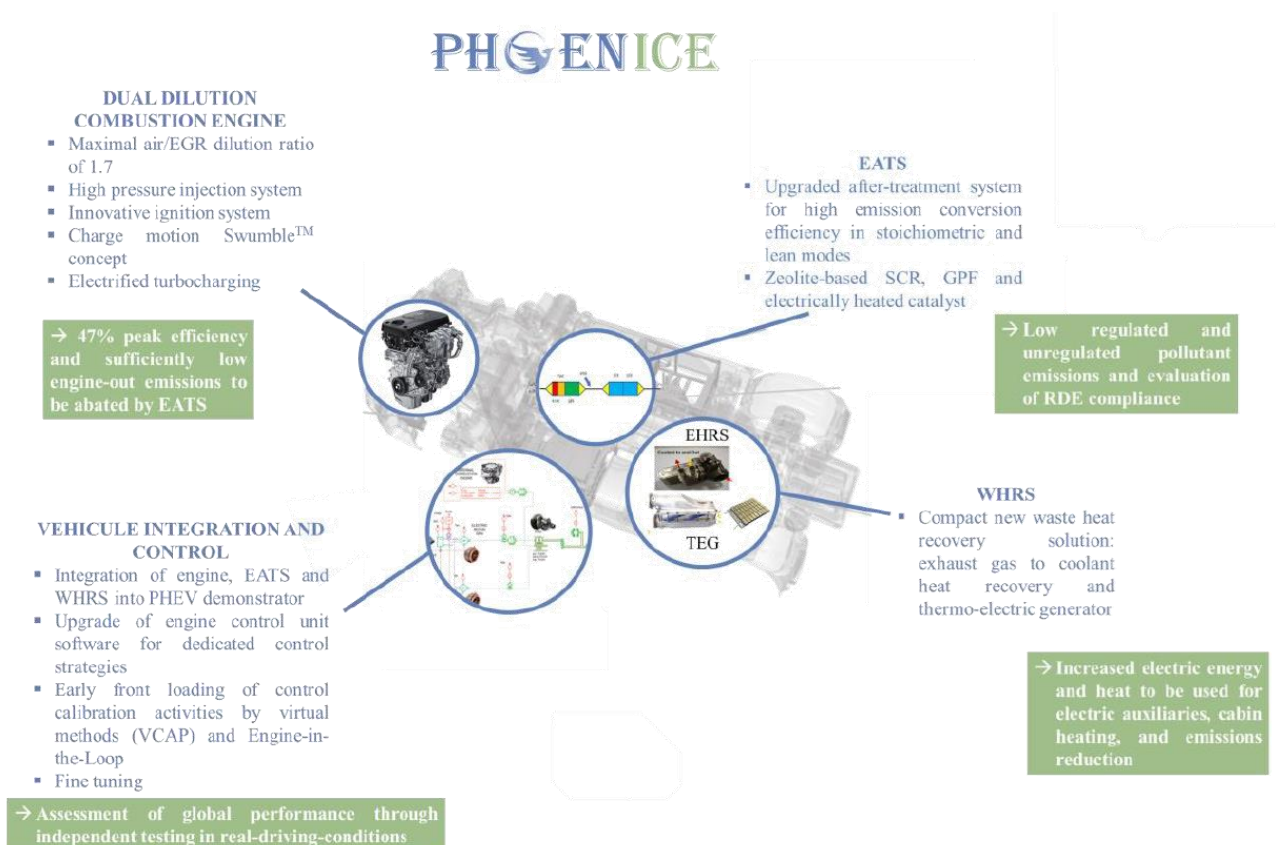


Figure 1-6 – PHOENICE GSE-T4 Tuning

### 1.4.1 Garrett E-Turbo

One of the upgraded components in the PHOENICE engine is the turbocharger. While the GSE-T4 is already a turbocharged engine, a larger electrified turbocharger is required to support the high dilution rates of DDCA while simultaneously providing the necessary boost pressure.

As a result of turbo matching analysis performed on the 1D virtual test rig, the turbocharger was designed by the partner company Garrett Motion and pairs a Variable Nozzle Turbine (VNT) with a compressor capable of providing the needed extra air. The Garrett unit is paired with a 48 V electric machine with an efficiency of  $\eta_{tot} = \eta_{Inverter} \cdot \eta_{Motor} = 0.828$  with a maximum rotational speed of 225 kRPM. The electrified turbocharger can regenerate energy from the turbo shaft's rotational speed. Moreover, although still primarily driven by exhaust gas enthalpy, the turbo shaft can also be driven by the e-motor whenever rapid acceleration is required.

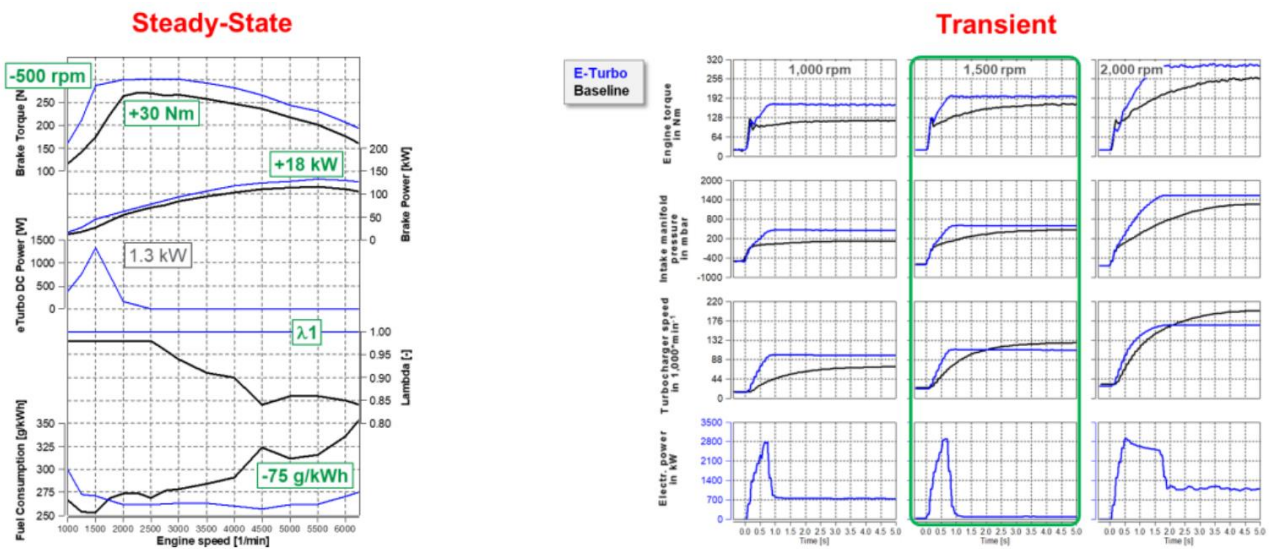


Figure 1-7 – E-Turbo Performance tested on a Mercedes A-Class prototype.

As can be seen from *Figure 1-8*, the two compressor maps are plotted. PHOENICE can reach peak efficiencies up to 4% higher and over a much larger area with respect to the baseline turbo.

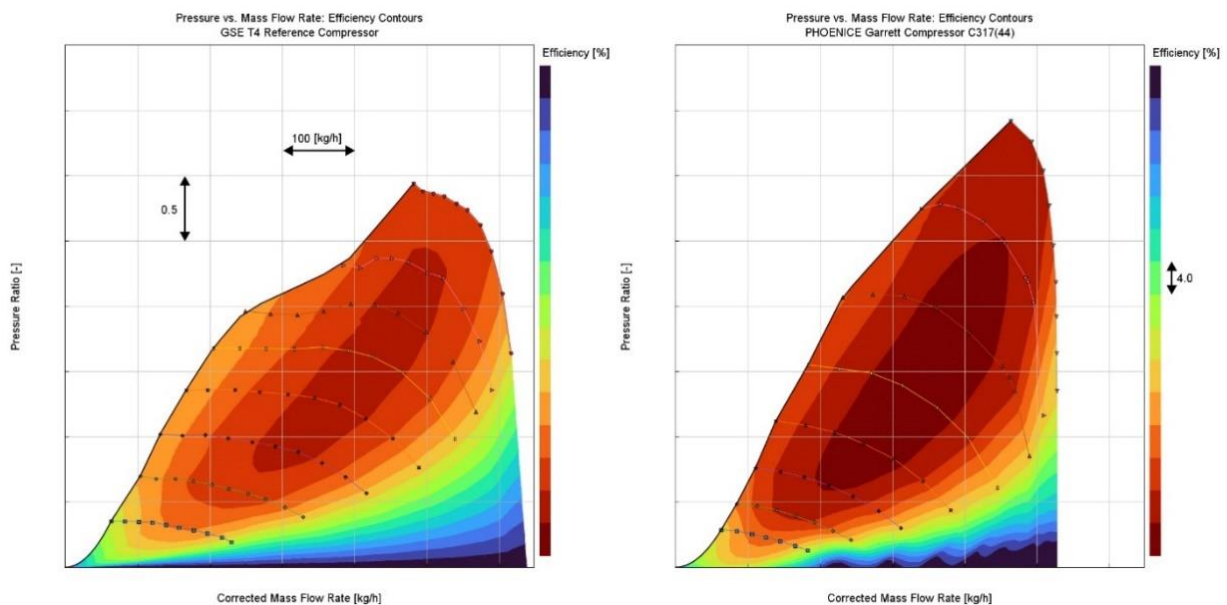


Figure 1-8 - Compressor Maps: Baseline vs. PHOENICE

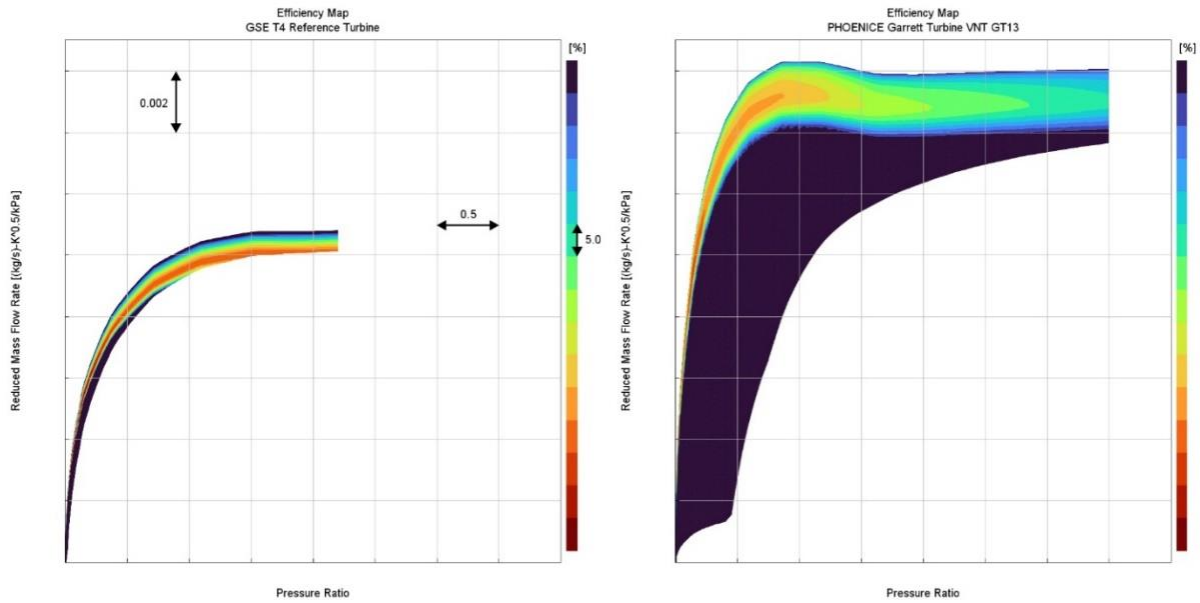


Figure 1-9 – Turbine Maps: Baseline vs. PHOENICE

Geometrically speaking, the baseline and the Garrett turbochargers also differ in terms of the actuation mechanism. The GSE-T4 turbine is controlled by a Waste Gate valve (WG), whereas the PHOENICE one employs a VNT.

The wastegate, a simple mechanical valve, is used by WG turbochargers to regulate exhaust gas flow through the turbine. When the exhaust system's pressure reaches a specific point, the wastegate valve opens, enabling some exhaust gases to bypass the turbine, preventing the engine from overheating and the turbocharger from spinning too quickly. As their operating principle is quite simple, this configuration is much cheaper, although less sophisticated. On the other hand, in a VNT turbocharger, the exhaust gas flow through the turbine can be adjusted by a set of moveable vanes, which are actuated depending on throttle position and engine load. The VNT turbocharger can maintain ideal turbine speed throughout a more extensive range of engine speeds by adjusting the angle of the vanes, which improves power delivery and efficiency. Moreover, the VNT turbocharger can run at lower engine RPMs, lessening turbo lag and enhancing responsiveness. Moreover, boost pressure settings on waste gate turbochargers are typically fixed and can only be altered by changing the wastegate spring or utilizing an electronic boost controller. In contrast, VNT turbochargers can alter the boost pressure according to what is needed resulting in better performance and fuel efficiency at a higher price and more complicated maintenance.

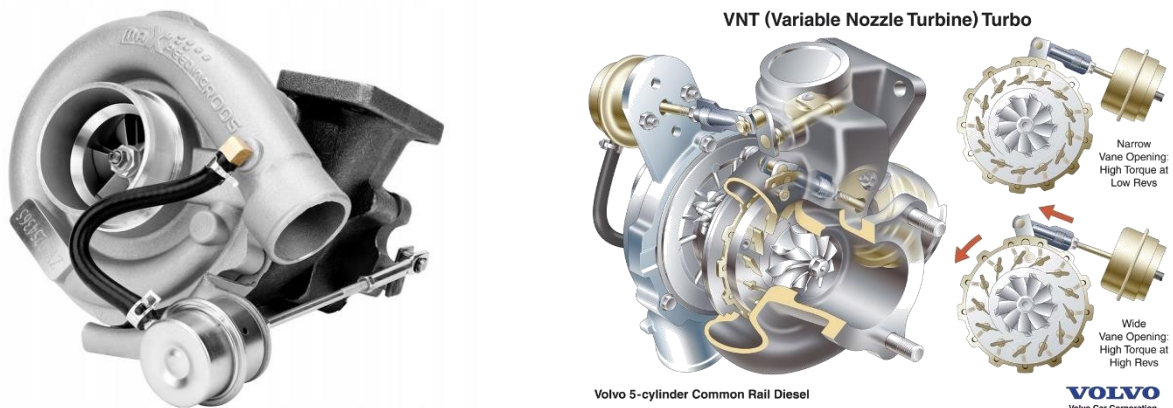


Figure 1-10 - WG Turbocharger (left) vs. VNT Turbocharger <sup>[11]</sup> (right)

### 1.4.2 Low-Pressure EGR

An Exhaust Gas Recirculation system was introduced in the PHOENICE engine to lower the combustion temperature and thus the  $\text{NO}_x$  emissions, which for GDI engines are not negligible.

The logic behind EGR is to introduce inert gasses in the cylinder, such as  $\text{CO}_2$ , which will steal some of the heat in the chamber without reacting, thus effectively diluting the mixture and lowering the combustion temperature. In addition, the introduced inert gasses will also go through side endothermic reactions, such as the dissociation of  $\text{CO}_2$  and  $\text{H}_2\text{O}$ , decreasing the available amount of heat for the reaction even further.

In the automotive world, two main kinds of EGR systems are used: high-pressure (or short route) EGR and low-pressure (or long route) EGR. The main difference between the two is where the gasses are recirculated from. The short route EGR recirculates the exhaust gasses before the turbine directly from the exhaust manifold. This way, the gasses are not expanded and can rapidly flow to the intake line. The main cons of this solution are to be found in the lower turbine efficiency due to a reduction in the MFR, which will inherently affect the compressor performances as well, and the increase in intake air temperature and particulates. On the other hand, the low-pressure solution recirculates the gasses after the close-coupled after-treatment bricks. In this way, the recirculates are not only at a lower pressure, as they are expanded in the turbine, but they are also filtered of all the impurities and pollutants which would act like nucleation points for SOOT formation. This second solution does not affect the turbine performances, as the Mass Flow Rate (MFR) through the turbine is not changed and does not change the intake air temperature, as the gasses are generally run through an EGR cooler. However, long route systems are characterized by worse transient performances as, when full load is required, the EGR line requires more time to be emptied due to the larger volume.

The system employed in the PHOENICE engine is of the low-pressure kind paired with an EGRC, as this solution yields the lowest possible BSFC.

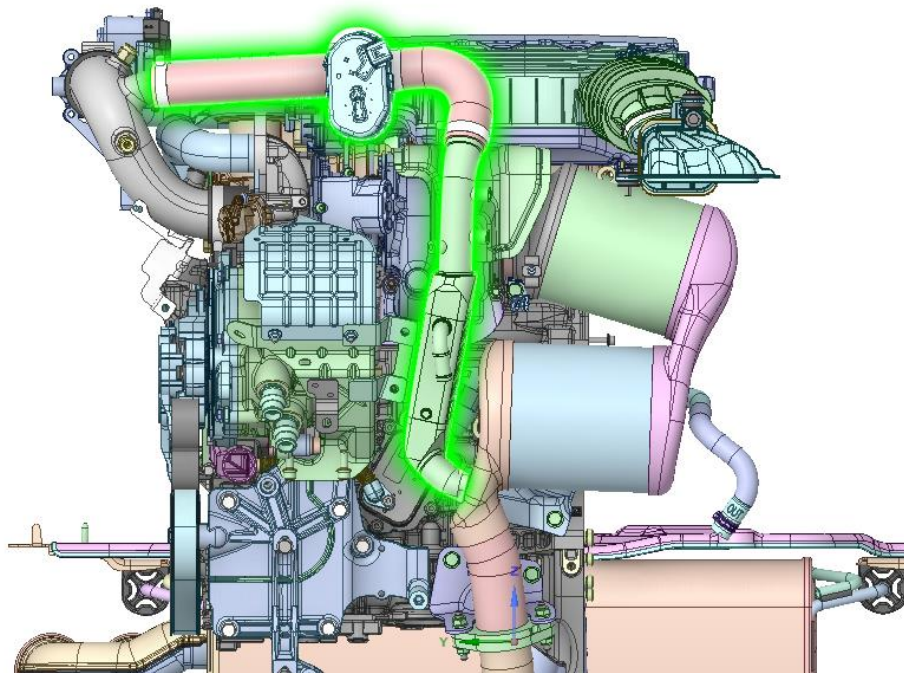


Figure 1-11 – PHOENICE Low Pressure EGR Line

### 1.4.3 Dual Diluted Combustion and Swumble™

The working principle of gasoline engines is based on flame front propagation, more specifically, with its speed. The burning mixture should be as close to stoichiometric as possible to achieve fast enough burn durations while at the same time ensuring proper oxidation of the fuel and high after-treatment efficiency. Under laminar flow operating conditions, no fuel can guarantee such a propagation speed. A laminar flame front must be faster to oxidize the whole mixture volume in the given time. A certain turbulence level is required to corrugate the flame front, increasing its surface area and thus increasing its propagation speed. A high enough turbulence level is usually achieved by employing proper intake ducts and piston head designs which will cause one of three principal phenomena: Swirl, Tumble, and squish.

A spiral motion of the intake air parallel to the combustion chamber axis characterizes swirl. Swirl enhances mixing in the case of a DI diesel engine. Tumble is characterized by a spiral motion of the intake air perpendicular to the combustion chamber axis. This solution enhances the turbulence level inside the chamber and, for this reason, is mainly used in SI engines. Lastly, Squish is characterized by a toroidal motion of charge at TDC due to a properly shaped piston head which will guide the flow during the compression phase. Although the benefits of this solution are lower with respect to swirl and tumble, it is usually used in gasoline and diesel engines to improve turbulence in the former and mixing in the latter.



Figure 1-12 – Swirl vs. Tumble vs. Squish [12,13]

The turbulence level will be even more relevant if the used mixture is not stoichiometric, like in the PHOENICE prototype. As shown in *Figure 1-13*, the leaner the mixture, the slower the combustion speed, and the higher the turbulence at the spark needed for petrol to ignite.

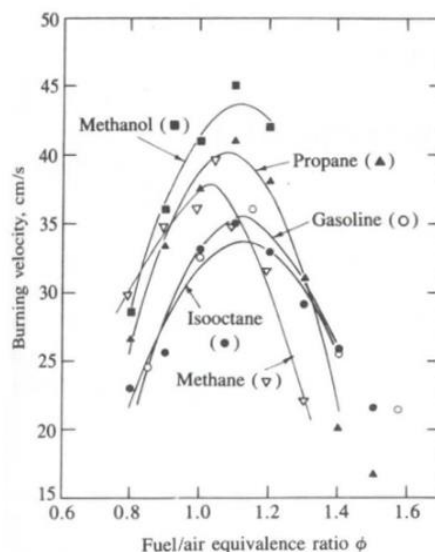


Figure 1-13 – Burning velocity as a function of the equivalence ratio  $\phi$  [14]

To overcome this issue, PHOENICE employs an innovative intake design solution, developed, and trademarked by IFPEN, allowing combustion for very lean mixtures. This solution is called Swumble™. Swumble™ is characterized by an increase of TKE at top dead center of about 40%, ensuring a fast enough flame front and combustion propagation, even at ultra-lean conditions, moreover, increased mixing for both GDI petrol and alcohol-based biofuels. Thanks to Swumble™-like charge motion, PHOENICE will achieve an overall faster and more efficient combustion to the base GSE-T4 engine.

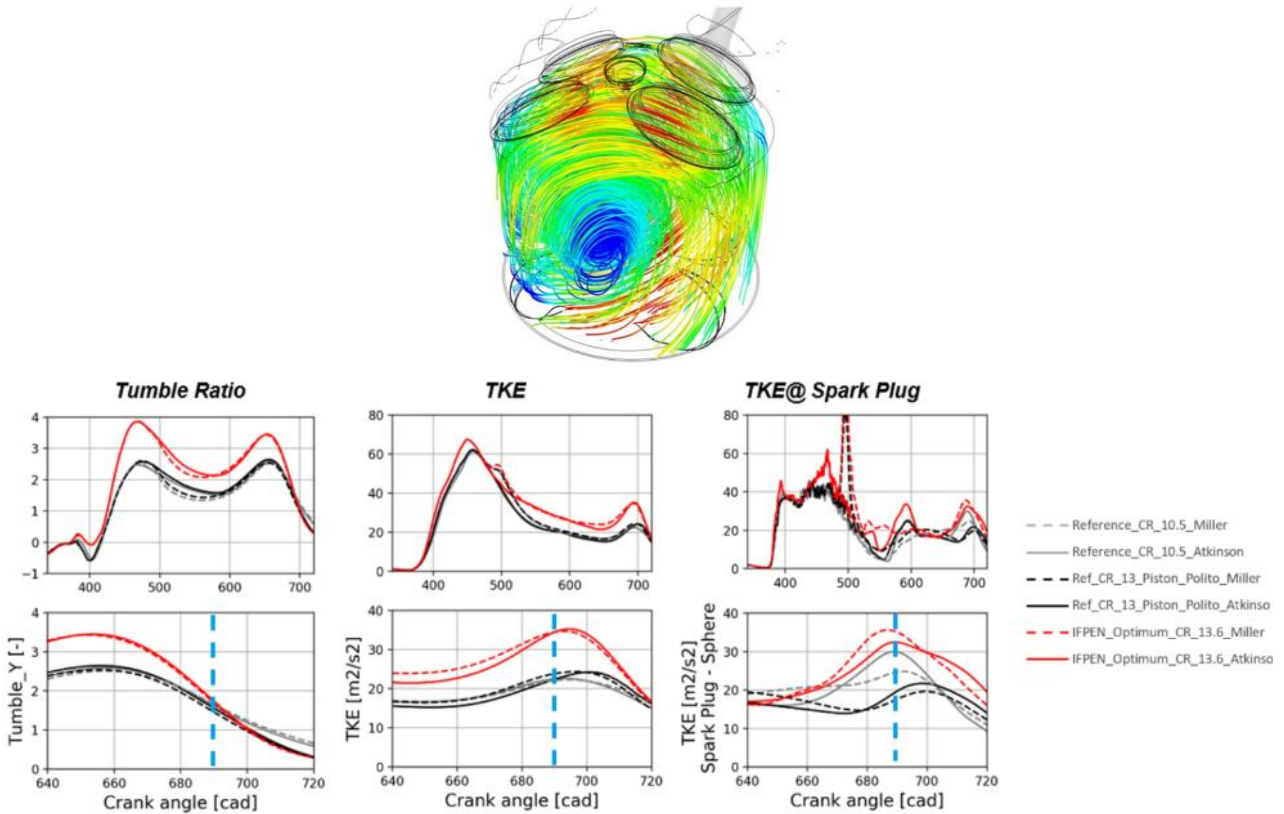


Figure 1-14 – Swumble™ Intake Air Charge Motion [15]

Swumble™ is especially effective when coupled with Miller cycles (EIVC or LIVC). Looking at Figure 1-15, one can see that Swumble™ makes Turbulent Jet Injection (TJI) levels of efficiency achievable even in a more standard GDI engine design. It must be noted that TJI, although employed on street-homologated vehicles (i.e., Maserati MC20, Nettuno Engine [16]), requires a much higher cost of implementation, making the results achieved by Swumble™ even more remarkable.

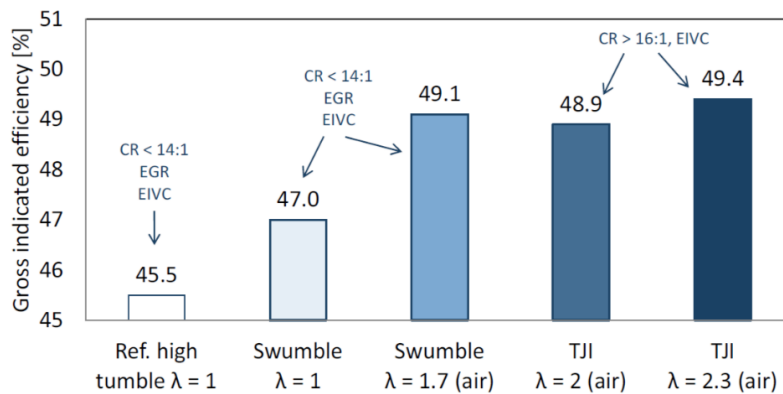


Figure 1-15 – Performance of Swumble™ concept in lean conditions [17]

#### 1.4.4 Water Charge Air Cooler

Although a Water Charge Air Cooler (WCAC) is already present in the base GSE-T4 engine, PHOENICE upgrades such a component to a larger and more efficient one to cool the larger quantity of intake air and EGR that the engine needs for DDCA.

A WCAC reduces the intake air temperature by running it through water-cooled fins. Cold air is denser, introducing a larger quantity of oxygen in the combustion chamber and consequently increasing the amount of fuel that can be oxidized per cycle, increasing the engine's power output.

The larger the volume of air to be cooled, the beefier and more efficient the heat exchanger should be. For this reason, the GSE-T4 WCAC was upgraded to an ad hoc designed heat exchanger by Valeo. The overall exchanger volume was increased from 1.8 L to 2.8 L.

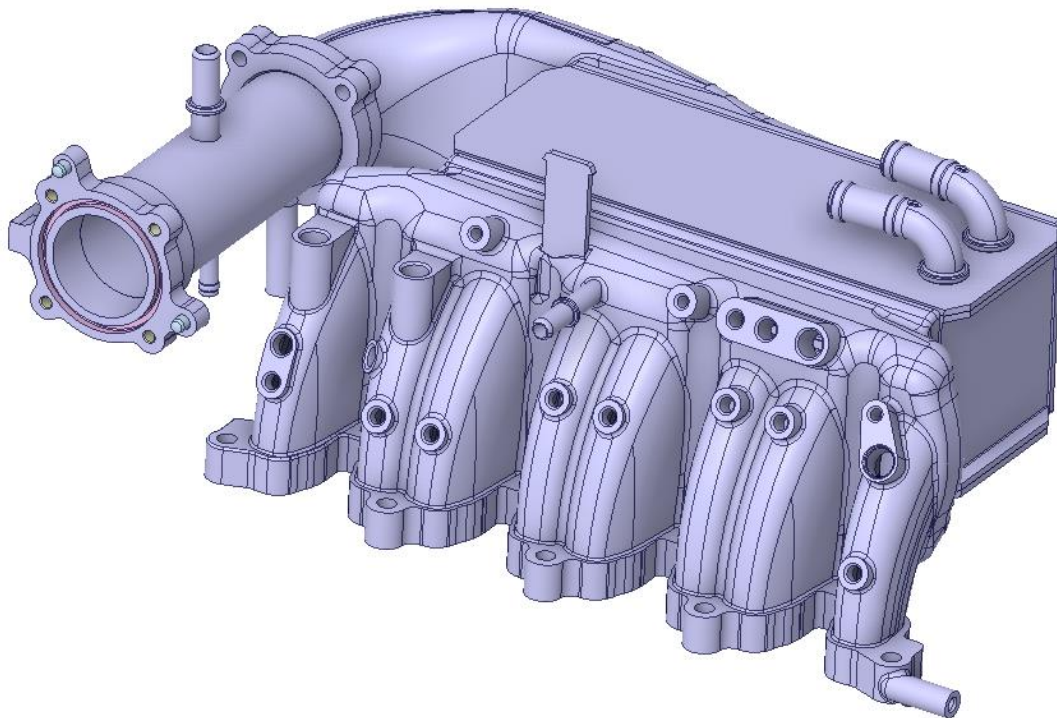


Figure 1-16 – PHOENICE WCAC CAD Render

### 1.4.5 Exhaust Line

The after-treatment system for the PHOENICE hybrid demonstrator must meet the more stringent Euro 7 standard over a wide range of real-world driving conditions. Furthermore, it must sustain both the lean environment consequence of the DDCA strategy and the stoichiometric conditions expected to occur during cold starts, high loads, and Start & Stop (S&S) maneuvers.

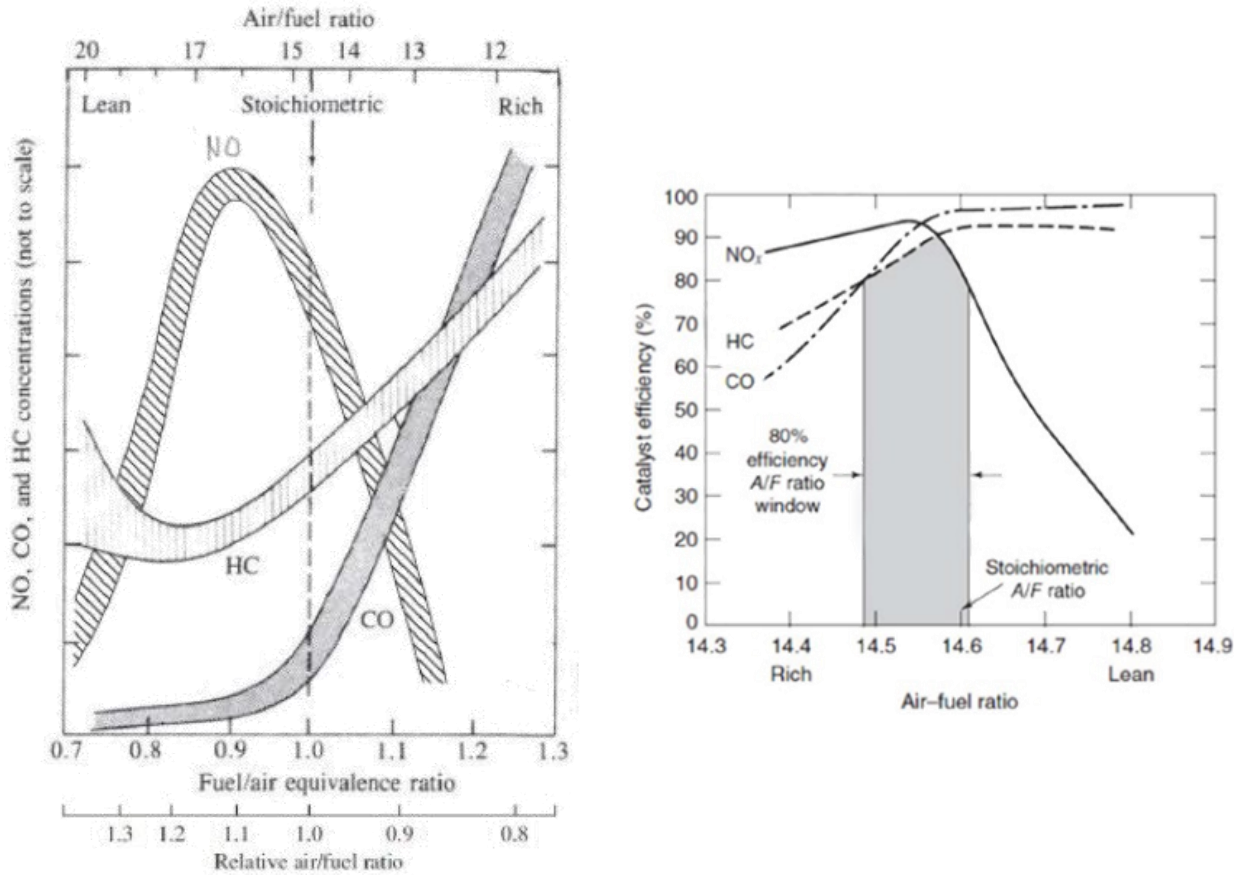


Figure 1-17 – Engine-out emissions function of  $\phi$  (left) TWC efficiency function of  $\alpha$  (right) [14]

Consequently, the TWC and GPF bricks of the baseline GSE-T4 powertrain were updated in geometry and formulation while others were added, such as SCR and NO-Ox. Table 1-2 shows a comparison in terms of After Treatment System (ATS) volume.

Component	Baseline Vol. [L]	PHOENICE Vol. [L]
EHC-TWC1 (CC)	0.82	1.5
GPF (CC)	1.4	2.5
NO-O <sub>x</sub> (UF)	N/A	1
SCR (UF)	N/A	2.5
ASC (UF)	N/A	2.5

Table 1-2 – Comparison between baseline and PHOENICE EATS components volume

Through an iterative process, the ATS was optimized, and the final layout, shown in *Figure 1-18*, was identified by Johnson Matthey.

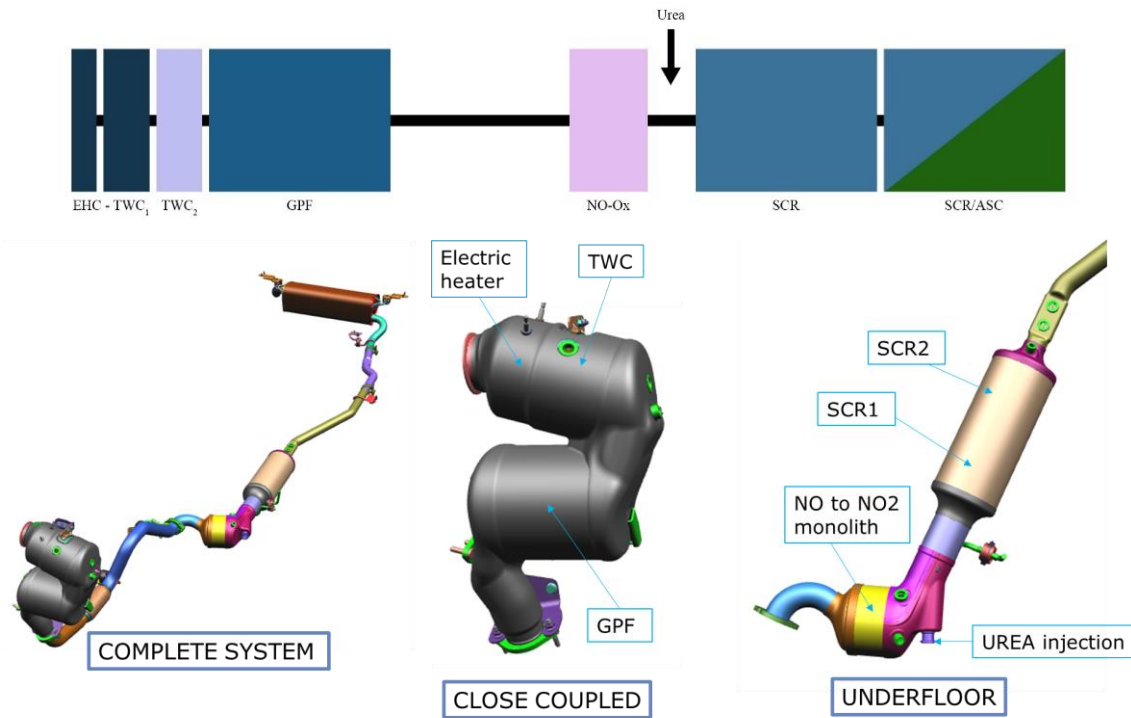


Figure 1-18 – PHOENICE EATS Layout

The system took advantage of the possibilities offered by the plug-in hybrid architecture. The Electrically Heated Three Way Catalyst (EHC-TWC) will use the vehicle's ability to start in EV mode to reach light-off temperature before the ICE is even started. While in EV mode, secondary air will be injected upstream of the EATS via the E-Turbo or an additional air pump to preheat the EHC and all the downstream components.

The Closed-Coupled Gasoline Particulate Filter (cc-GPF), in addition to its primary function of lowering Particulate Matter (PM) emission without excessive backpressure, is coated with TWC technology to reduce gaseous emissions further. Johnson Matthey utilized the latest technologies, specially developed for Euro 7 applications, to achieve this.

The underfloor section of the EATS comprises the lean NO<sub>x</sub> oxidation systems. The exhaust gasses first go through a NO-Oxidation catalyst (NO-Ox), which converts the engine-produced NO to NO<sub>2</sub> to increase the downstream Selective Reduction Catalyst (SCR) conversion efficiency. As a matter of fact, by increasing the NO<sub>2</sub>/NO ratio in the exhaust gas, the SCR conversion efficiency increases. Finally, the Ammonia Selective Catalyst (ASC) traps any ammonia (NH<sub>3</sub>) content that may slip through the SCR to the ambient environment due to excessive urea dosing, as a by-product of the TWC reactions or from the release of the stored NH<sub>3</sub> in the SCR due to a too high temperature.

While the underfloor position of the NO<sub>x</sub> after-treatment prevents its components from overheating and allows them to work within the ideal temperature range, this limits the minimum time to reach light-off temperature. Consequently, during a cold start, the engine will have to run under stoichiometric conditions and switch to lean mixtures once the SCR has reached the ideal temperature of about 200°C.

### 1.4.6 Waste Heat Recovery System (WHRS)

Regarding WHRS, two different technologies were considered to determine the best trade-off between vehicle overall efficiency and cost: Exhaust gas-to-coolant Heat Recovery System (EHRS) and Thermo-Electric Generator (TEG).

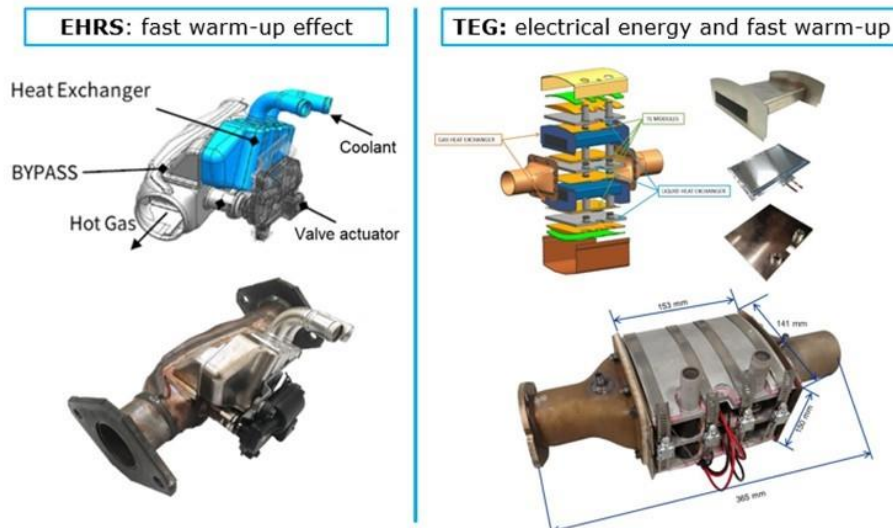


Figure 1-19 – Exhaust Heat Recovery System (EHRS) vs. Thermo-Electric Generator (TEG) [18]

EHRS can be employed to accelerate engine warm-up and enable a smart cabin heating strategy. The device consists of a Heat Exchanger (HE) and a bypass valve which, when closed, allows the exhaust gas to flow through the HE, transferring part of its thermal energy to the engine coolant for a faster warm-up with a consequent efficiency increase. On the other hand, when the ideal engine temperature is reached, the valve is opened, and the exhaust gas flow is stopped. The main con of this solution is the substantial occupied volume. TEG can provide additional power to the vehicle’s electrical network. In this multi-layer component, Thermoelectric Modules (TEMs) are sandwiched between HES in which exhaust gas flows (hot side) and HEs where coolant flows (cold side). The temperature difference between the two sides is converted into electric voltage via a thermocouple (Seebeck effect [19]). On top of the faster engine warm-up, like in the EHRS case, the low-voltage battery charge TEG can provide will ease the alternator’s work, lowering fuel consumption further. However, reliability and affordability are the most significant issues for this solution.

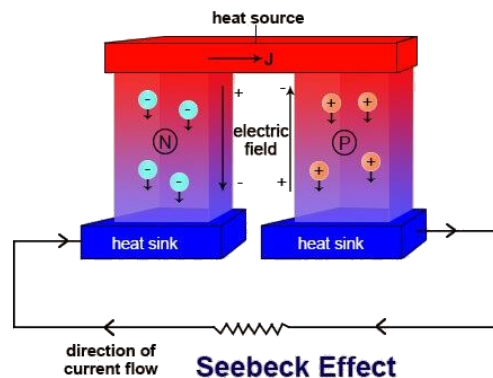


Figure 1-20 – Working principle of the Seebeck effect [19]

Both components were designed by Centro Ricerche Fiat (CRF), and their performances were evaluated on the test bench to select the optimal configuration. While EHRS is already adopted on some PHEVs and Full Hybrid EVs, TEG is not yet adopted on cars; At the time of writing, additional tests are still required to determine if and which system, or combination of the two, will be used in the final vehicle demonstrator.

## 1.5 Used Software

The primary computational tool utilized throughout this research activity is GT-Suite V2022. GT-POWER is the industry-leading multi-physics simulation tool with various applications that offer functionalities ranging from fast concept design to detailed system or subsystem/component analysis, including optimizations, DoE, and root cause investigations.

The primary suite software utilized was:

- GT-ISE, for the 1D-CFD model creation.
- GT-POST, for simulation results post-processing.
- SpaceClaim, for CAD geometries clean-up and generic pre-processing of step files.
- GEM 3D, for CAD geometries discretization into 1D elements, to be imported into the GT-ISE model.
- GT-Optimizer, to find the optimal parameter values to reach a given target.

The software license and the computational power were kindly provided by the e<sup>3</sup> – Engines, Energy, and Environment research group where this thesis was carried out.

Other note-worthy software is Microsoft Office Suite (especially Excel, Word, and PowerPoint) and MATLAB®. Moreover, Adobe Suite was used for the redacted thesis's aesthetic traits.



Figure 1-21 – Used Software icons

## 2 Model Development

### 2.1 CAD Discretization

The first step of developing the virtual test rig is to update the GSE-T4 flow lines to the PHOENICE ones. A precise representation of the flow lines ensures the highest accuracy for the model. In this chapter, the general discretization procedure will first be explained, and then each sub-assembly will be shown.

First, a brief explanation of the main GT-POWER 1D flow elements will be given in *Table 2-1*.

Template Name	Template Icon	Template Description
PipeRound		This template models a pipe with a round cross-section and an optional bend.
PipeRectangle		This template models a pipe with a rectangular cross-section and an optional bend.
FlowSplitGeneral		This template models any arbitrarily shaped flow volume. It often has more than 2 flow ports, and acts to split flow; however, it is not required.
CatalystBrick		This template represents a flow-through catalyst or a packed bed reactor.
OrificConn		This template models an orifice, defined by diameter or area and discharge coefficients, which calculates the mass flow rate between the adjacent flow volumes.
ActuatorConn		This template is a link between the control's library and the multi-physics library (i.e., flow, mechanical, thermal, etc.).
SensorConn		This template provides a control sensor link between "physical" (i.e., non-control) parts and control components parts.
SubAssExternalConn		This template is used in an external subassembly model to define the linking interface between parts in subassembly and the "main" model.
HeatExchangerConn		This template is specifically intended to be used to impose the gas temperature at a particular point in a flow system.
ReceiveSignal		This template allows a controls signal to be connected without a traditional link arrow on the map in the .gfm file.
RLTCreator		This template allows the user to create customized RLT variables when an RLT quantity is desired that is not available in the standard GT-SUITE software.
BoundaryPressure		This template describes boundary conditions of pressure, temperature, and fluid properties.
BoundaryFlow		This template represents a boundary condition that imposes flow through a specified mass flow rate, volume flow rate, velocity, or mass flux.

Table 2-1 – Principal 1D GT-POWER Templates

### 2.1.1 Discretization Work Procedure

The starting point of flow line discretization is the CAD geometries provided by the partner companies in either step or STL format. The procedure continued as follows:

1. These geometries were imported and pre-processed into GT-SpaceClaim to remove all the unnecessary components. Non-functional holes and openings were closed, and multi-piece components were merged into a single volume.
2. Pipes volumes were extracted starting from the inner surfaces, and possible overlaps between volumes were resolved by keeping the smaller one between the two. Additionally, the components were split into volumes, straight and single-bend pipes to ease the discretization process of the next steps.
3. The cleaned-up geometry was then imported into GEM3D, where the flow discretization was made. The discretization process divides a large volume assembly into smaller, connected ones. Each volume and pipe were parametrized accordingly as a Flowsplit or pipe element.
4. The discretized line was exported to GT-POWER and rearranged to look more organized and explicit. The model was finally saved as a sub-assembly model.

The flow chart in *Figure 2-1* can summarize the above procedure.



Figure 2-1 - Flow lines discretization procedure flowchart

### 2.1.2 Low-Pressure Intake Line

The first of five sub-assemblies that were updated is the low-pressure intake line. This sub-assembly comprises the ambient air intake, the airbox with its filter, the EGR throttle, which ensures the required pressure difference at high EGR rates, and the compressor inlet.

1. The CAD geometry was imported to SpaceClaim for clean-up (*Figure 2-2*), the unnecessary holes were patched (*Figure 2-3*), and the multi-piece airbox was merged into one.

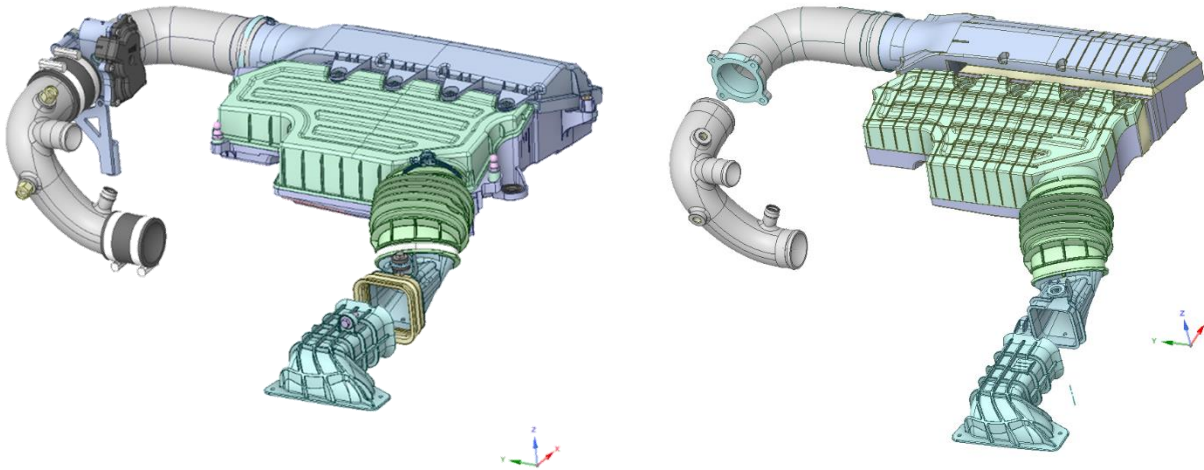


Figure 2-2 – Low-Pressure Intake Line CAD geometry: before clean-up (left) and after (right)

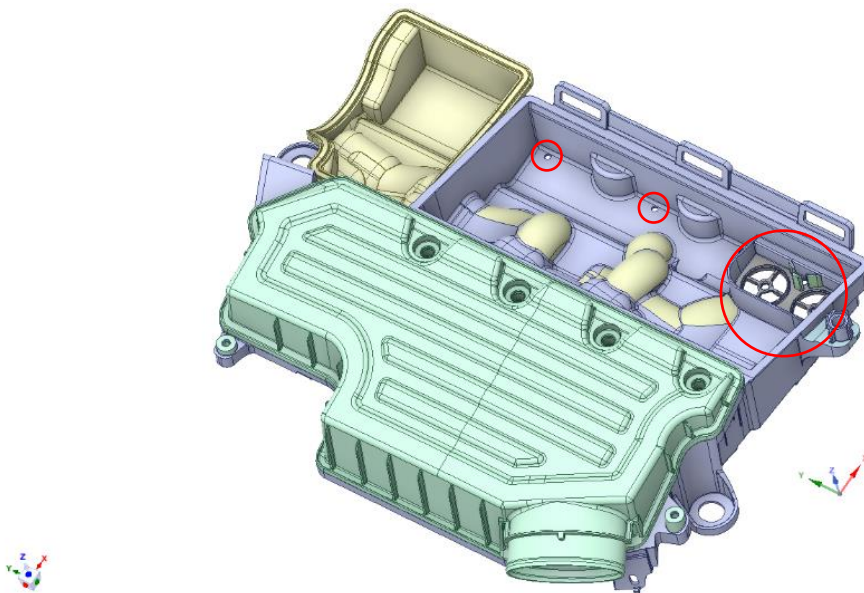


Figure 2-3 – Low-Pressure Intake Line Airbox holes

2. Volumes were extracted and overlaps removed (Figure 2-4).

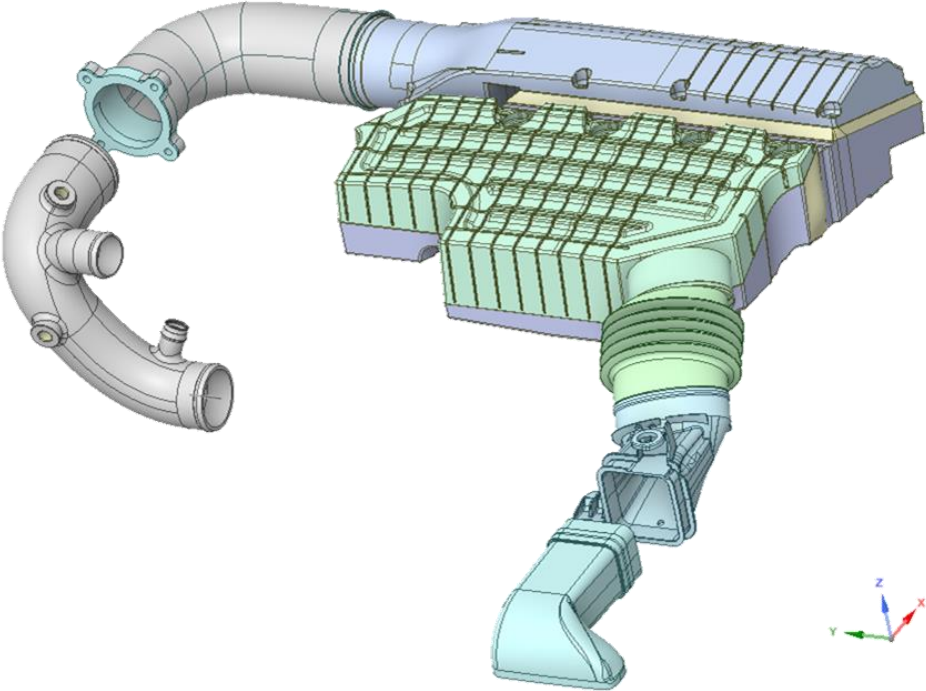


Figure 2-4 – Low-Pressure Intake Line Final Cleaned-up Geometry

3. The cleaned-up geometry was imported into GEM3D, and the various components were discretized (Figure 2-5).

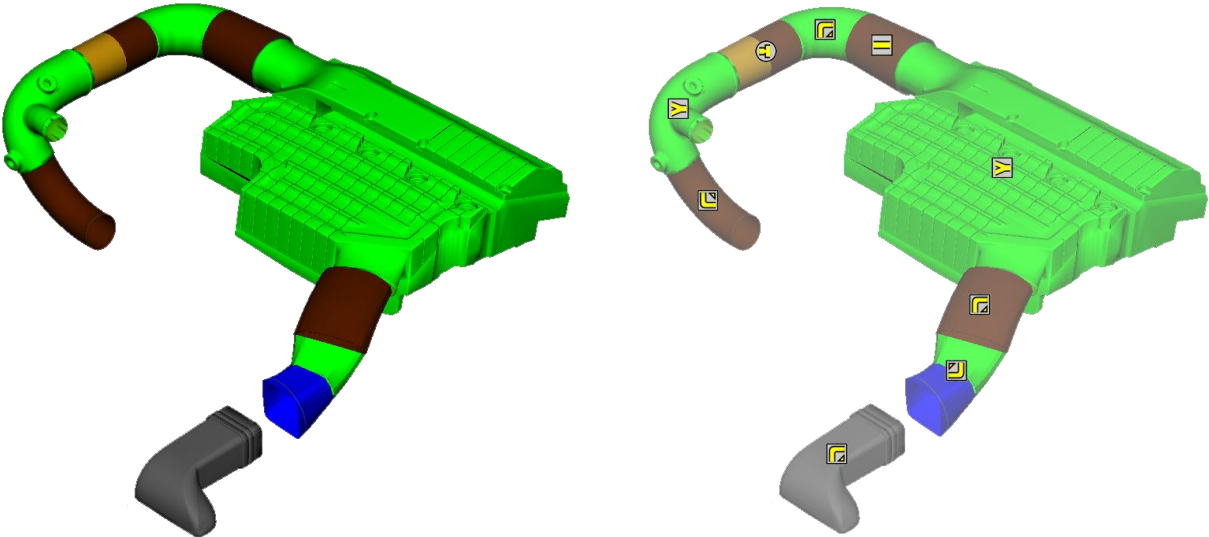


Figure 2-5 - Low-Pressure Intake Line GEM3D Discretization



### 2.1.3 Intake Manifold

The intake manifold, or high-pressure intake line, was the following sub-assembly. It includes the pipeline from the compressor outlet and the WCAC intake manifold.

1. The CAD geometry was imported to SpaceClaim for clean-up (*Figure 2-7*).

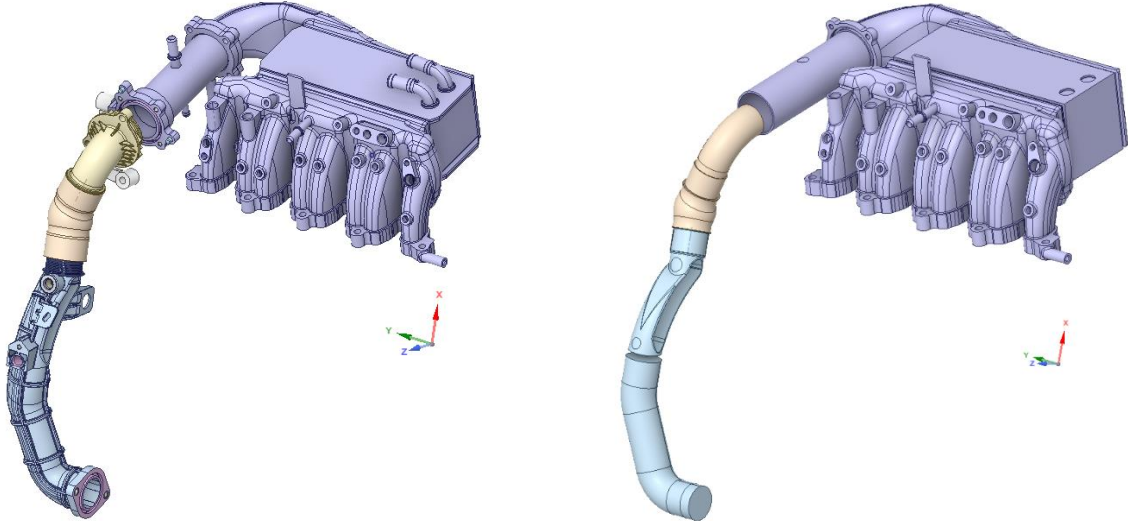


Figure 2-7 – High-Pressure Intake Line CAD geometry: before clean-up (left) and after (right)

2. Volumes were extracted and overlaps removed (*Figure 2-8*).

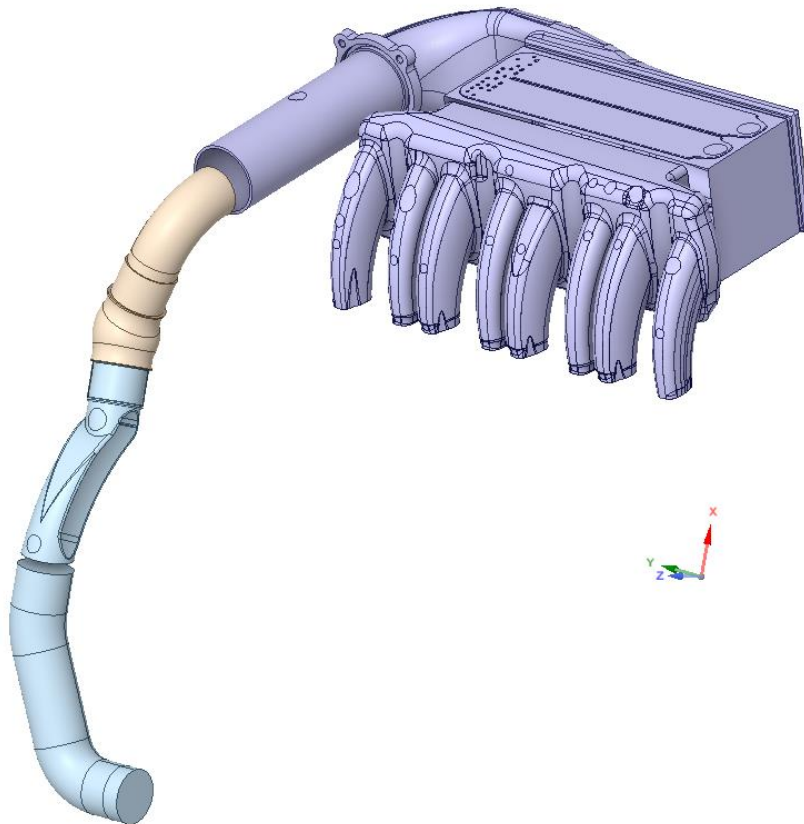


Figure 2-8 – High-Pressure Intake Line Final Cleaned-up Geometry

- The cleaned-up geometry was imported into GEM3D, and the various components were discretized (*Figure 2-9*).

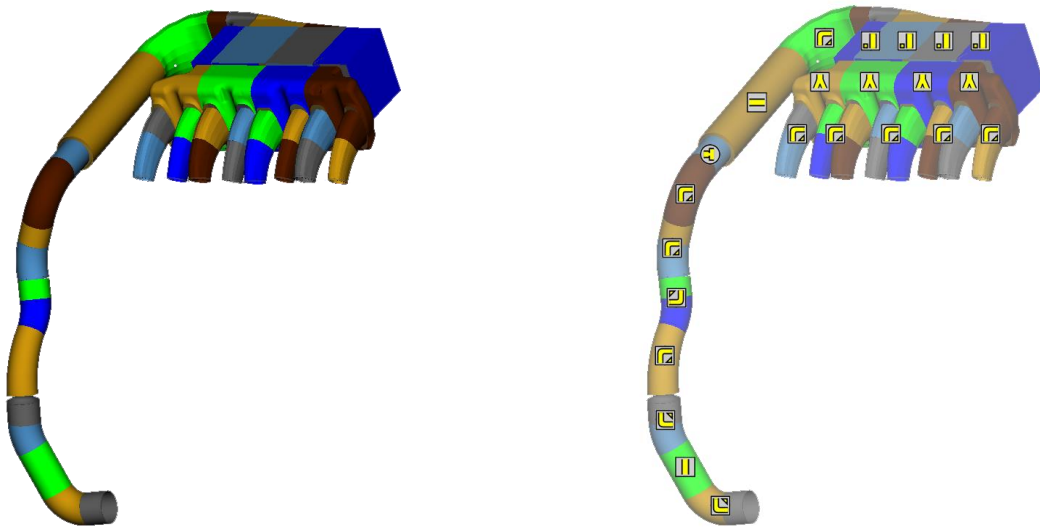


Figure 2-9 - High-Pressure Intake Line GEM3D Discretization

- Finally, the discretized line was exported to GT-POWER (*Figure 2-10*).

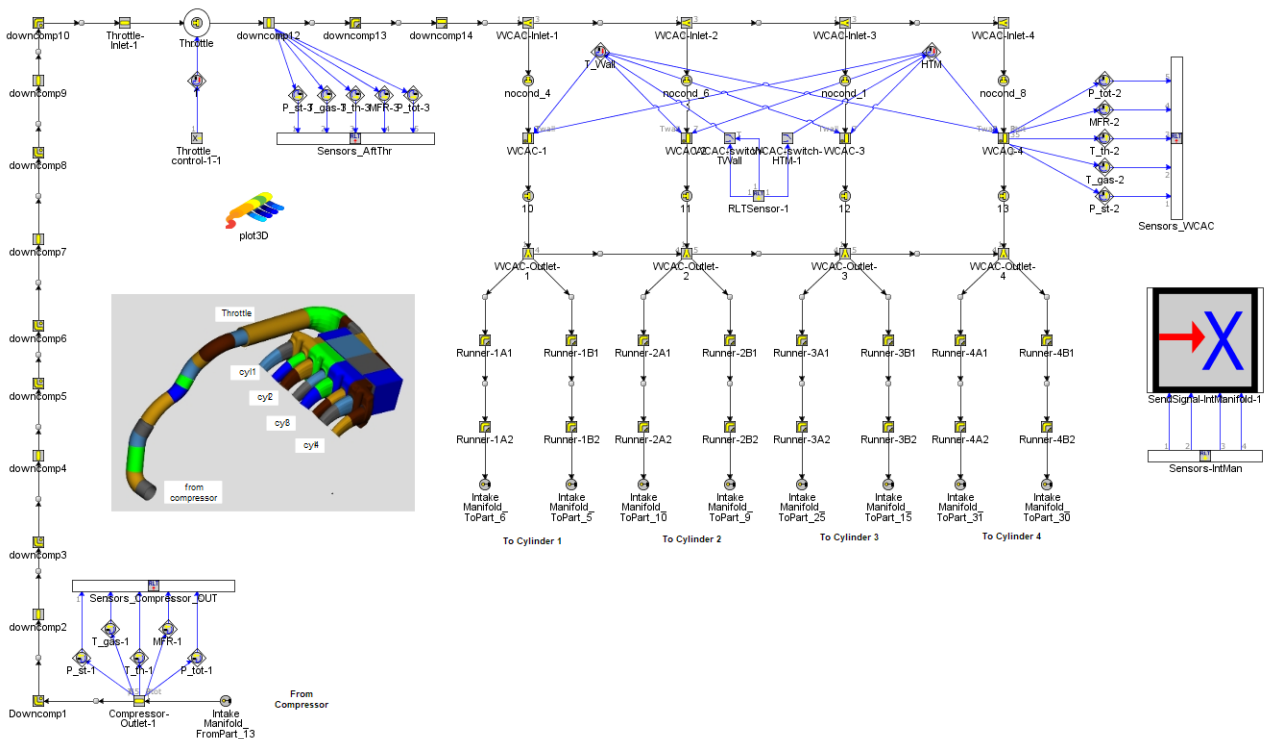


Figure 2-10 – High- Pressure Intake Line GT-POWER sub-assembly model

Note that in *Figure 2-10*, some extra elements with respect to the discretization are present, such as three sets of sensors, one signal receiver used to control the engine throttle, and the WCAC outlet temperature control logic, which imposes a given temperature at the exit of the cooler.

### 2.1.4 Exhaust Line

To fit the new EATS, the exhaust line geometry was revolutionized. Starting from the turbine outlet, the closed-coupled bricks are characterized by the typical telephone junction. Following the pipeline, the NO-Ox and SCR+ASC combo and the final TEG brick can be seen. Finally, the exhaust muffler and tailpipes are represented. It is worth noting that while the TEG was part of the provided geometry, the decision on which WHRS to use still needed to be made. Nevertheless, the system was included in the model as a straight pipe to, on the one hand, ease the transition to the brick model if TEG is confirmed and, on the other hand, not affect the flow pressure drops.

1. The CAD geometry was imported to SpaceClaim for clean-up (*Figure 2-11*).

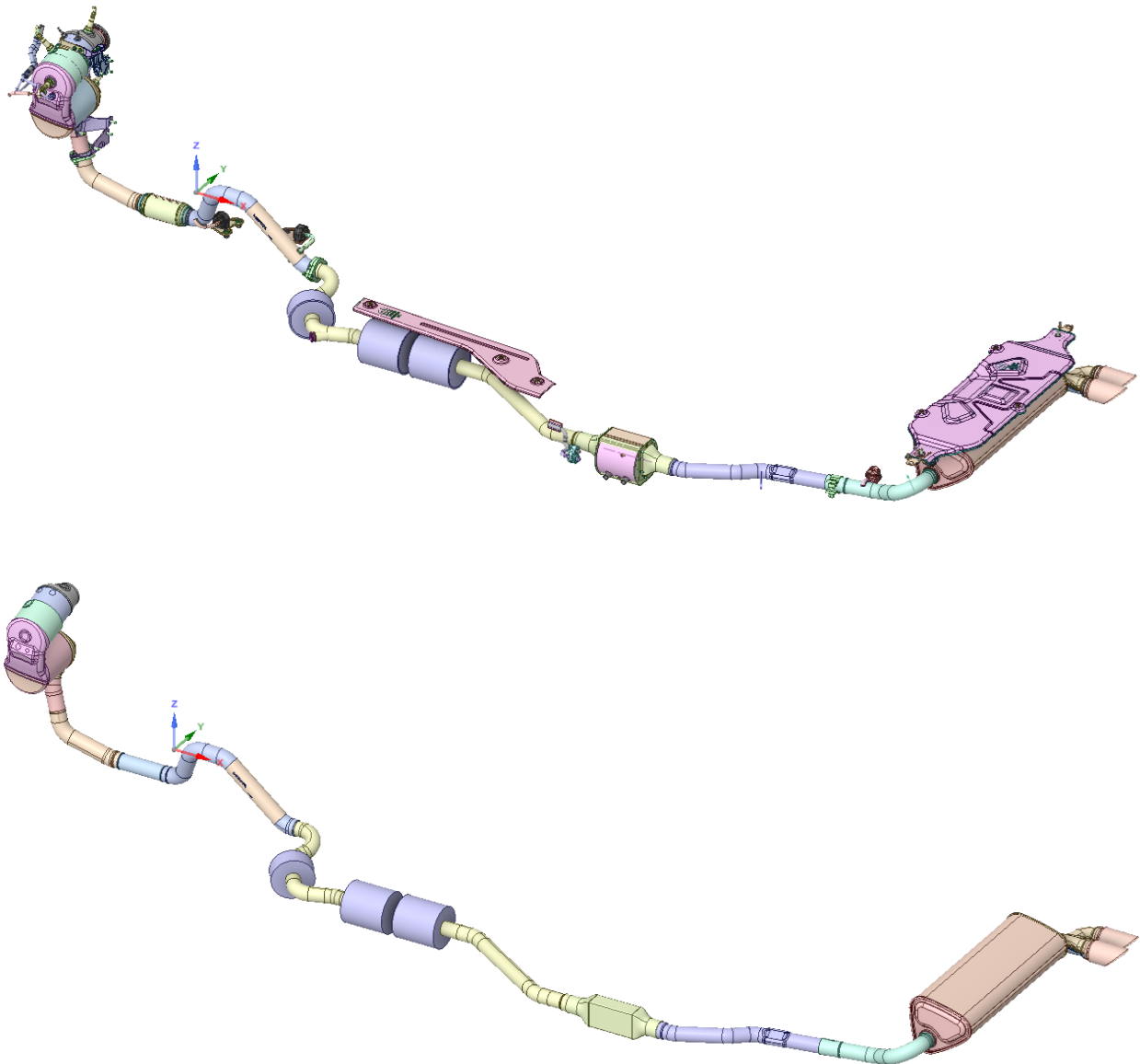


Figure 2-11 – Exhaust Line CAD geometry: before clean-up (left) and after (right)

2. Volumes were extracted and overlaps removed (*Figure 2-12*).

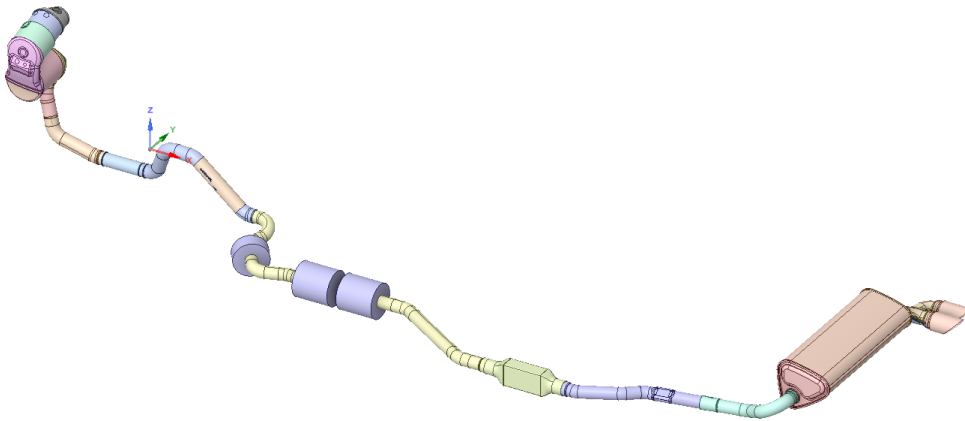


Figure 2-12 – Exhaust Line Final Cleaned-up Geometry

3. The cleaned-up geometry was imported into GEM3D, and the various components were discretized (*Figure 2-13*). Note that the components downstream of the TEG were not discretized because they were not changed from the original GSE-T4. Thus, their discretization was taken from the original Stellantis model.

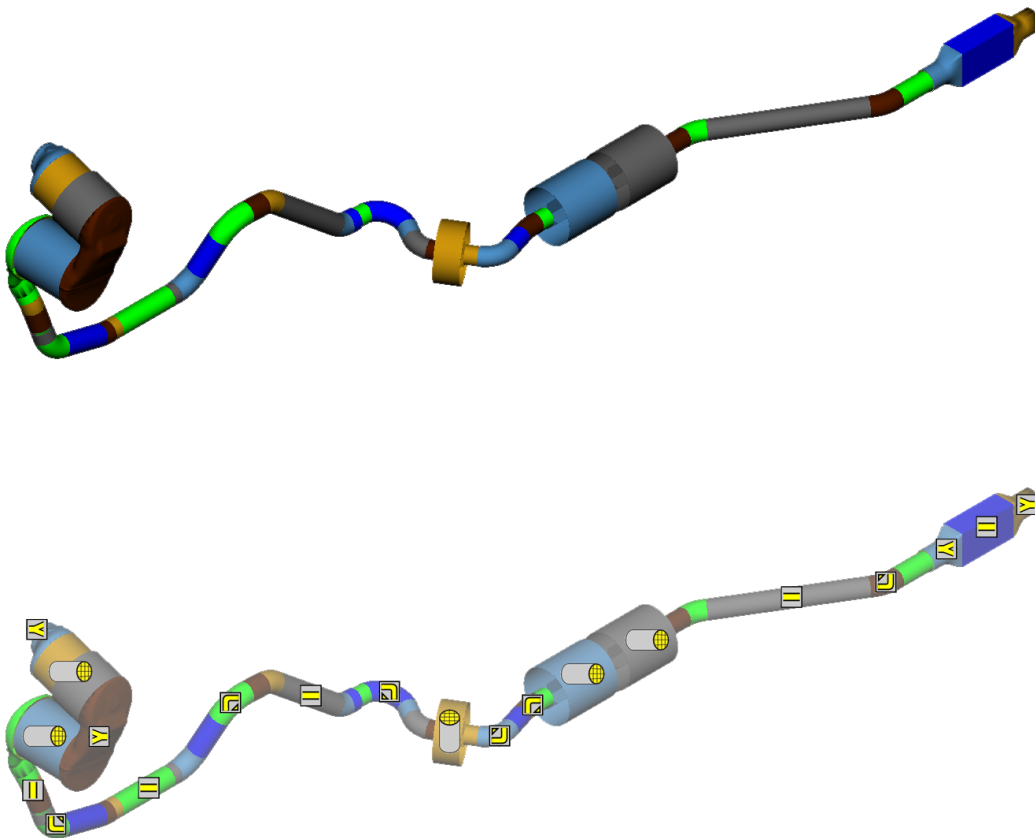


Figure 2-13 – Exhaust Line GEM3D Discretization

4. Finally, the discretized geometry was exported to GT-POWER (*Figure 2-14*).

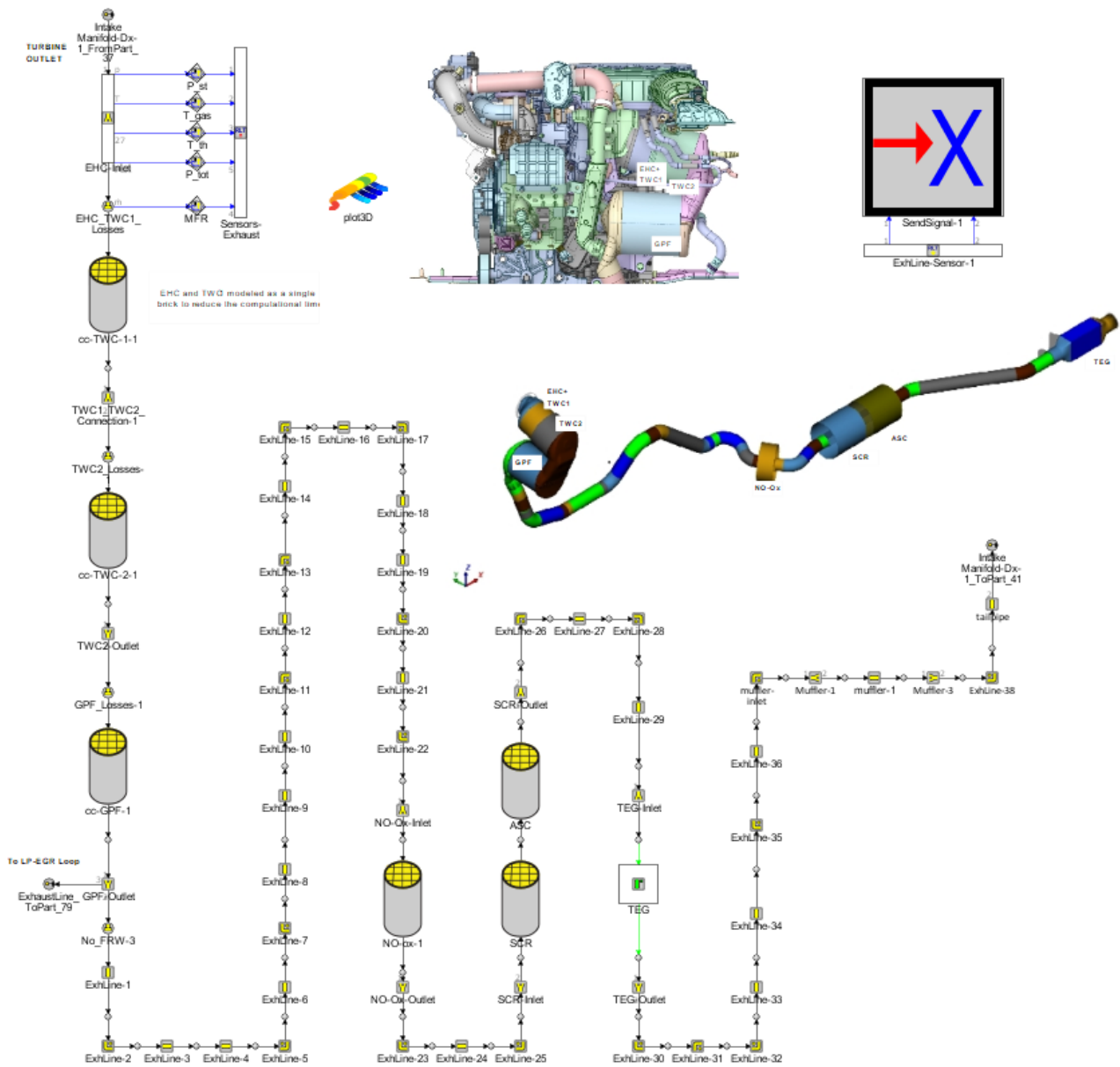


Figure 2-14 – Exhaust Line GT-POWER sub-assembly model

Note that in *Figure 2-14*, some extra elements with respect to the discretization are present, such as one set of sensors at the turbine outlet and one SendSignal to controllers. As previously explained in *Chapter 2.1.4*, note that TEG is colored in green to indicate that it is not definitive.

### 2.1.5 EGR Loop

The EGR loop is the only flow line under analysis that is not an update. The original GSE-T4 did not employ an EGR line; it is thus a PHOENICE exclusive. The circuit is composed of the loop inlet, which receives a part of the exhaust gasses from after the closed-coupled GPF, the EGR Cooler (EGRC), the EGR valve, which regulates the delivered amount of EGR, and, finally, the loop outlet connected to the low-pressure intake line upstream the compressor.

1. The CAD geometry was imported into SpaceClaim for clean-up and hole patching (*Figure 2-15*).

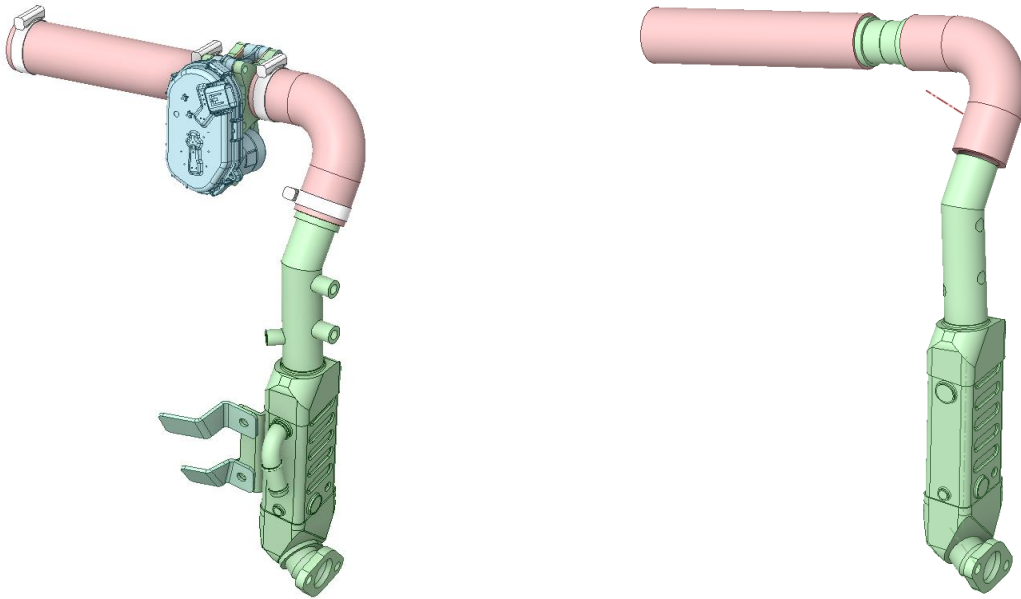


Figure 2-15 – EGR Loop CAD geometry: before clean-up (left) and after (right)

2. Volumes were extracted, and the overlaps were resolved (*Figure 2-16*).

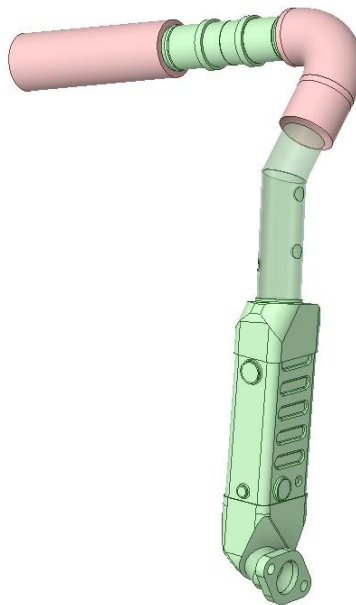


Figure 2-16 – EGR Loop Final Cleaned-up Geometry

3. Once imported into GEM3D, the various components were discretized (*Figure 2-17*).

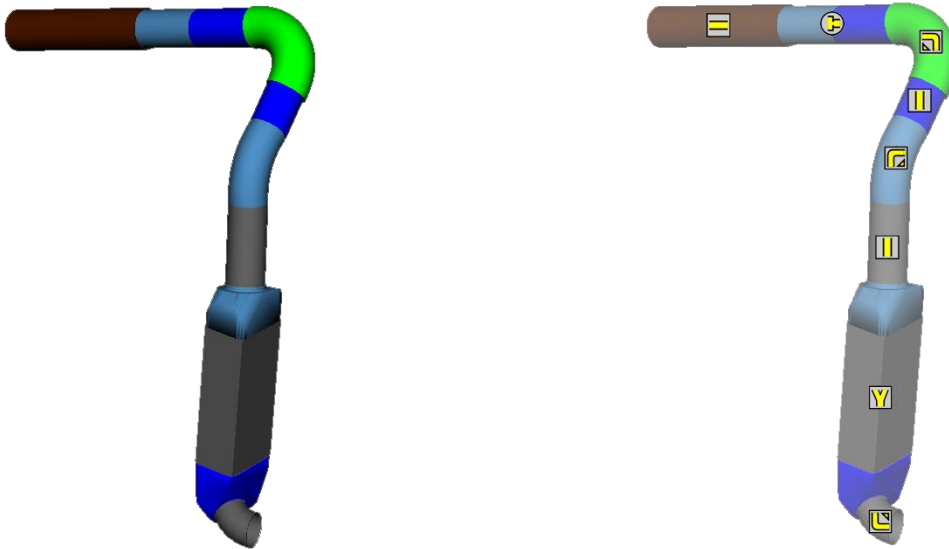


Figure 2-17 – EGR Loop GEM3D Discretization

4. Finally, the discretized line was exported to GT-Power (*Figure 2-18*).

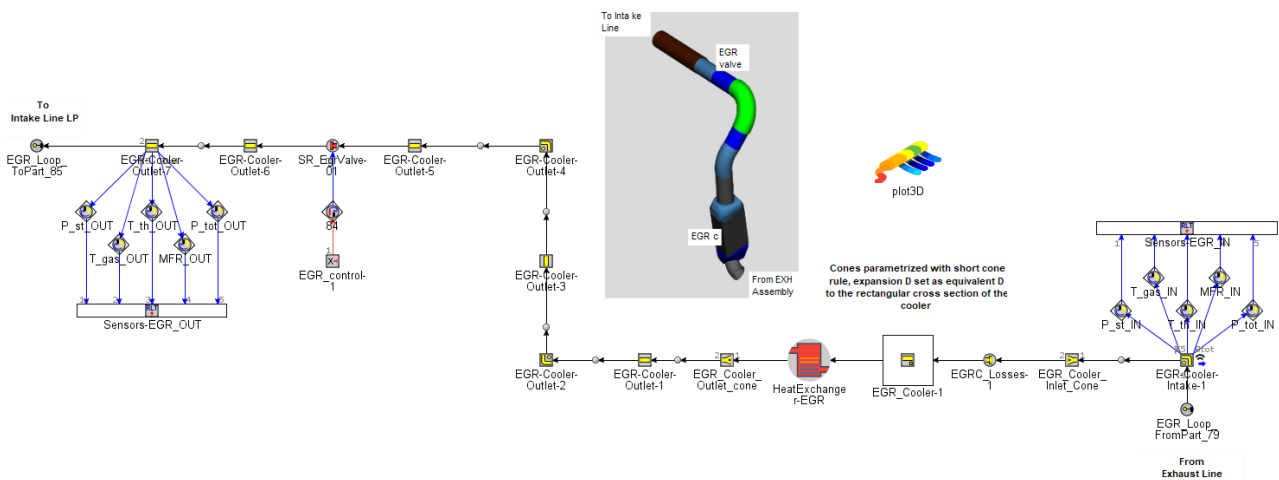


Figure 2-18 – EGR Loop GT-POWER sub-assembly model

Note that in *Figure 2-18*, some extra elements with respect to the discretization are present, such as two sets of sensors, one signal receiver used to control the EGR valve, and the EGRC outlet temperature control, which imposes a given temperature at the exit of the cooler.

### 2.1.6 Intake and Exhaust Conduits

Finally, the intake and exhaust ports' geometries were updated to represent the new cylinder head design. The same procedure was followed except that, as no clean-up was needed, the STL geometry was imported directly into GEM3D for discretization.

1. No clean-up was needed for this component (*Figure 2-19*).

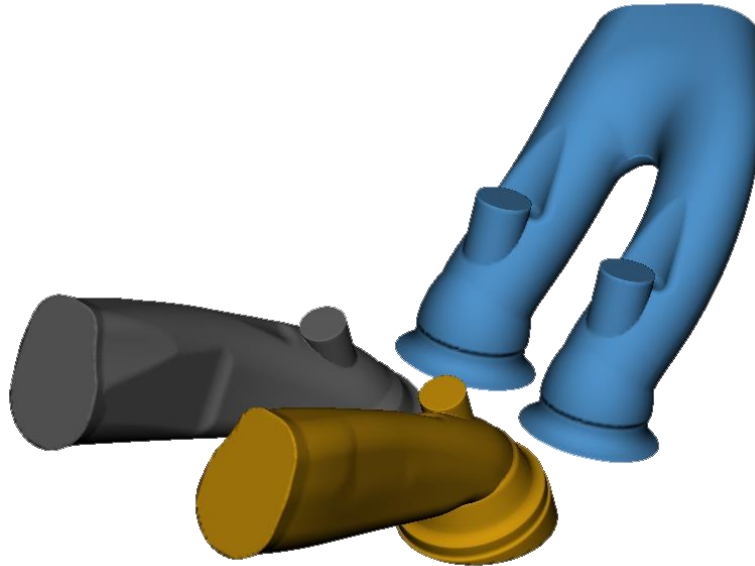


Figure 2-19 – Conduits CAD geometry

2. The CAD geometry was directly imported into GEM3D for flow discretization (*Figure 2-20*).

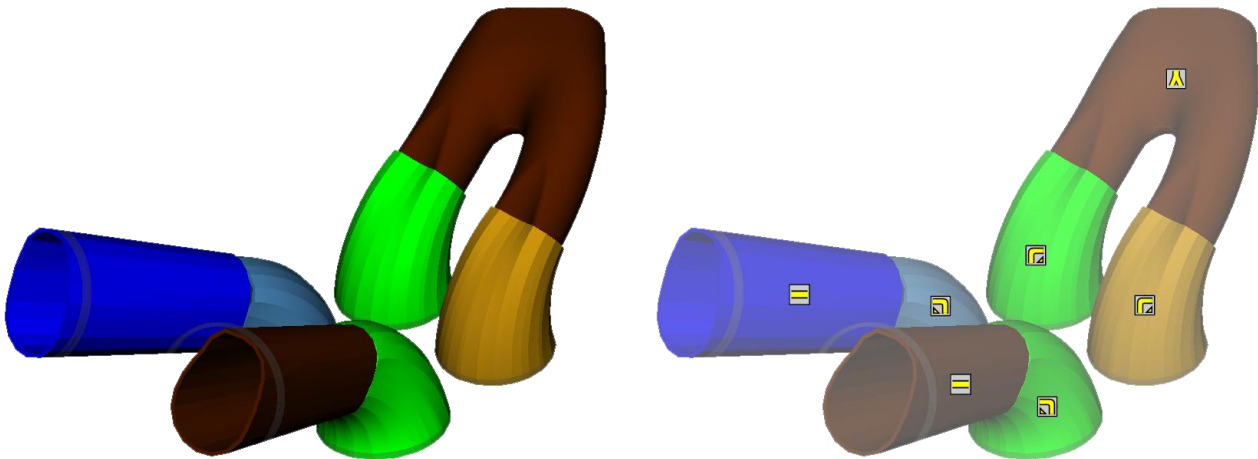


Figure 2-20 – Conduits GEM3D Discretization

3. Finally, the discretized line was exported to GT-POWER (*Figure 2-21*).

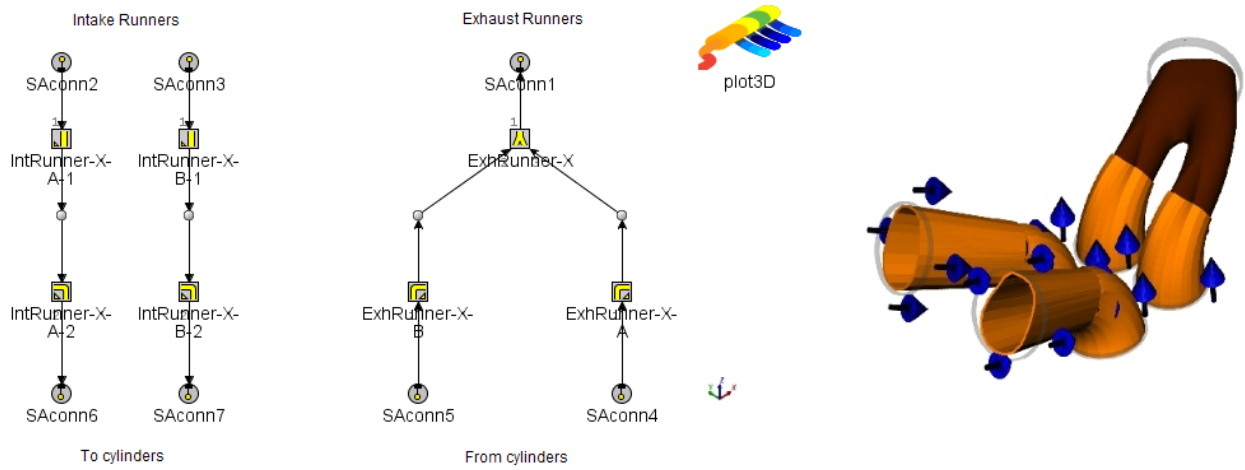


Figure 2-21 – Conduits GT-POWER sub-assembly model

Note that, as all cylinders have the same runner's geometry, in *Figure 2-21*, only one set of ports is represented.

## 2.2 Engine Model Updates

Alongside the new CAD geometries, other data was provided to update the existing GSE-T4 GT-POWER model. Indeed, the existing turbo model must be updated to the Garrett E-Turbo, and the intake valves must be changed to account for the new Swumble™ effect. Moreover, the combustion model must consider the new piston and head design. This chapter will focus on the upgrade of such parts of the model.

### 2.2.1 Garrett E-Turbo & Efficiency Map

Regarding the GT-POWER turbo model, the primary thing to change is the geometric details and the operating maps of both the turbine and compressor wheels. The model templates remain unchanged. Both a VNT and a WG turbo use the same Turbine template library.

Other than geometrical differences, from a model point of view, the only difference between the two turbocharger models is the MotorGeneratorMap template, which must be used in the e-turbo model to account for energy regeneration and, if needed, e-turbo boost.

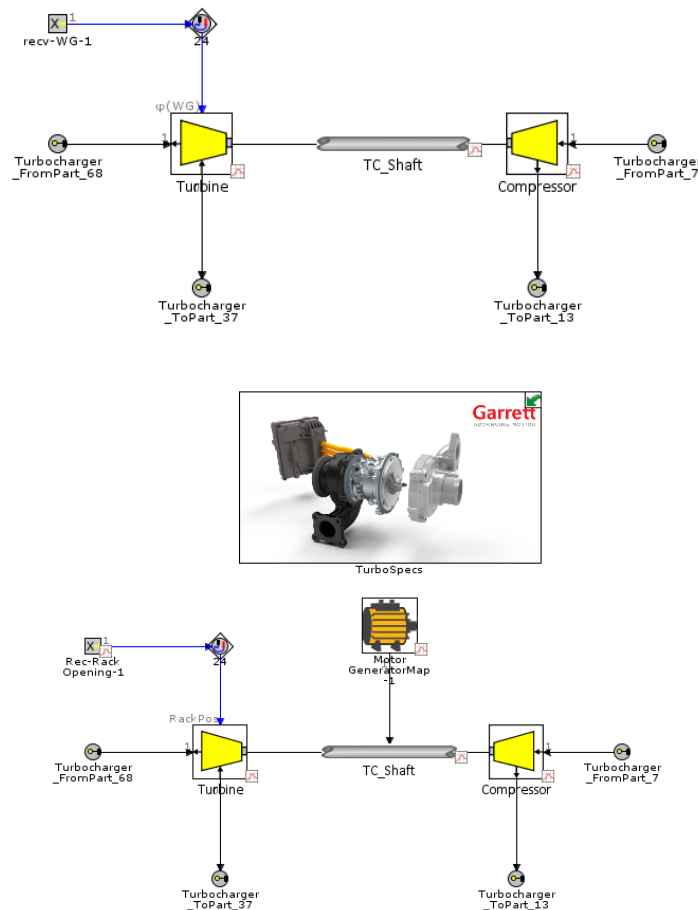


Figure 2-22 – Baseline GSE-T4 Turbocharger model (above) vs. PHOENICE E-Turbo (bottom)

It is worth noting how *Figure 2-22* shows the different control strategies needed for the two turbines. In the baseline turbo, the receive signal, alongside the actuator connection in the top left part of the image, forces a value of WG diameter, whereas, in the PHOENICE case, it forces a certain rack position. While the efficiency map is fixed for the baseline turbo, the e-turbo has a map for each rack position.

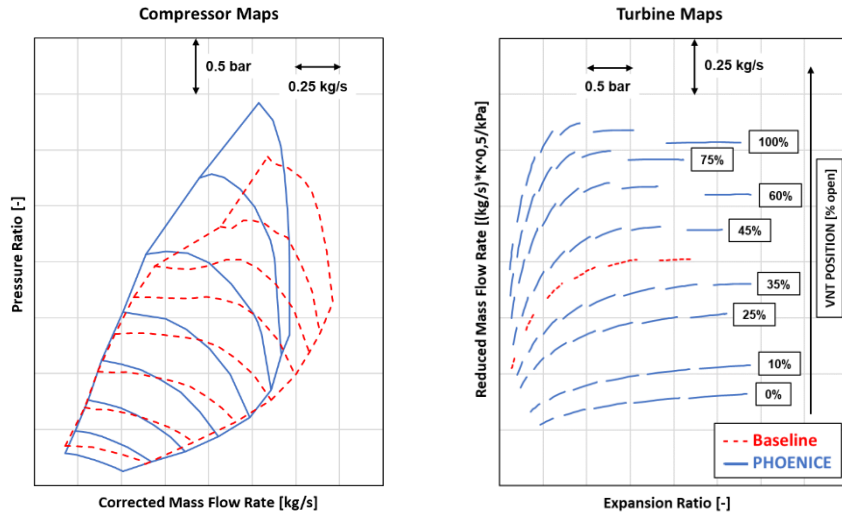


Figure 2-23 – Compressor and Turbine Maps: GSE-T4 vs. PHOENICE

To set up the MotorGeneratorMap, only a few variables are needed, shown in *Figure 2-24*, such as the electromechanical conversion efficiency, which can be either a fixed value or an operating map, and the minimum and maximum torque curves.

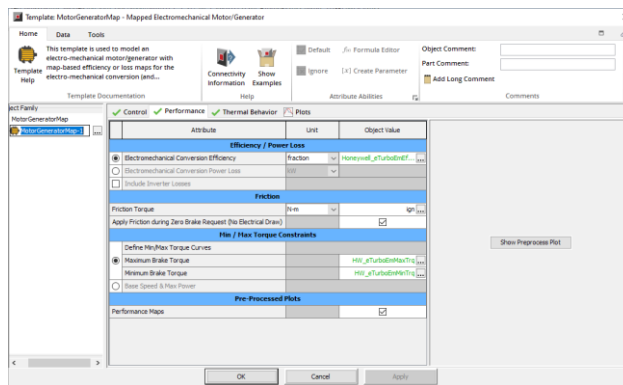


Figure 2-24 – MotorGeneratorMap GT-POWER Template

All this data was provided by the partner company Garrett Motion and was directly linked to an Excel spreadsheet to ease any future efficiency updates.

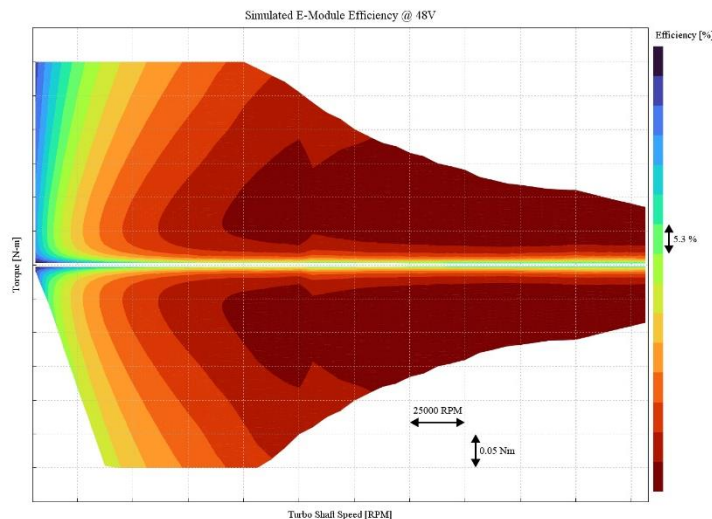


Figure 2-25 – Electric Motor Efficiency Map as a Function of Torque and Rotational Speed

### 2.2.2 Intake Valves Flow and Turbulence Coefficients

In GT-POWER, valve elements require that flow Discharge Coefficients ( $C_D$ ) are entered for both directions.  $C_D$  is defined as the ratio of the effective flow area to the reference flow area, originating from the isentropic velocity equation for a flow through an orifice [20].

A high degree of accuracy over these parameters is required as they account for friction losses and errors in the velocity profile of the orifice equation.

An experimental flow measurement is required to evaluate a gas's discharge coefficients.  $C_D$  is defined as:

$$\dot{m} = A_{eff}\rho_{is}U_{is} = C_D A_R \rho_{is} U_{is} \rightarrow C_D = \frac{\dot{m}}{A_R \rho_{is} U_{is}}$$

Where,

$$\rho_{is} = \rho_0 (P_r)^{1/\gamma}$$

And,

$$U_{is} = \sqrt{RT_0} \left\{ \frac{2\gamma}{\gamma-1} \left[ 1 - P_r^{\frac{\gamma-1}{\gamma}} \right] \right\}^{\frac{1}{2}}$$

$\dot{m}$  = mass flow rate

$A_{eff}$  = effective flow area

$\rho_{is}$  = density at the throat

$\rho_0$  = upstream stagnation density

$U_{is}$  = isentropic velocity at the throat

$C_D$  = discharge coefficient

$A_R$  = reference flow area

$P_r$  = absolute pressure ratio

$R$  = gas constant

$T_0$  = upstream stagnation temperature

$\gamma$  = specific heat ratio (1.4 for air at 300°C)

For cam-driven valves, the value of  $A_R$  can be computed in two ways. The first one, which is the one used in the PHOENICE model, keeps the value of  $A_R$  constant for all Lift over Diameter (L/D) values.

$$A_R^1 = \frac{\pi}{4} \cdot d_{ref}^2$$

The second one, on the other hand, evaluated  $A_R$  uniquely for each lift position in the L/D array as the valve curtain area:

$$A_R^2 = \pi \cdot d_{ref} \cdot L$$

The difference between the two methods is the initial value of the  $C_D$  array. When using the first method, the first value of the  $C_D$  array must be zero, whereas, with the second, it must be a non-zero value.

While GT-POWER provides an excel sheet to compute the  $C_D$  from experimental flow data, in this research activity, the  $C_D$  array was directly provided by IFPEN. Thus a simple import was sufficient.

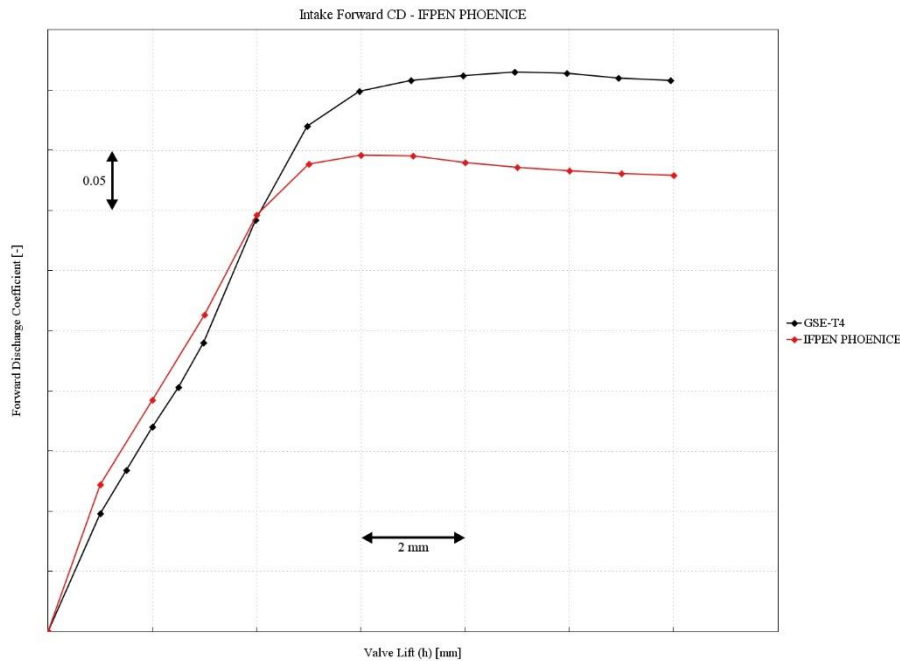


Figure 2-26 – Intake Valves Forward Discharge Coefficient PHOENICE vs. GSE-T4

It is worth noting that *Figure 2-26* shows forward coefficients only as the reverse coefficients are assumed equal to the forward ones since no information was provided. Moreover, only the  $C_{DS}$  of the intake valves were to be changed as the exhaust side was unchanged in the PHOENICE engine.

Finally, one could argue that PHOENICE has higher losses with respect to the baseline GSE-T4 since the  $C_D$ s are lower. This is correct as with increasing swirl and tumble, as a consequence of Swumble™, a higher degree of losses is to be expected.

A similar procedure is applied to evaluate the intake valves' swirl and tumble coefficients ( $C_s$  and  $C_t$ ). Swirl and tumble coefficients are used to calculate the swirl and tumble torque applied to the in-cylinder gasses and can be defined as the ratio of the angular momentum flux to the linear momentum flux [21]. The greater the coefficients, the greater the swirl and tumble level through the valve.

They are evaluated as follows:

$$C_s = \frac{2T}{\dot{m}U_{is}B} \text{ and } C_t = \frac{2T}{m\dot{U}_{is}B}$$

$T$  = torque

$\dot{m}$  = mass flow rate

$U_{is}$  = isentropic valve velocity

$B$  = cylinder bore

$P_R$  = absolute pressure ratio

$R$  = gas constant

$T_0$  = upstream stagnation temperature

$\gamma$  = specific heat ratio (1.4 for air at 300°C)

Differently from  $C_D$ ,  $C_s$  and  $C_t$  can be negative, affecting the swirl and tumble motion direction. However, as swirl and tumble coefficients are defined as the fraction of linear flow that is converted into angular motion, the following constraint is valid:

$$|C_s| + |C_t| \leq 1$$

As for the  $C_D$ , data regarding  $C_t$  was directly provided by IFPEN.

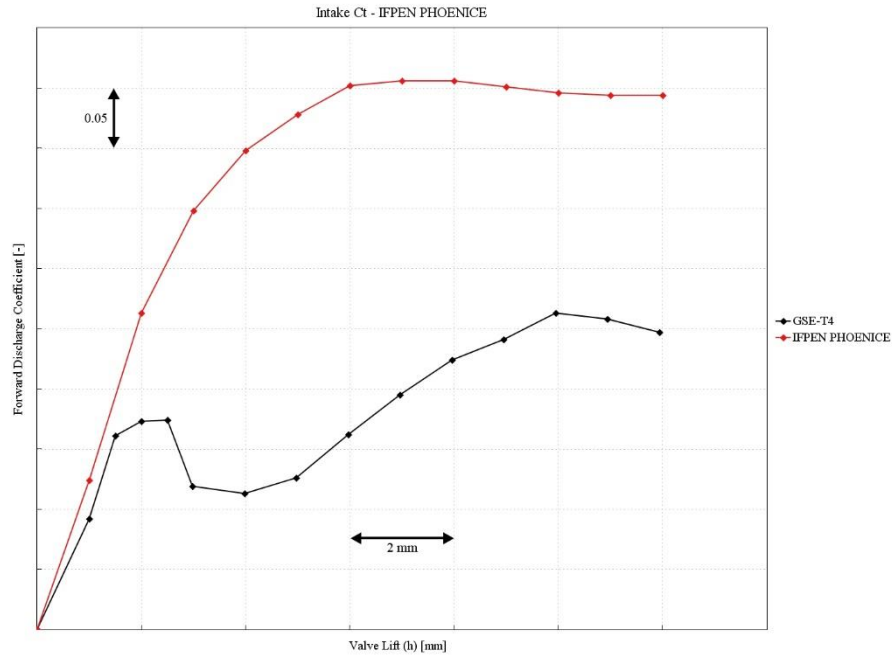


Figure 2-27 – Intake Valves Tumble Coefficient PHOENICE vs. GSE-T4

It is worth noting how different the two curves in *Figure 2-27* are. However, it is plausible that to evaluate the tumble coefficients, Stellantis has used a different approach with respect to the one covered in this thesis (i.e., paddle wheel measurements <sup>[21]</sup> or others). When IFPEN simulated the  $C_D$  and  $C_t$  of the original GSE-T4 engine, blue curves in *Figure 2-28*, similar results emerged in terms of  $C_D$  between the Stellantis and the IFPEN simulation. On the other hand, the  $C_t$  resembled the PHOENICE simulation ones closer.

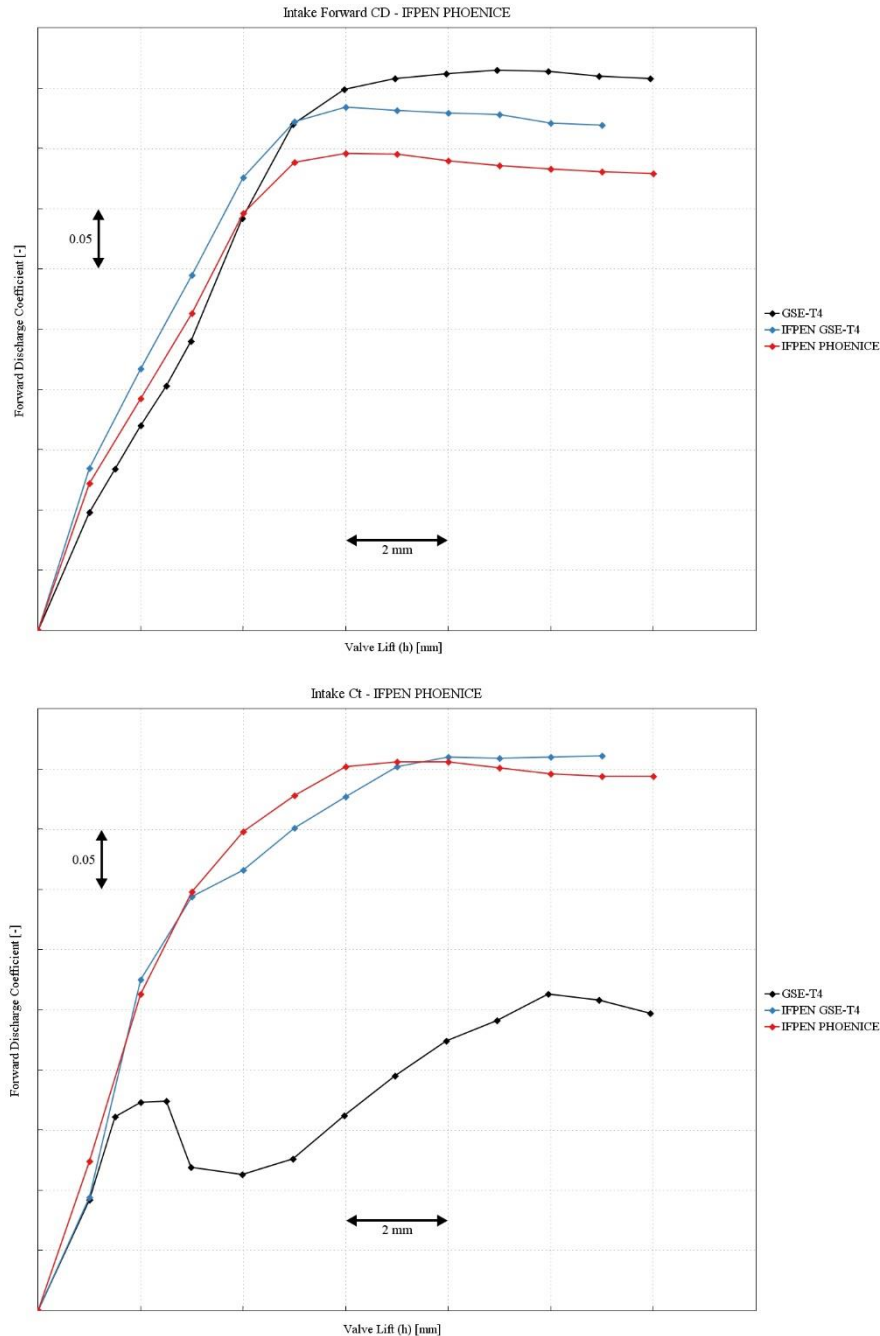


Figure 2-28 –  $C_D$  and  $C_t$  Coefficients: GSE-T4 vs. IFPEN GSE-T4 vs. IFPEN PHOENICE

For this reason, the original GSE-T4 tumble coefficients were temporarily imported into the model.

Moreover, no information was available regarding the swirl level, thus the attribute was temporarily left blank. Both issues will eventually need to be fixed once the data is available.

### 2.2.3 Combustion Chamber Geometry

Finally, the combustion chamber must be updated. An optimization of the combustion chamber geometry was performed by IFPEN to increase the Compression Ratio (CR) to 13.6 with a consequent increase in thermodynamic efficiency. The optimization process results are the piston shown in *Figure 2-29* and the cylinder head whose piston-side surface is shown in *Figure 2-30*.



Figure 2-29 – PHOENICE new piston design with CR 13.6



Figure 2-30 – PHOENICE new cylinder head design

These STL geometries are needed in the combustion model to correctly predict how the flame front will evolve during the combustion.

To model the combustion in GT-POWER, two prominent families of templates are available: predictive and non-predictive models. Non-predictive models work on the basis of an imposed burn rate, thus requiring experimental combustion data for every conducted test. Moreover, as the burn rate is fixed, it is independent of any engine parameter and can thus reduce the computational time. Predictive models, on the other hand, require experimental measurements only for the initial model correlation. Once tuned, the model can self-adjust for transient conditions and provide more detailed outputs, such as information on  $\text{NO}_x$ , knock, and heat transfers.

In this research activity, both combustion models will be used, indeed *Chapter 5.2* and *Chapter 5.3* will deal with non-predictive combustion, whereas *Chapter 5.4* will go through the tuning procedure of a predictive combustion model, which is required to use the digital twin as a virtual test rig. The respective chapters will explain the combustion models used in more in-depth. For now, the combustion template present in the model is of the predictive family and is called EngCylCombSITurb. This model, alongside the knock and in-cylinder flow model, was derived from a previously calibrated modified GSE-T3 engine research activity. Although these models are not tuned for the PHOENICE application, the modified engine had a similar compression ratio and, as discussed in *Chapter 1.3*, similar characteristics to the larger GSE-T4, thus making the derived models an acceptable approximation for preliminary analysis.



### 3 Model Calibration

#### 3.1 Aftertreatment Bricks Calibration

The EATS bricks will now be included in the exhaust flow line discretized in *Chapter 2.1.4*. Johnson Matthey gave the geometry of each component alongside experimental results on the pressured drop of each one. The following chapter describes the modelization and tuning of the brick components.

##### 3.1.1 Calibration Procedure

Aftertreatment systems can be divided into two primary families: through flow and cross flow. Throughflow bricks are characterized by many small parallel catalyst-coated channels in which exhaust gas flows from one side of the brick to the other. They are typically more efficient due to the longer contact time and lower back pressure. Aftertreatment systems such as TWC, SCR, Diesel Oxidation Catalyst (DOC), and Lean NO<sub>x</sub> Trap (LNT), are all of the through type.

Crossflow bricks, on the other hand, are designed so that the exhaust gas flows perpendicularly with respect to the brick's longitudinal axis, passing through porous channels that run parallel to the length of the brick. As a matter of fact, the exhaust gasses enter from one side and, following the back-and-forth path inside the brick, exit on the other side. Gasoline Particulate Filters (GPF) and Diesel Particulate Filters (DPF) are of this second kind as, when the gasses flow from one channel to the other, the Particulate Mass (PM) gets stuck on the porous wall.

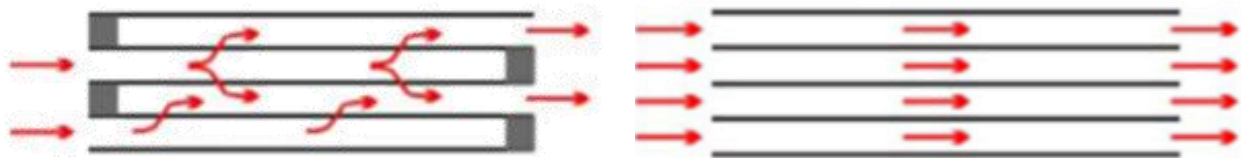


Figure 3-1 – Crossflow brick (left) vs. Throughflow brick (right)

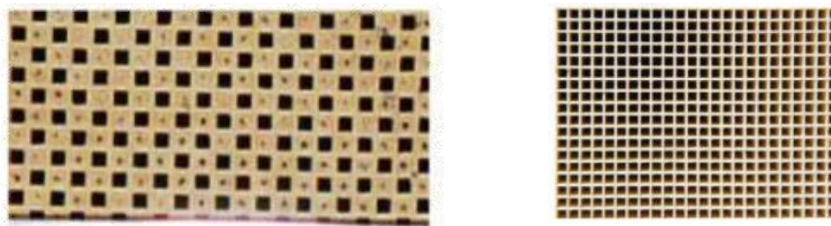


Figure 3-2 – Crossflow brick cross-section (left) vs. Throughflow brick cross-section (right)

In GT-POWER, on the other hand, the difference between the two model templates is more complicated. As a matter of fact, the ParticulateFilter template requires a lot more information to be used as, on top of the pressure drop, it accounts for pollutants calculation and filter regeneration. In this research activity, as the focus is engine performance, little interest is given to the pollutants conversion efficiency and optimal Platinum-Group Metal (PGM) loading. For this reason, all ATS bricks will be parametrized as throughflow bricks with the CatalystBrick template.



Figure 3-3 – CatalystBrick vs. ParticulateFilter GT-POWER templates

As previously stated, alongside the geometrical dimension of each ATS element, JM provided some experimental measurements to tune the back pressures. The conducted tests consisted of individual brick flow analysis, where each brick was independently tested at different exhaust mass flow rates provided by a real engine. The test set-up was thus equal for each component, ensuring the same initial conditions.



Figure 3-4 – Visual representation of the ATS bricks testing conditions

The provided data was the same for each brick and was expressed as a function of the test time:

- Ambient pressure and temperature ( $P_{amb}$  and  $T_{amb}$ ).
- Pressure and temperature in the intake manifold of each brick element ( $P_1$  and  $T_1$ ).
- Pressure in the outlet manifold of each brick element ( $P_2$ ).
- Exhaust mass flow rate.
- Engine RPM related to that MFR.

The first step in the tuning process is to convert the time data into time-averaged data. Starting from the mass flow rate, *Figure 3-5* shows that each engine RPM is kept constant for 60 seconds. Consequently, seven time-averaged operating conditions can be obtained and simulated on GT-POWER. Moreover, the time-averaged pressure drop can be evaluated as the difference between the inlet and outlet pressure. This time-averaged pressure drop is the target value that the individual brick model should obtain.

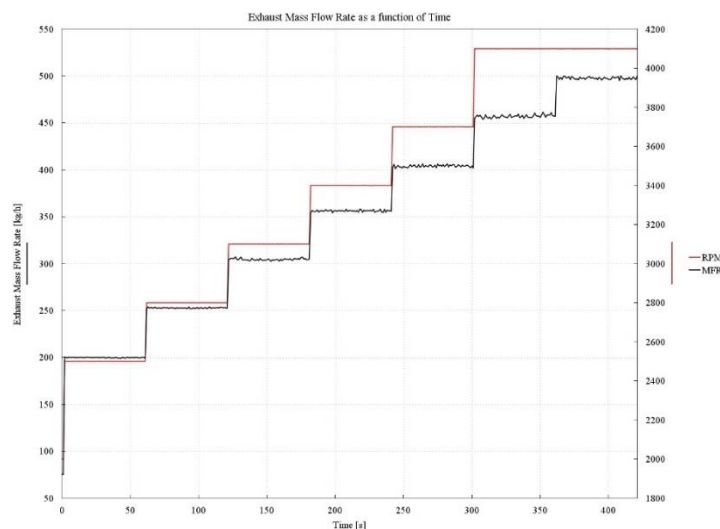


Figure 3-5 – Exhaust Mass Flow Rate as a function of Time

Now that the initial conditions are set, the individual brick GT-POWER model can be constructed.

Figure 3-6 shows the constructed individual brick model for back pressure tuning. The model works as follows: a BoundaryFlow element provides the experimental exhaust gas MFR which flows at a temperature  $T_1$  through the intake pipe and intake cone to arrive at the CatalystBrick. After the brick element, the exhaust gasses flow to the outlet environment, represented by the BoundaryPressure template, at the pressure  $P_2$ . While the simulation runs, two sensor connections read the intake and outlet static pressure values. These pressures are then subtracted from one another and averaged by the summation block and the RLTCreator.

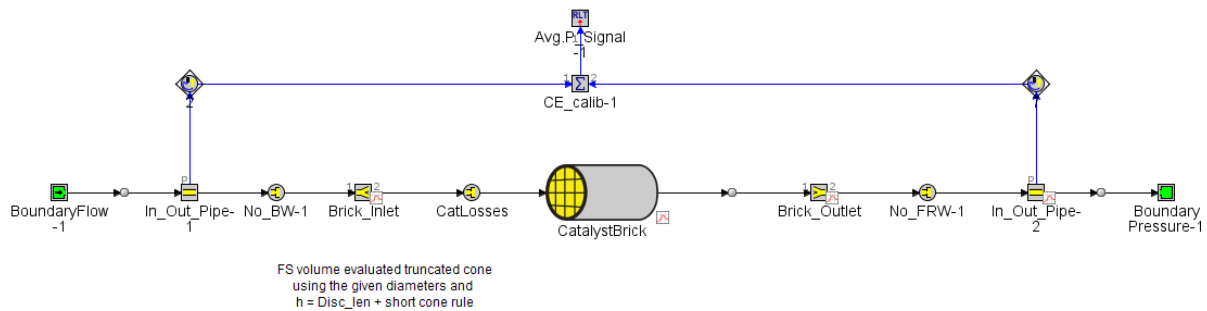


Figure 3-6 – Individual Brick Model

It must be noted that, as the inlet and outlet cone geometrical information was not provided, they were discretized according to the short cone rule, as suggested in the GT-POWER flow manual [20]. The flow manual suggests that when two pipes of different diameters are connected through a cone whose axial length is smaller than the discretization length of the model, the cone should be parametrized as a Flowsplit element with the largest diameter on both sides and that, to ensure that no backflow losses occur, the orifice upstream the inlet cone is set to have a reverse  $C_D$  equal to one. Similar considerations can be made for the outlet cone. As no information regarding the cone length was also given, they were parametrized with a length equal to the discretization length.

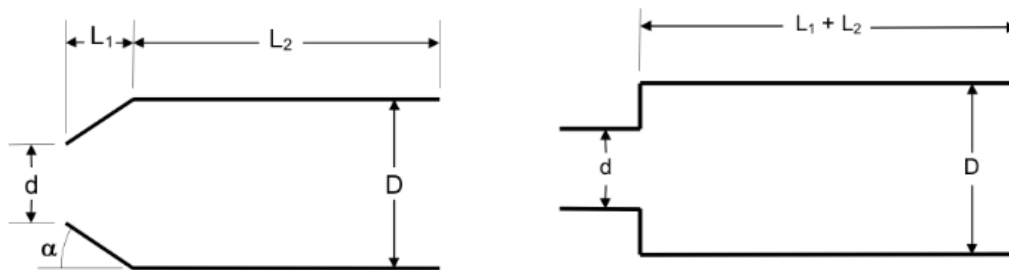


Figure 3-7 – Short cone discretization: actual system (left) equivalent discretized system (right)

Moreover, the MFR data must be tuned before it can be used in the BoundaryFlow template. As the provided pressure drop was evaluated by connecting the bricks to a running engine, the mass flow rate should represent the oscillations in a real engine on a crank angle basis.

To obtain such a pulsated MFR, the baseline GSE-T4 model was run to target the time-averaged mass flow rates at the turbine inlet. The pulsated MFRs shown in Figure 3-8 were then exported to the individual brick model.

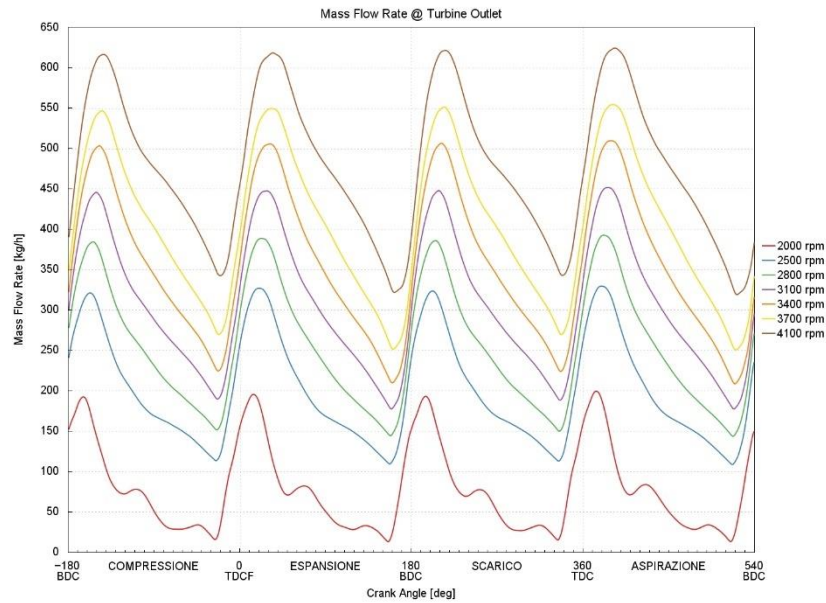


Figure 3-8 – Pulsated MFR at Turbine Outlet

Finally, the GT-POWER optimizer can be set to vary the forward  $C_D$  of the CatLosses orifice and the Friction Multiplier (FM) of the CatalystBrick such that the RLTCreator pressure drop vs. mass flow rate matches the target experimental quadratic trend like the one shown in *Figure 3-9*.

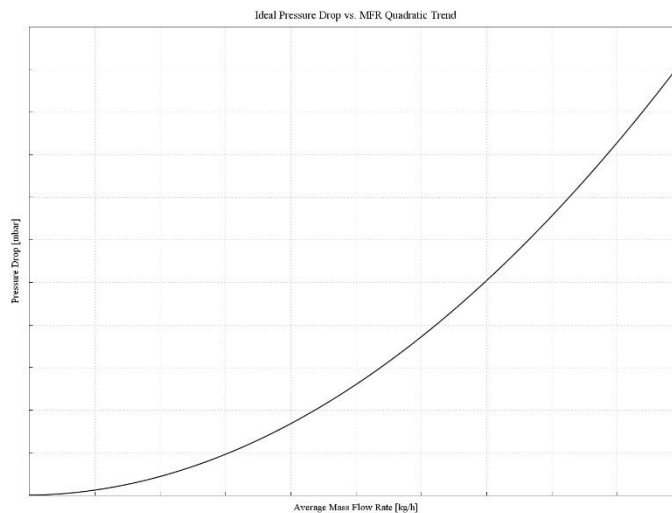


Figure 3-9 – Ideal Pressure Drop vs. Mass Flow Rate Quadratic Trend

Having said this, the procedure to follow to model and tune the aftertreatment bricks is the following:

1. Build the CatalystBrick template according to the given geometry.
2. Build the individual brick model with the pulsated MFR and  $T_1$ .
3. Optimize the  $C_D$  and FM to match experimental results.
4. Check for results consistency and, if needed, manually tune the parameters.



Figure 3-10 – EATS Bricks Calibration procedure flowchart

### 3.1.2 EHC + TWC<sub>1</sub>

Located at the turbine outlet, the first closed coupled (CC) EATS is the Electrically Heated Catalyst (EHC) and Three-Way Catalyst (TWC) Euro 7 ready combo, both enclosed in the same canister. The EHC is needed to quickly reach light-off temperature while the vehicle demonstrator runs in EV mode. This way, once the thermal engine is switched on, the ATS is at optimal operating temperature, providing the highest conversion efficiency.

1. The first step is building the CatalystBrick templates for both the EHC and TWC<sub>1</sub>. As they are in the same canister, they will be tuned as one single unit. The main geometric information is summarized in *Table 3-1*.

	Substrate Material	Diameter [mm]	Length [mm]	Cell density [cpsi]	Web Thickness [mm]
EHC	Metallic	130	11	130	0.050
TWC <sub>1</sub>	Metallic	130	40	600	0.040

Table 3-1 – EHC+TWC<sub>1</sub> main geometrical characteristics

2. The individual brick model in *Figure 3-12* was then built.



Figure 3-11 – Visual representation of the EHC-TWC<sub>1</sub> ATS brick testing conditions

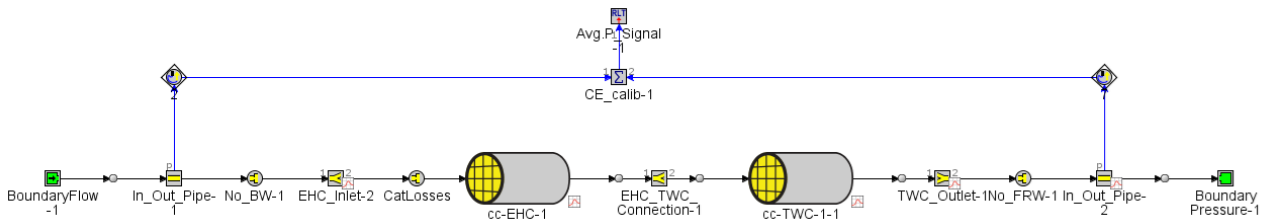


Figure 3-12 – EHC+TWC<sub>1</sub> 1D CFD GT-POWER individual brick model

It must be noted that since in GT-POWER two brick elements cannot be connected to one another, an additional Flowsplit between the two was needed. This element was parametrized as to ignore any losses not to affect the simulation results. The model's initial conditions are summarized in *Table 3-2*.

EHC+TWC <sub>1</sub>	GT-POWER cases						
RPM	4100	3700	3400	3100	2800	2500	2000
Average MFR [Kg/h]	477.37	403.95	356.24	304.52	252.79	199.90	75.5
Target P <sub>drop</sub> [mbar]	122.87	88.12	69.43	52.73	37.25	22.26	2.77
Average T <sub>1</sub> [C]	801.39	775.53	756.34	743.93	718.39	668.72	442.51
Average P <sub>2</sub> [mbar]	1042.93	1032.98	1027.03	1022.11	1019.07	1015.89	1007.41

Table 3-2 – EHC+TWC<sub>1</sub> Initial Conditions

3. The model was optimized to match the experimental pressure losses. The optimized values were  $C_D = 0.1967$  and  $FM = 1.6284$ , with a maximum error of 3.81 mbar at a mass flow rate of 199 Kg/h.

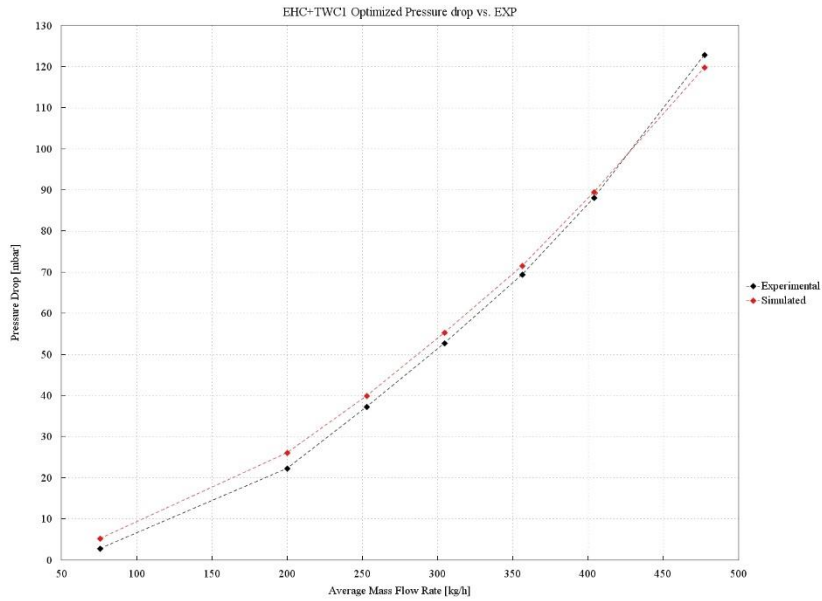


Figure 3-13 – EHC+TWC<sub>1</sub> optimized  $P_{drop}$

4. As shown in *Figure 3-13*, despite the optimizer getting close to the experimental results, it is still not a perfect match. To obtain more accurate results, a manual optimization was made. As a matter of fact, the optimizer does not know the physical effect of the discharge coefficient and the friction multiplier. Indeed, changing one or the other does not have the same effect on the pressure drop curve. As shown in *Figure 3-14*, varying the  $C_D$  will mainly affect the high-MFR portion of the parabolic trend, whereas changing the FM will affect the low-MFR part.

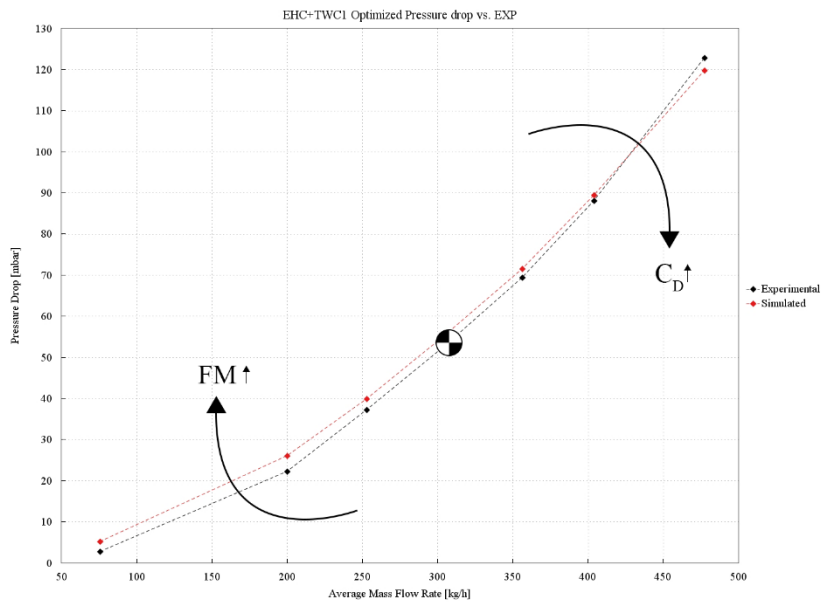


Figure 3-14 – Physical effect of  $C_D$  and FM on pressure drop

Consequently, after a couple of iterations, the final EHC+TWC<sub>1</sub> pressure drop tuning resulted in a C<sub>D</sub> of 0.1695 and a FM of 0.850 with a maximum error of -2.46 mbar at a mass flow rate of 477 Kg/h. The new trend is shown in *Figure 3-15*.

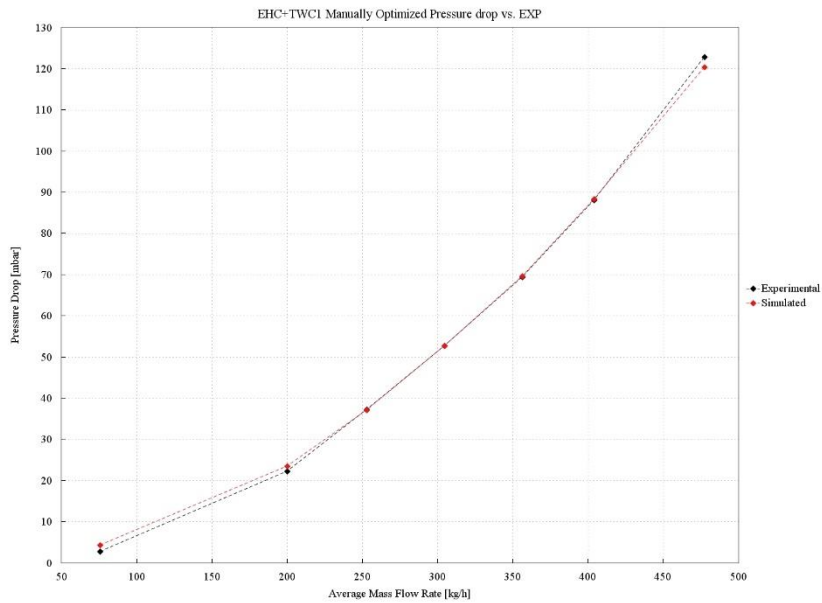


Figure 3-15 – EHC+TWC<sub>1</sub> manually calibrated P<sub>drop</sub>

However, after a first test run, the simulation results proved that the EHC+TWC<sub>1</sub> discretization slowed the computational time by a large margin. The reason behind this is the very short axial length of the EHC brick, which was less than half of the discretization length. As a matter of fact, while the discretization length of the exhaust line was chosen as  $0.3 \cdot Bore = 25 \text{ mm}$ , as suggested by the GT-POWER manuals, the EHC was only 11 mm long. This implies that GT-POWER will not be able to discretize the element by itself, which slows the computation.

To solve this issue, the EHC disk was incorporated into the TWC<sub>1</sub>, regardless of the cpsi difference (130 for the EHC and 600 for the TWC<sub>1</sub>). A new CatalystBrick template was thus built.

	Substrate Material	Diameter [mm]	Length [mm]	Cell density [cpsi]	Web Thickness [mm]
TWC <sub>1</sub>	Metallic	130	40+11 = 51	600	0.040

Table 3-3 – Updated TWC<sub>1</sub> main geometrical characteristics

The new brick was substituted into the individual brick model, as shown in *Figure 3-16*.

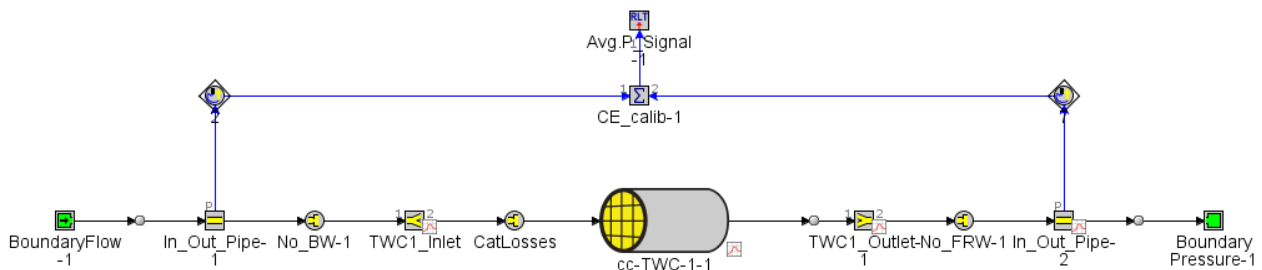


Figure 3-16 – Updated TWC<sub>1</sub> 1D CFD GT-POWER individual brick model

The tuning procedure was repeated. The optimizer yielded a  $C_D$  of 0.1864 and a FM of 0.9859 with a maximum error of -2.49 mbar at a mass flow rate of 199.90 Kg/h.

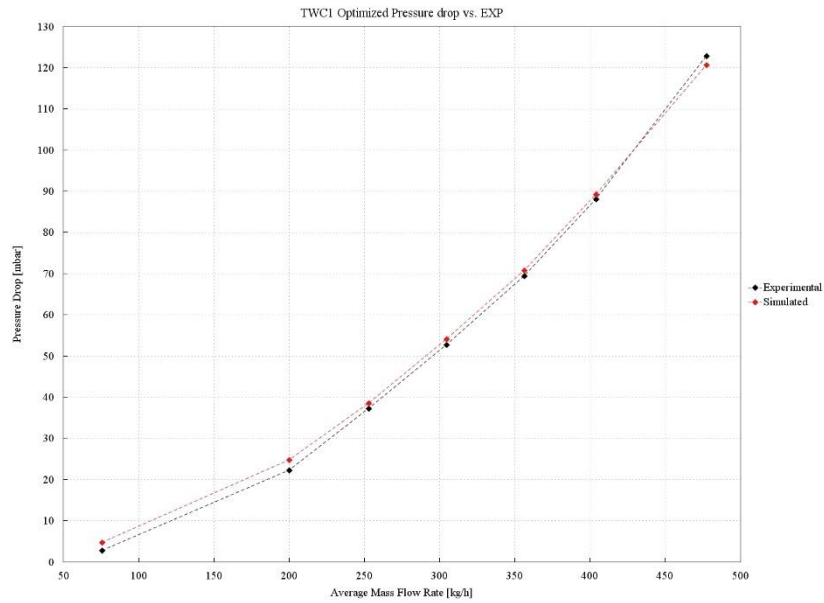


Figure 3-17 – Updated  $TWC_1$  optimized  $P_{drop}$

While the manual optimization managed to lower the maximum error to 1.9 mbar at a mass flow rate of 477 Kg/h, as seen in *Figure 3-18*.

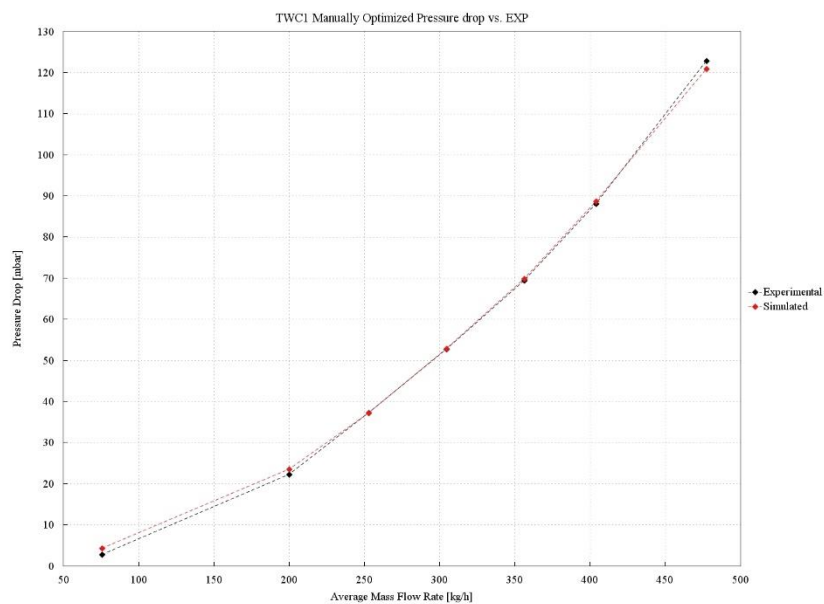


Figure 3-18 – Updated  $TWC_1$  manually calibrated  $P_{drop}$

### 3.1.3 TWC<sub>2</sub>

Downstream the EHC+TWC<sub>1</sub> combo, a second TWC<sub>2</sub> can be found to reduce the emitted HC and CO further.

1. Slightly larger and longer than TWC<sub>1</sub>, TWC<sub>2</sub> has a more packed substrate to increase conversion efficiency. However, this will cause higher back pressure. The CatalystBrick was created as follows.

	Substrate Material	Diameter [mm]	Length [mm]	Cell density [cpsi]	Web Thickness [mm]
TWC <sub>2</sub>	Ceramic	132.1	55	750	0.064

Table 3-4 – TWC<sub>2</sub> main geometrical characteristics

2. The individual brick model in *Figure 3-20* was then built.

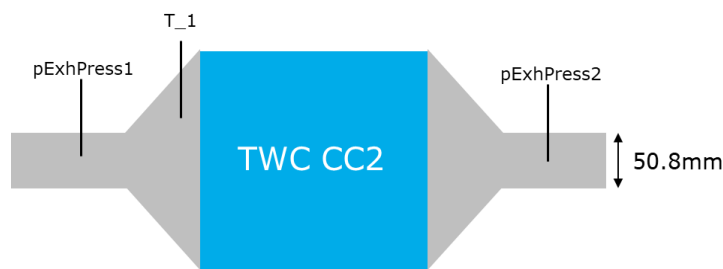


Figure 3-19 – Visual representation of the TWC<sub>2</sub> ATS brick testing conditions

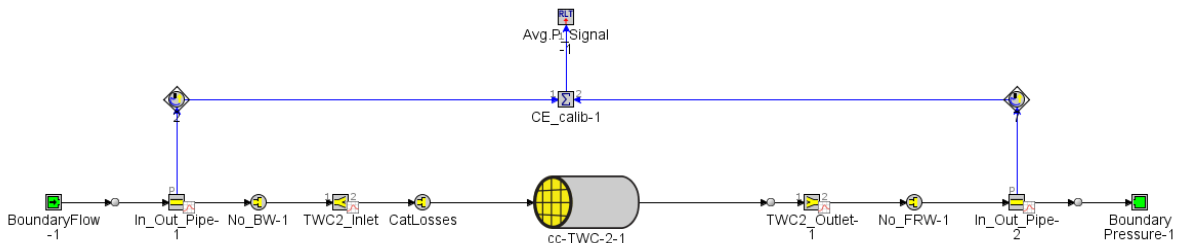


Figure 3-20 – TWC<sub>2</sub> 1D CFD GT-POWER individual brick model

The model's initial conditions are summarized in *Table 3-5*.

TWC <sub>2</sub>	GT-POWER cases						
RPM	4100	3700	3400	3100	2800	2500	2000
Average MFR [Kg/h]	477.37	403.95	356.24	304.52	252.79	199.90	75.5
Target P <sub>drop</sub> [mbar]	145.12	111.36	88.70	69.68	50.99	36.45	3.35
Average T <sub>1</sub> [C]	801.87	778.64	760.32	751.53	726.31	679.47	466.91
Average P <sub>2</sub> [mbar]	1041.16	1031.51	1025.96	1022.34	1015.48	1011.35	1006.79

Table 3-5 – TWC<sub>2</sub> Initial Conditions

3. The model was optimized to match the experimental pressure drops. The optimized values were  $C_D = 0.3310$  and  $FM = 2.8056$ , with a maximum error of 5.61 mbar at a mass flow rate of 252 Kg/h.

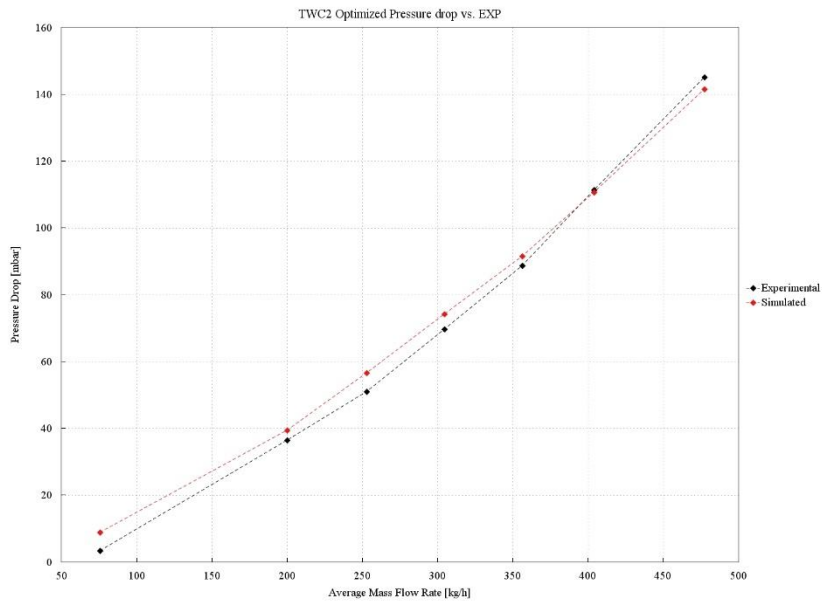


Figure 3-21 – TWC<sub>2</sub> optimized P<sub>drop</sub>

4. The TWC<sub>2</sub> simulation was also tuned to get more accurate results. The final TWC<sub>2</sub> pressure drop tuning resulted in a  $C_D$  of 0.2 and a FM of 1.850 with a maximum error of 3.88 mbar at a mass flow rate of 75.5 Kg/h. The new trend is shown in *Figure 3-22*.

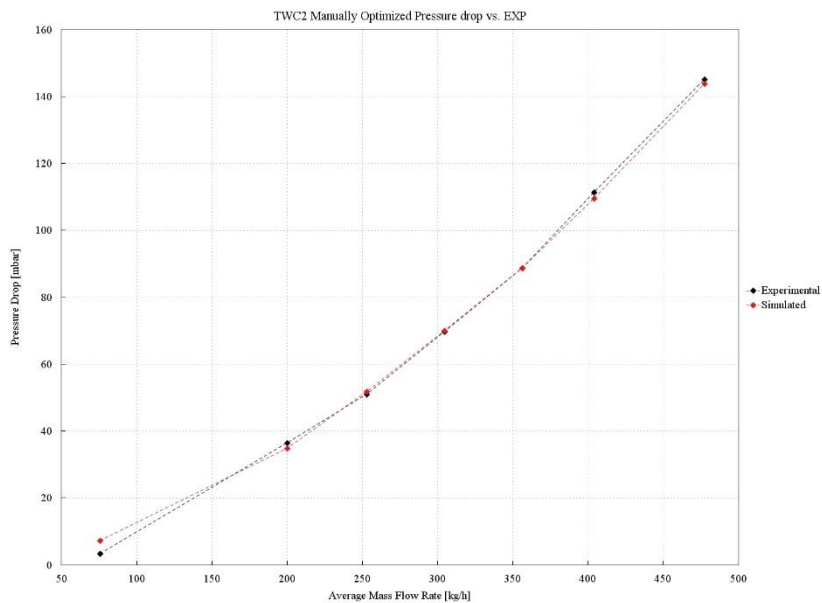


Figure 3-22 – TWC<sub>2</sub> manually calibrated P<sub>drop</sub>

### 3.1.4 GPF

Finally, the last closed coupled brick is a GPF. As stated in the chapter introduction, although GPFs are of the wall flow type, in this research activity they will nonetheless be parametrized as through flow bricks via the CatalystBrick template.

1. The CatalystBrick was created with the following geometrical features. As this is the only GPF in the car's ATS, its longitudinal dimension will be significant to ensure that the Euro 7 target for PM can be achieved.

	Substrate Material	Diameter [mm]	Length [mm]	Cell density [cps]	Web Thickness [mm]
GPF	Ceramic	143.8	150	300	0.203

Table 3-6 – GPF main geometrical characteristics

2. The individual brick model was then built as shown in *Figure 3-24*.



Figure 3-23 – Visual representation of the GPF ATS brick testing conditions

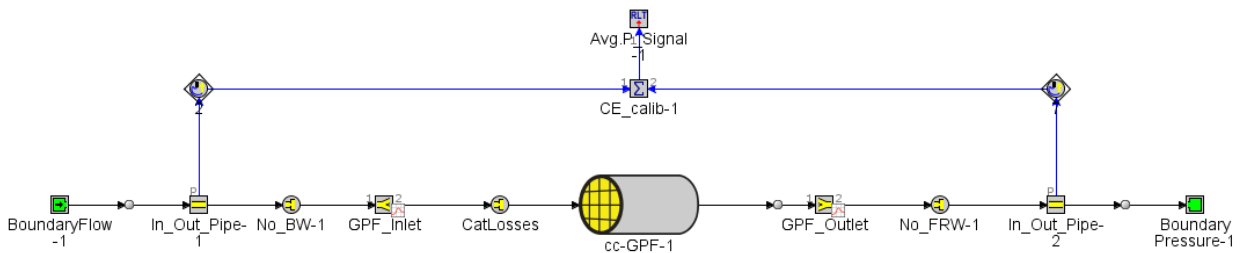


Figure 3-24 – GPF 1D CFD GT-POWER individual brick model

The model's initial conditions are summarized in *Table 3-7*.

GPF	GT-POWER cases						
RPM	4100	3700	3400	3100	2800	2500	2000
Average MFR [Kg/h]	477.37	403.95	356.24	304.52	252.79	199.90	75.5
Target $P_{drop}$ [mbar]	191.81	147.29	122.18	99.89	77.74	51.90	16.42
Average $T_1$ [C]	796.35	774.13	759.99	754.41	736.06	686.10	549.54
Average $P_2$ [mbar]	1038.43	1030.18	1023.98	1021.02	1015.68	1011.76	1005.82

Table 3-7 – GPF Initial Conditions

- The model was optimized to match the experimental pressure drops. The optimized values were  $C_D = 0.6163$  and  $FM = 3.8156$ , with a maximum error of  $-8.12$  mbar at a mass flow rate of  $477$  Kg/h.

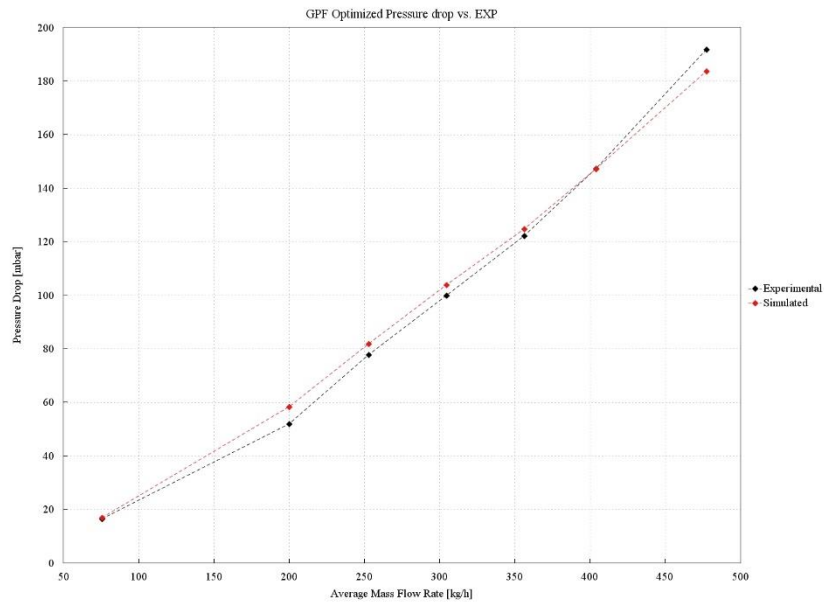


Figure 3-25 – GPF optimized  $P_{drop}$

- The GPF simulation was also tuned to get more accurate results. The final GPF pressure drop tuning resulted in a  $C_D$  of  $0.211$  and a  $FM$  of  $2.990$  with a maximum error of  $-2.88$  mbar at a mass flow rate of  $477$  Kg/h. The new trend is shown in *Figure 3-26*.

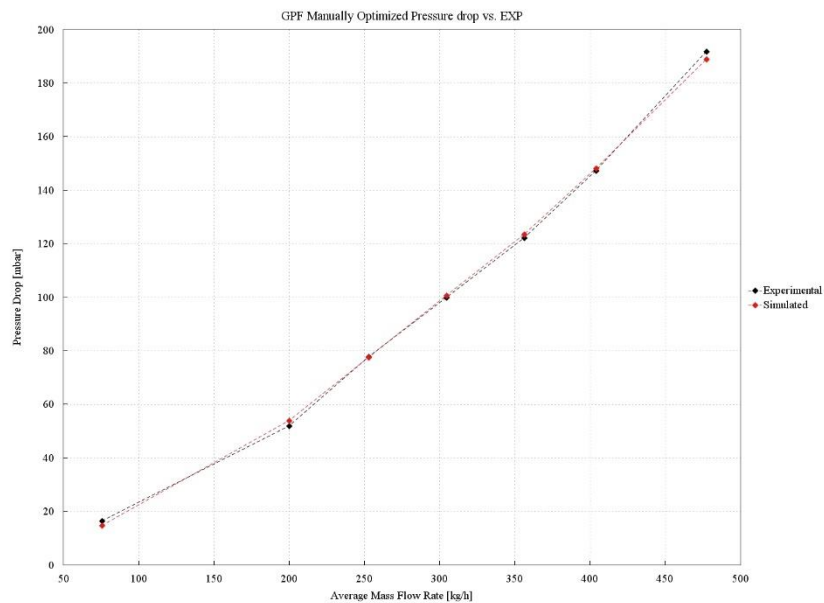


Figure 3-26 – GPF manually calibrated  $P_{drop}$

### 3.1.5 NO-Ox

The NO-Ox is the first brick belonging to the Under Floor (UF) portion of the exhaust line. These bricks are characterized by a lower ideal operating temperature with respect to the closed coupled ones. Thus, their thermal safety can be guaranteed by placing them far away from the engine. The underfloor bricks are characterized by the same data set as their CC counterpart; their calibration procedure will hence be equivalent.

1. The CatalystBrick was created with the following characteristics.

	Substrate Material	Diameter [mm]	Length [mm]	Cell density [cps]	Web Thickness [mm]
NO-Ox	Ceramic	143.8	62.5	400	0.102

Table 3-8 – NO-Ox main geometrical characteristics

2. Consequently, the individual brick model was built as in *Figure 3-28*.

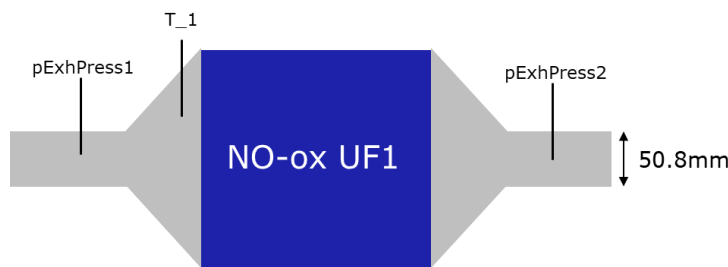


Figure 3-27 – Virtual representation of the NO-Ox ATS brick testing conditions

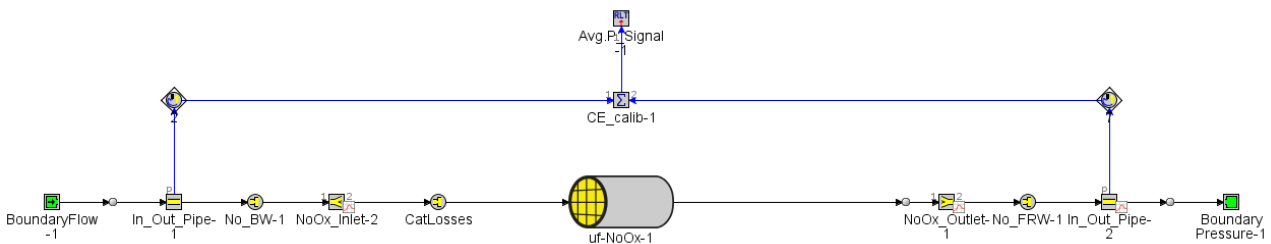


Figure 3-28 – NO-Ox 1D CFD GT-POWER individual brick model

The model's initial conditions are summarized in *Table 3-9*.

NO-Ox	GT-POWER cases						
RPM	4100	3700	3400	3100	2800	2500	2000
Average MFR [Kg/h]	477.37	403.95	356.24	304.52	252.79	199.90	75.5
Target P <sub>drop</sub> [mbar]	103.36	75.55	59.93	44.21	29.70	22.60	3.10
Average T <sub>1</sub> [C]	797.46	780.01	765.09	752.15	729.46	683.10	461.23
Average P <sub>2</sub> [mbar]	1041.47	1029.75	1023.45	1018.95	1016.00	1010.87	1003.48

Table 3-9 – NO-Ox Initial Conditions

- The model was optimized to match the experimental pressure drops. The optimized values were  $C_D = 0.4618$  and  $FM = 2.6818$ , with a maximum error of 5.62 mbar at a mass flow rate of 477 Kg/h.

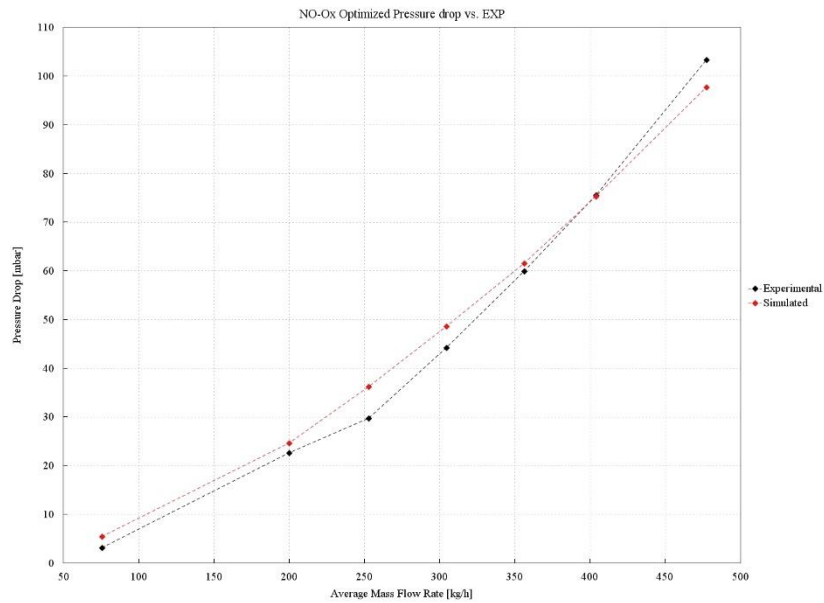


Figure 3-29 – NO-Ox optimized  $P_{drop}$

- After manual tuning, the final NO-Ox pressure drop simulation resulted in a  $C_D$  of 0.300 and a FM of 2.200 with a maximum error of 4.32 mbar at a mass flow rate of 477 Kg/h. The new trend is shown in *Figure 3-30*.

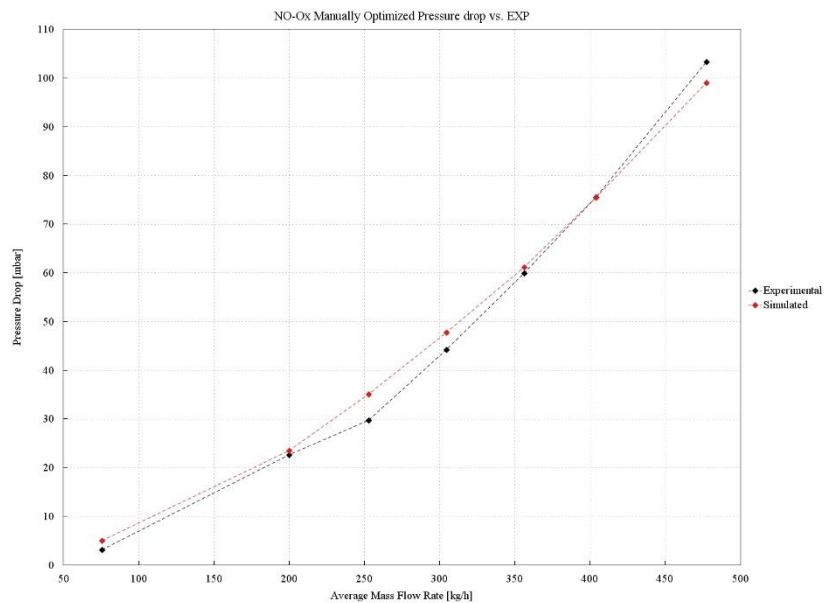


Figure 3-30 – NO-Ox manually calibrated  $P_{drop}$

### 3.1.6 SCR<sub>1</sub> & SCR<sub>2</sub>

The two SCR devices are next. The ultra-lean operating conditions of PHOENICE make SCR devices mandatory to abate the not negligible NO<sub>x</sub> emissions. As both the geometrical characteristics and initial conditions were the same between the two components, a single optimization was performed. Both bricks will then use the same C<sub>D</sub> and FM coefficients.

1. As usual, the CatalystBrick template was built following the provided characteristics.

	Substrate Material	Diameter [mm]	Length [mm]	Cell density [cps]	Web Thickness [mm]
SCR <sub>1</sub>	Ceramic	143.8	152.4	600	0.102

Table 3-10 – SCR<sub>1</sub> main geometrical characteristics

2. The individual brick model in *Figure 3-32* followed right after.



Figure 3-31 – Visual representation of the SCR<sub>1</sub> ATS brick testing conditions

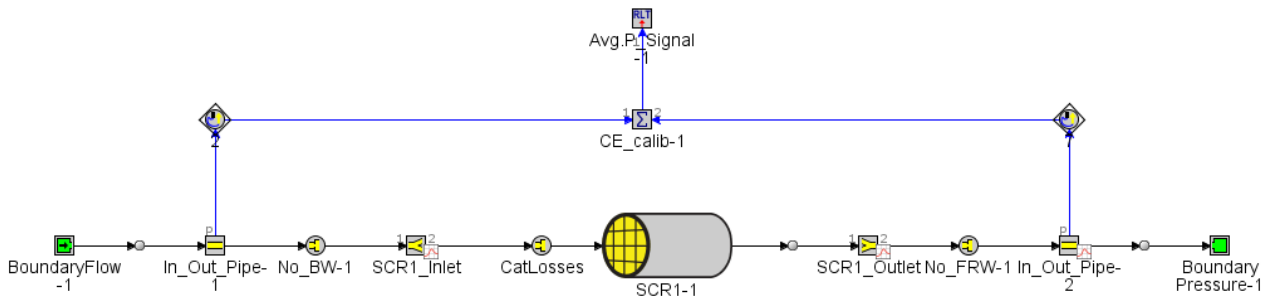


Figure 3-32 – SCR<sub>1</sub> 1D CFD GT-POWER individual brick model

The model's initial conditions are summarized in *Table 3-11*.

SCR <sub>1</sub>	GT-POWER cases						
RPM	4100	3700	3400	3100	2800	2500	2000
Average MFR [Kg/h]	477.37	403.95	356.24	304.52	252.79	199.90	75.5
Target P <sub>drop</sub> [mbar]	193.73	154.42	129.92	106.35	83.43	56.60	10.34
Average T <sub>1</sub> [C]	794.60	772.03	752.54	739.68	714.80	671.62	458.96
Average P <sub>2</sub> [mbar]	1033.03	1023.59	1017.77	1013.96	1006.21	1004.32	1001.04

Table 3-11 – SCR<sub>1</sub> Initial Conditions

3. The model was optimized to match the experimental pressure drops. The optimized values were  $C_D = 0.3727$  and  $FM = 2.3130$ , with a maximum error of  $-5.449$  mbar at a mass flow rate of  $75.5$  Kg/h.

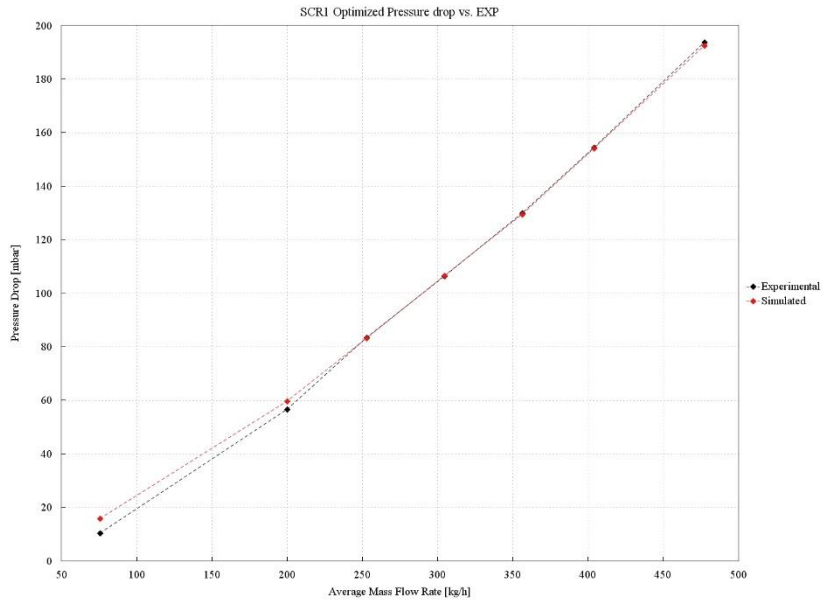


Figure 3-33 – SCR<sub>1</sub> optimized P<sub>drop</sub>

4. In the case of SCR<sub>1</sub> and SCR<sub>2</sub>, the match with experimental data was already very good. As a matter of fact, manual tuning did not produce any significant results. The best manual tuning results were obtained with  $C_D$  and  $FM$  similar to the optimizer.  $C_D = 0.3700$  and  $FM = 2.3100$ , with a maximum error of  $-5.435$  mbar at a mass flow rate of  $75.5$  Kg/h.

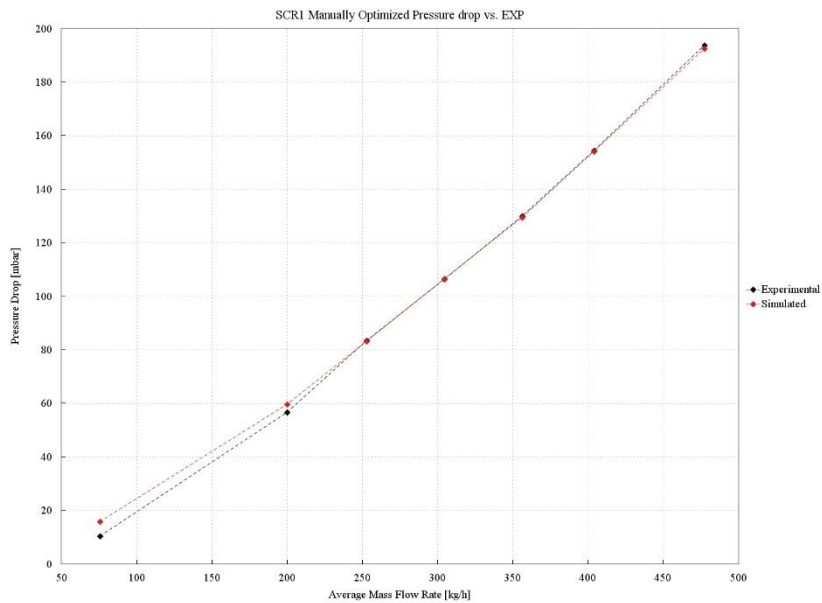


Figure 3-34 – SCR<sub>1</sub> manually calibrated P<sub>drop</sub>

## 3.2 Heat Exchangers Pressure Drop Calibration

In *Chapter 2.1*, the EGR and intake lines were discretized. However, the internal geometries of the Water Charge Air Cooler (WCAC) and EGR Cooler (EGRC) were not provided. Thus, the 1D model cannot represent the pressure losses of such components. This chapter will deal with the modeling and tuning of both components.

### 3.2.1 Calibration Procedure

Tuning the coolers' 1D model is quite like the brick tuning carried out in *Chapter 3.1*. The goal of this study, is to increase the losses through the component until they match the experimental results despite lacking the internal geometry which causes these drops in pressure.

The following steps summarize the procedure to follow:

1. Create the digital twin model representative of the experimental tests.
2. Impose the experimental initial conditions.
3. Tune the loss coefficients with the optimizer.
4. Tweak manually for higher accuracy.



Figure 3-35 – Coolers' Calibration Procedure Flowchart

### 3.2.2 EGR Cooler Calibration

The first cooler under analysis is the EGR Cooler. The EGRC accepts clean exhaust gas flow from the GPF outlet, lowers its temperature, and delivers it to the intake line, upstream of the compressor, through the EGR valve. This research activity will only focus on calibrating the exhaust gas pressure loss. No tuning of the cooling line will be reported. The experimental test set-up can be seen in *Figure 3-36*.



Figure 3-36 – EGRC Experimental Test set-up

1. The digital twin, starting from the discretized line, was built to match the test bench set-up.

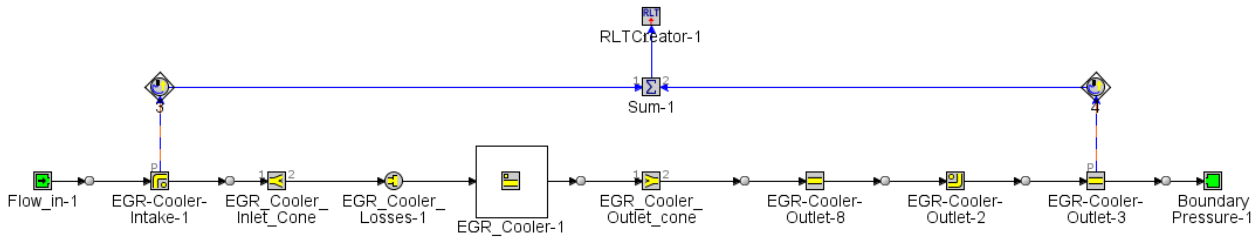


Figure 3-37 – EGRC 1D CFD GT-POWER test bench digital twin

2. As for the bricks' calibration, the model's initial conditions were imposed. The provided data included:
  - Inlet average mass flow rate measures.
  - Inlet Pressure and temperature ( $P_1$  and  $T_2$ ).
  - Measured pressured drop over the tested component.
  - Measured heat released by the EGRC during the test.
  - Outlet Temperature ( $T_2$ ).

Inlet temperature and mass flow rate were imposed on the BoundaryFlow element, whereas the EGRC block was set to match the experimental heat released. Finally, the pressure drops were used as the target values for the optimizer.

The initial conditions are summarized in *Table 3-12*.

EGRC	GT-POWER cases					
Average MFR [Kg/h]	108	90	72	54	36	18
Target $P_{drop}$ [mbar]	36.06	25.46	16.69	9.75	4.64	1.36
Average $T_1$ [°C]	280	280	280	280	280	280
Heat Released [kW]	4.96	4.32	3.60	2.81	1.95	1.01

Table 3-12 – EGRC Initial Conditions

- The optimizer was then run to optimize the forward Discharge Coefficient  $C_D$  and the Friction Multiplier FM to match the experimental pressure losses. The optimizer yielded a  $C_D$  of 0.2348 and a FM of 3.9471 with a maximum error of 0.76 mbar at a mass flow rate of 54 Kg/h.

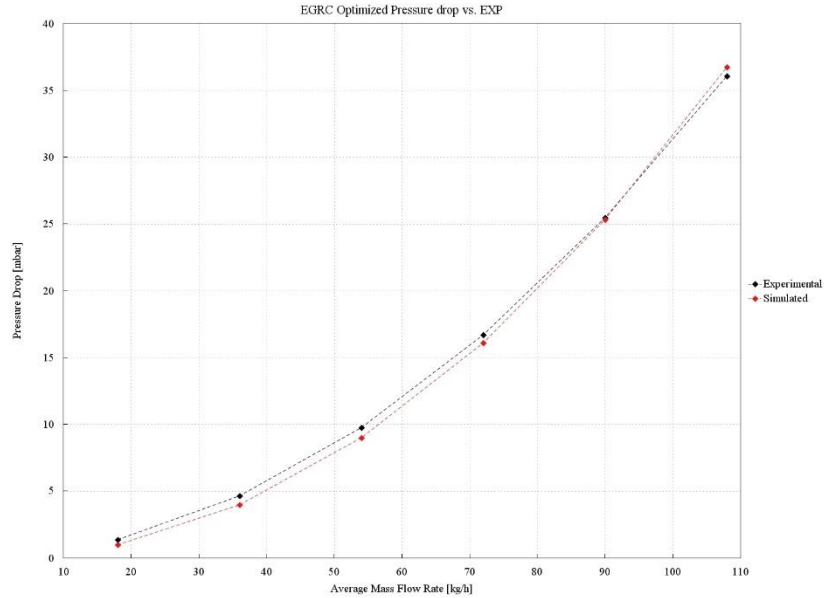


Figure 3-38 – EGRC optimized  $P_{\text{drop}}$

- As for the SCR1 in *Chapter 3.1.6*, the optimizer matched the experimental results. Thus little improvements were obtained by manual tuning. A  $C_D$  of 0.235 and a FM of 5 resulted in a maximum error of 0.75 mbar at a mass flow rate of 108 Kg/h.

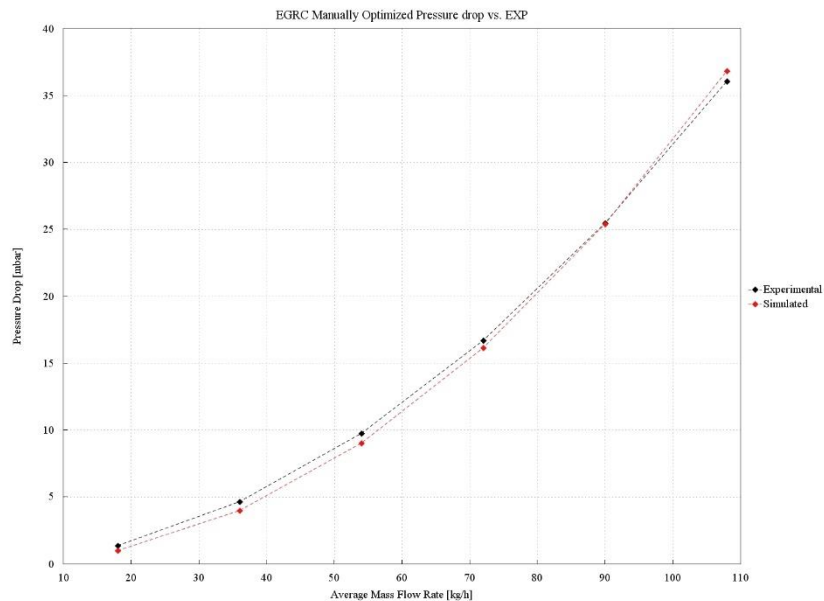


Figure 3-39 – EGRC manually calibrated  $P_{\text{drop}}$

It is worth noting how different from the bricks' simulations, looking at *Figure 3-38* and *Figure 3-39*, although a difference of 1.06 in the friction multiplier, little to no effect at low mass flow rates can be noticed. This behavior is due to the EGRC being parametrized as a single square pipe, whereas multiple channels characterized the CatalystBrick elements. The friction multiplier only affects the gas-to-wall interaction; thus, it is irrelevant in single-pipe components.

### 3.2.3 Water Charge Air Cooler Calibration

Following the same steps as the EGRC, the WCAC was also tuned. However, pressure drop experimental measurements could not be used. 3D CFD simulation results were thus used.

Although test bench data were available, they lacked information regarding the connections between the WCAC and the test bench. Indeed, the dimensions of the test bench outlet connection shown in *Figure 3-40* were unknown.

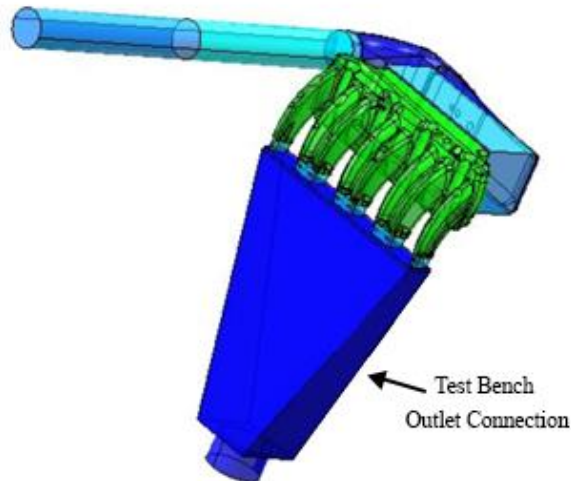


Figure 3-40 – Visual representation of the WCAC test bench set-up

As the pressure drop was experimentally measured with this trapezoidal connection, not having precise geometrical measurements would lead to too much inaccuracy and approximation. Despite being a simulation, basing the tuning on the 3D CFD would result in lower errors with respect to making wrong assumptions on the trapezoidal connection.

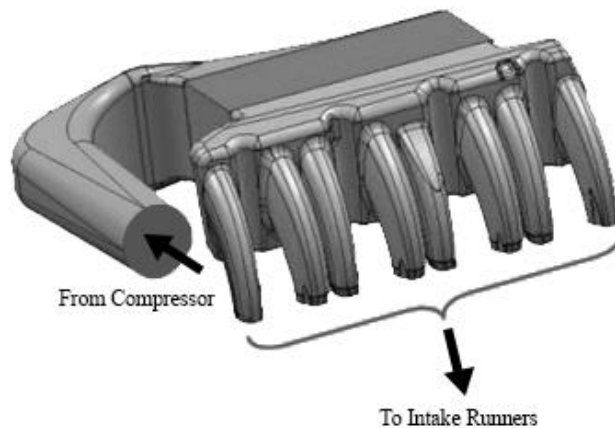


Figure 3-41 – WCAC 3D-CFD Simulation model set-up

1. The 1D model was thus built based on the CFD set-up.

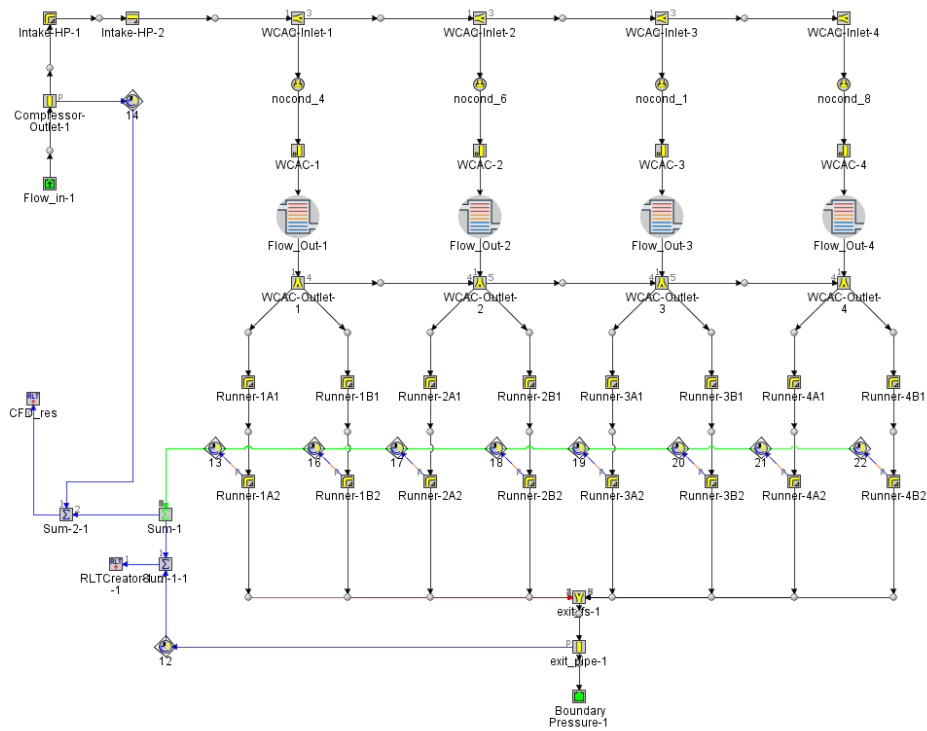


Figure 3-42 – WCAC 1D CFD GT-POWER Calibration Model

To properly evaluate the pressure drop, an average of the eight outlet runners' static pressure is made, as can be seen in *Figure 3-42*. Moreover, the four HeatExchangerConnections are used to force an outlet temperature of 50°C per the original GSE-T4 model. Finally, to represent the WCAC core passages, whose internal geometry is unknown, the total core volume was divided into four rectangular pipes, one per cylinder, which were further divided into 18 channels each for a total of 72 channels. The value of 72 was derived from the original GSE-T4 model. However, to account for the part of the core volume occupied by the cooler fins, only half of the cross-section area was assumed to allow air to flow through, leading to a total air volume of 0.8 L. This reduced volume was used to size the 72 channels.

2. The initial conditions for this analysis were similar to the EGRC test. The simulation pressured drops were given as a function of the inlet air mass flow rate at a fixed temperature. No indication of the heat released was given, however, as previously explained, a fixed outlet temperature of 50°C was forced. *Table 3-13* summarizes the initial conditions.

WCAC	GT-POWER cases			
Average MFR [Kg/h]	600	450	300	150
Target P <sub>drop</sub> [mbar]	29.7	15.6	8.8	3.8
Inlet Temp [°C]	180	180	180	180
Outlet Temp. [°C]	50	50	50	50

Table 3-13 – WCAC Initial Conditions

- The optimizer was then run to optimize the forward Discharge Coefficient  $C_D$  and the Forward Losses coefficient  $FL$  to match the 3D CFD pressure losses. The optimizer yielded a  $C_D$  of 0.3133 and a  $FL$  of 2.0617 with a maximum error of -1.88 mbar at a mass flow rate of 150 Kg/h.

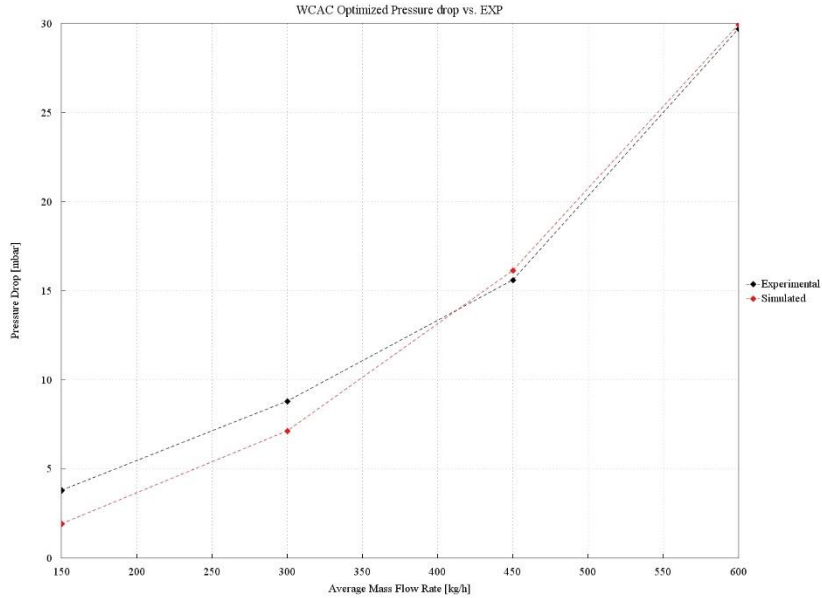


Figure 3-43 – WCAC optimized  $P_{drop}$

- As for the  $SCR_1$  and the EGRC, the optimizer matched the experimental results, thus, little improvements were obtained by manual tuning. A  $C_D$  of 0.32 and a  $FL$  of 3 resulted in a maximum error of -1.81 mbar at a mass flow rate of 150 Kg/h.

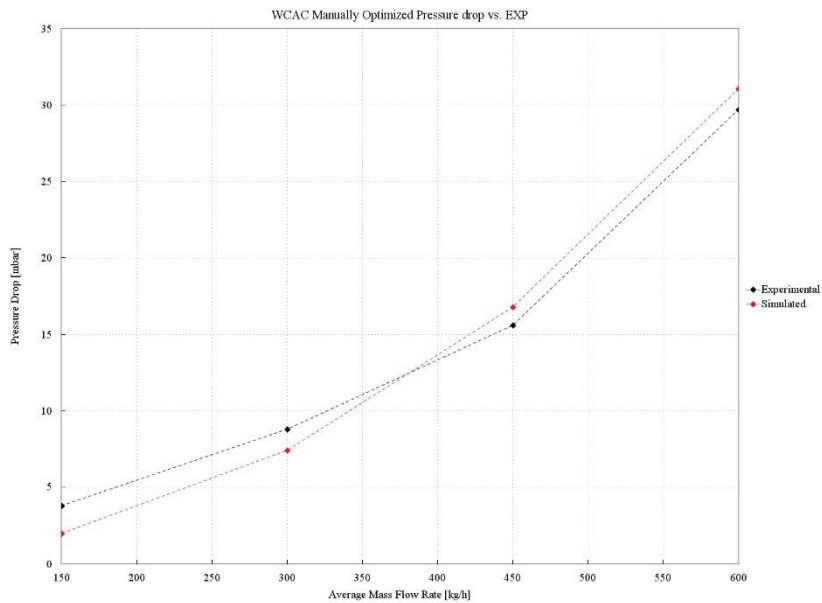


Figure 3-44 – WCAC manually optimized  $P_{drop}$

A fixed WCAC outlet temperature of 50°C was assumed. This value was imposed in the original GSE-T4 1D model and was thus carried over.

However, in order to understand whether this value could influence the obtained tuning, a sensitivity analysis was carried out. The given Valeo dataset shows that a temperature of 75°C should never be reached as the coolant may start to boil. The sensitivity analysis was thus carried out in a neighborhood of 50°C.

The calibration model in *Figure 3-42* was kept the same except for the WCAC outlet temperature. The sensitivity analysis was conducted for the not-calibrated conditions, meaning that the  $C_D$  and  $F_L$  were left at the default values. The considered temperature values are 40°C, 50°C, 60°C, and 70°C.

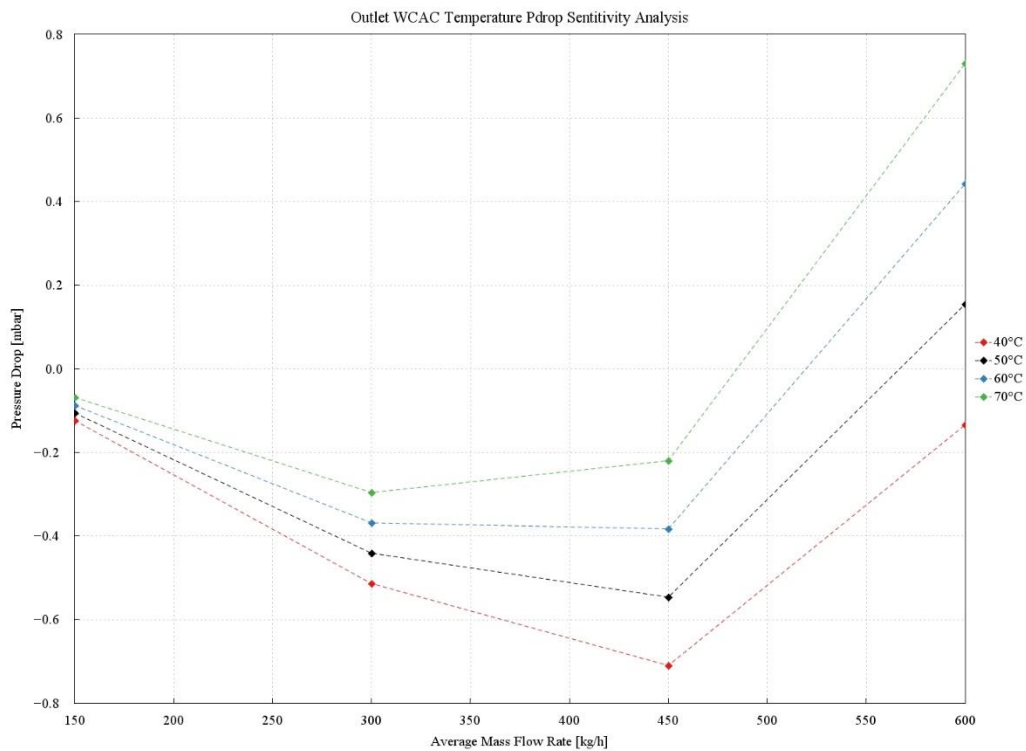


Figure 3-45 – WCAC Outlet Temperature Sensitivity Analysis

As the pressure drop differences between the various temperatures in *Figure 3-45* were negligible, the assumed temperature for the calibration procedure was chosen to be 50°C, like in the GSE-T4 model. A more precise tuning will be possible once a parametric evaluation of such temperature is available.

## 4 Preliminary Engine Calibration

A preliminary set of engine calibrations was conducted to study the consequences of changing different parameters in the engine model and whether such changes affected the performances. It is worth recalling that the following study was carried out with the modified GSE-T3 combustion model, as defined in *Chapter 2.2.3*. Nevertheless, the similar no-EGR stoichiometric conditions make this approximation acceptable.

### 4.1 Intake Charge Temperature Sensitivity Analysis

In *Chapter 3.2.3*, the effect of different WCAC outlet temperatures was investigated in terms of cooler pressure drop. Here, on the other hand, the focus of the study will be related to overall engine performance. As a matter of fact, the WCAC outlet temperature directly controls the intake charge temperature. This value is very relevant in high compression ratio engines, such as the PHOENICE one, as a low temperature mitigates the occurrence of knock and thus significantly affects the engine efficiency. The complete engine model was used to run a full load simulation, investigating the effect of different intake charge temperatures. Specific attention was given to the changes in Mean Effective Pressure (MEP), combustion efficiency, and volumetric efficiency for three different values of temperature: 40°C, 50°C, and 60°C.

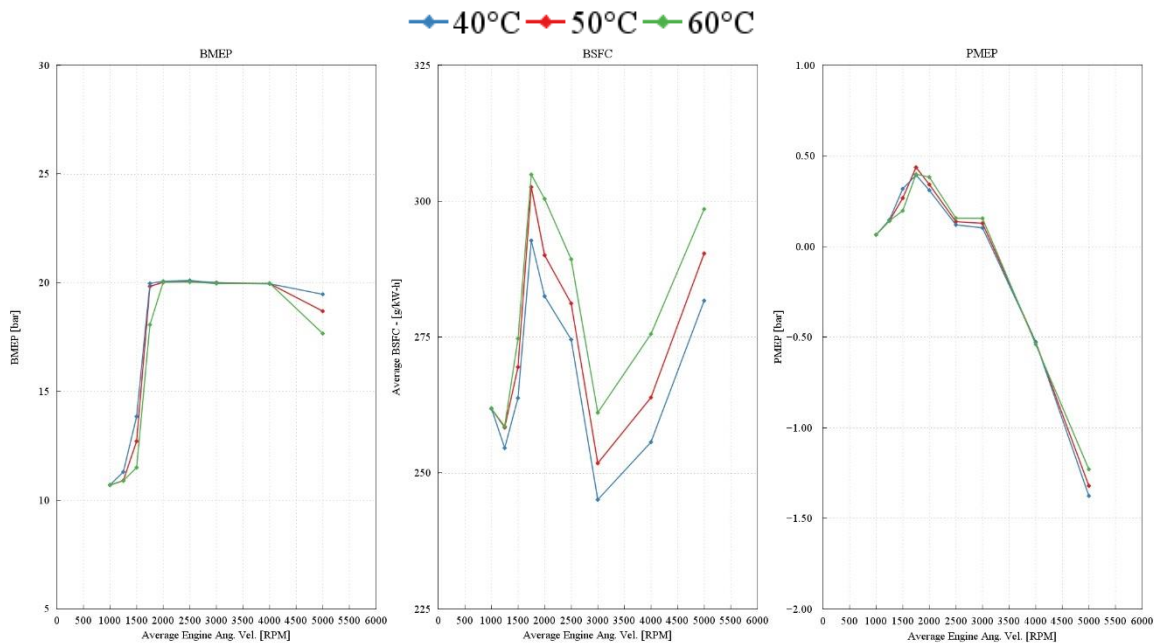


Figure 4-1 – PHOENICE Engine Performance for Different WCAC Outlet Temperatures – MEP

*Figure 4-1* shows how all three temperature values do not limit the achievable BMEP, which is fixed to a maximum of 20 bar. The only exception is the last operating point at 5000 RPM, where the lowest WCAC temperature of 40°C can achieve a BMEP 1 bar higher than 50°C and 2 bar higher than 60°C. Consequently, the lower intake charge temperature leads to a lower Brake Specific Fuel Consumption (BSFC). The Pumping Mean Effective Pressure (PMEP) remains similar for all three cases. As can be seen from *Figure 4-2*, the difference in BSFC is explained by the faster burn duration obtained by the 40°C case, which increases the brake efficiency as the anchor point of the combustion (MFB50) is closer to the ideal range of 8-10°. In the 50°C and 60°C cases, the MFB50 is retarded, and the combustion duration is increased to limit the knocking phenomenon. However, this will negatively affect the combustion efficiency.

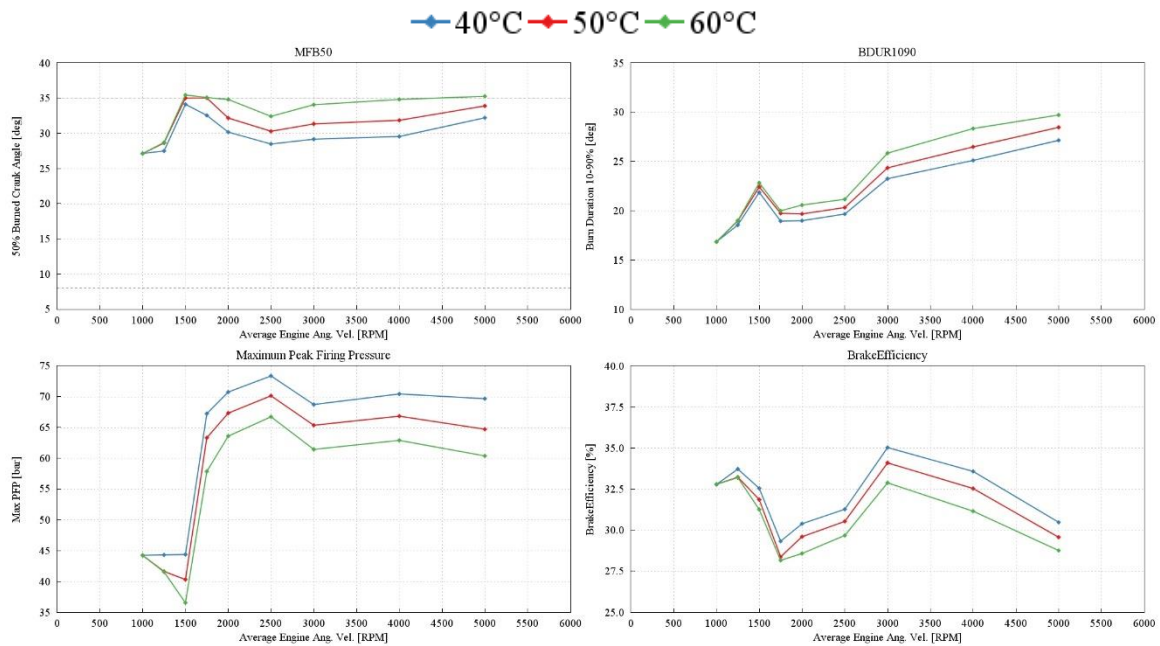


Figure 4-2 – PHOENICE Engine Performance for Different WCAC Outlet Temperatures – Combustion Efficiency

Finally, looking at *Figure 4-3*, it is worth noting how, despite the higher outlet temperature, the 60°C oddly proved to have a slightly higher volumetric efficiency  $\lambda_v$ . The reason behind this is that the turbocharger controller provided a higher boost to compensate for the less dense intake air. As a matter of fact, the compressor speed is also higher.

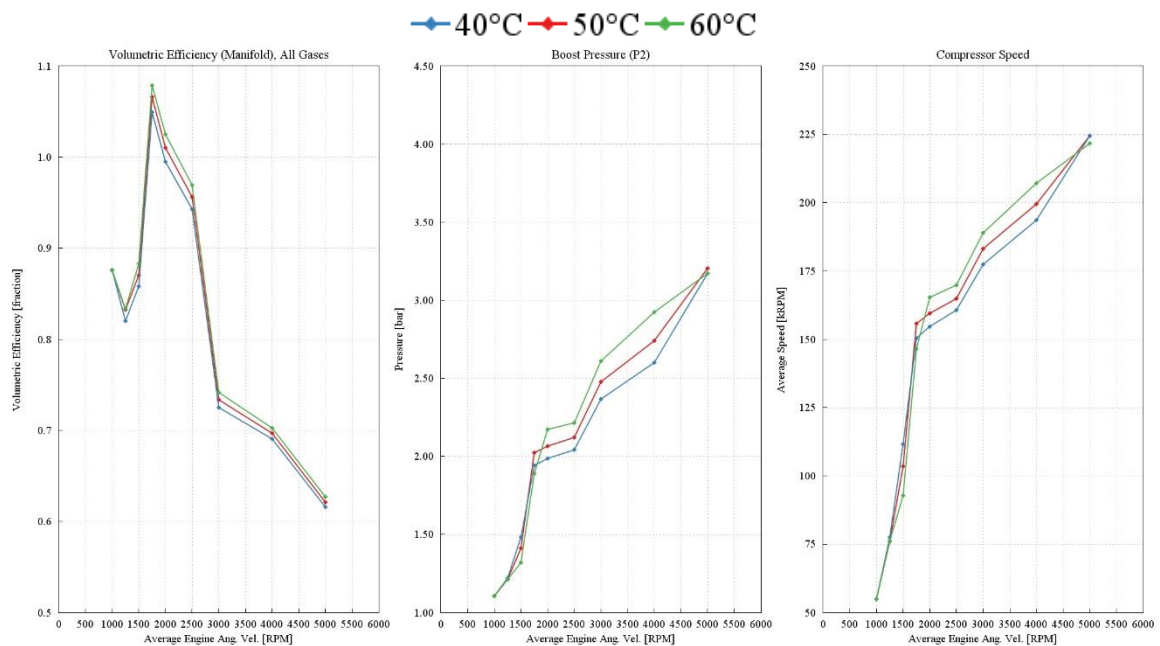


Figure 4-3 – PHOENICE Engine Performance for Different WCAC Outlet Temperatures – Volumetric Efficiency

In conclusion, while the WCAC outlet temperature had a negligible effect on the sub-assembly pressure drop, it certainly does not in terms of performance. A lower temperature will lead to a less prone to knock combustion, which can be optimally phased by increasing the spark advance to increase the BTE.

## 4.2 Maximum E-Turbo Rotational Speed Sensitivity Analysis

While the maximum achievable turbo speed in the user manual is 225 kRPM, Garrett suggests limiting the speed to 215 kRPM for a longer-lasting experience. Consequently, to study whether the lower speed was sufficient to provide adequate intake airflow, the complete engine model was used to simulate how such changes would affect the performances of PHOENICE.

As in the previous analysis, the sensitivity analysis follows the full load profile. A fixed intake charge temperature of 50°C is assumed in both cases. Moreover, while the PHOENICE engine will be mainly run with a maximum BMEP of 20 bar due to its Dedicated Hybrid Engine (DHE) application (acceptable performance scenario), the different maximum turbocharger speed is evaluated for the maximum performance scenario too.

### 4.2.1 Acceptable Performance Scenario

Figure 4-4 shows that a lower e-turbo maximum speed has a negligible effect on performance until we reach the highest engine speed. At such high RPMs, the engine needs a higher boost than what can be achieved at 215 kRPM. The decrease in BMEP is about 0.8 bar. It is worth noting that the BSFC being lower in the 215 kRPM case does not mean that a lower maximum speed lowers the BSFC. As a matter of fact, the engine is effectively producing less power, thus consuming less fuel.

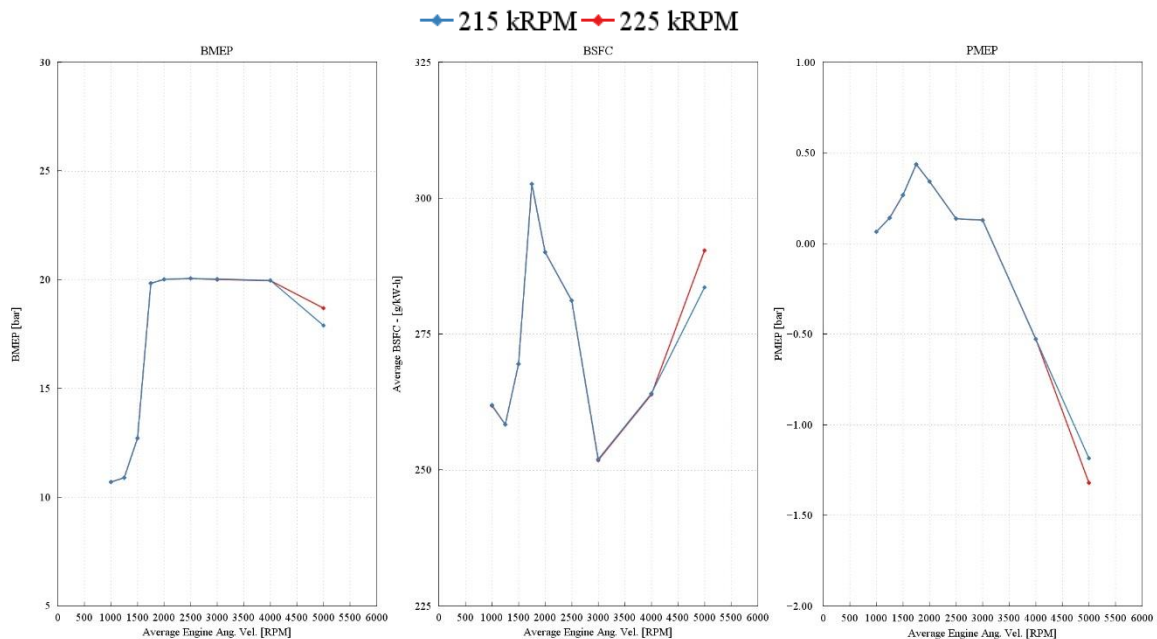


Figure 4-4 – PHOENICE Engine Performance for Different Maximum Turbocharger Speeds– MEP

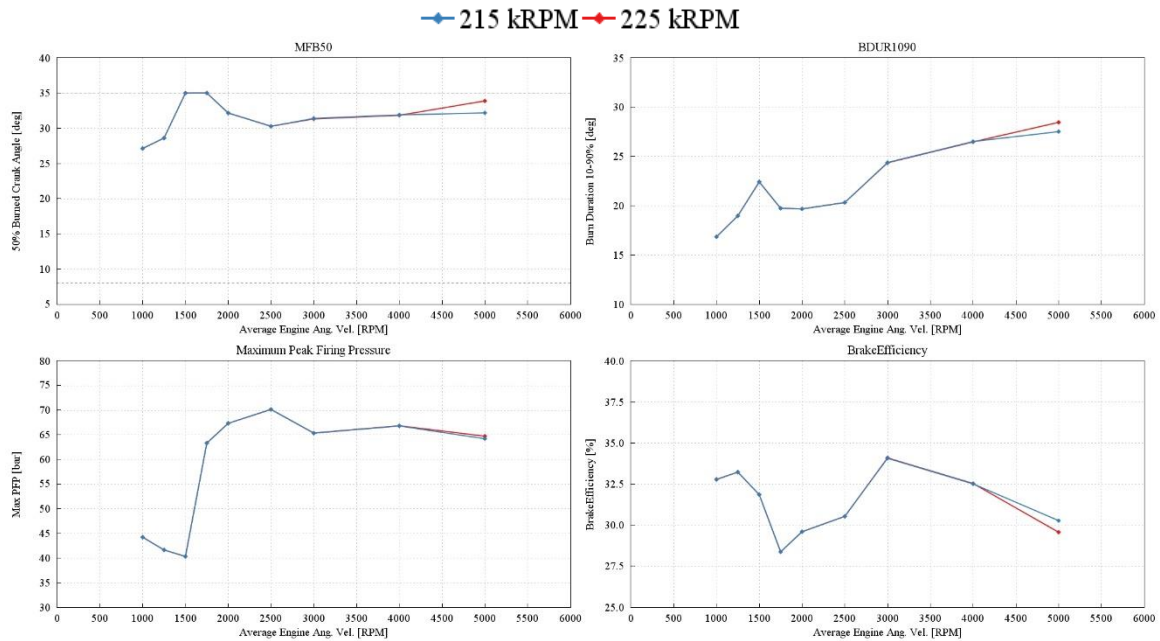


Figure 4-5 – PHOENICE Engine Performance for Different Maximum Turbocharger Speeds – Combustion Efficiency

A similar argument is evident in *Figure 4-5*, where the only difference between the two cases is at 5000 RPM. The lower BMEP of the 215 kRPM case ensures that a less retarded MFB50 can be achieved without any risk of knock. Consequently, a larger engine brake efficiency was achieved.

Finally, while the volumetric efficiency remains unchanged, lower boost pressure and a lower compressor speed are achieved in the 215 kRPM case, as shown in *Figure 4-6*.

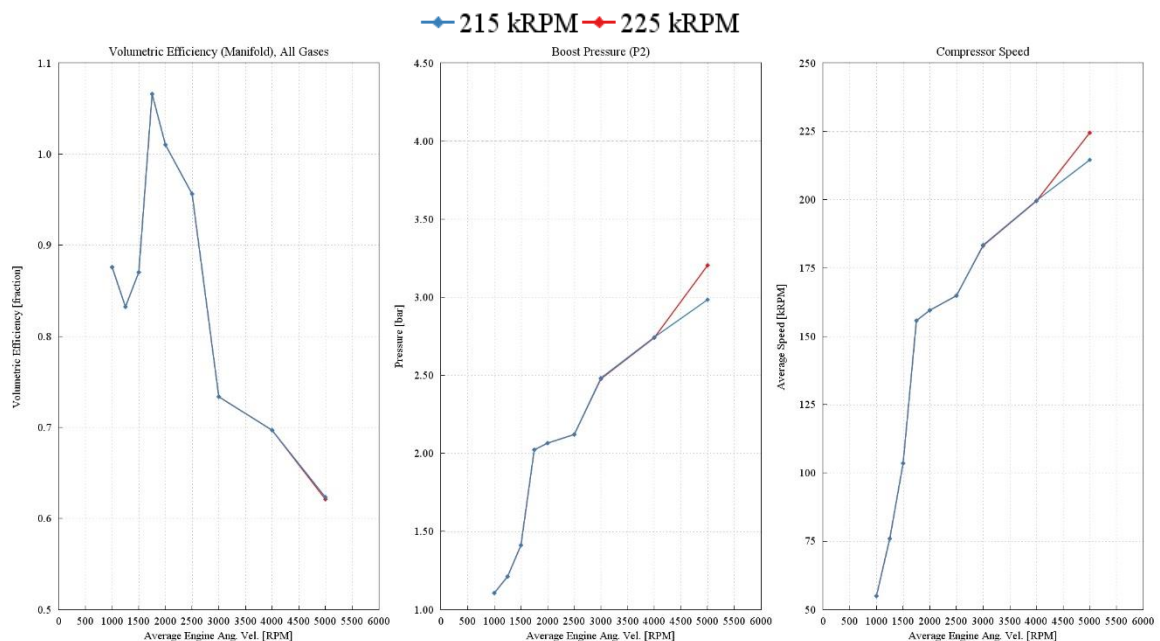


Figure 4-6 – PHOENICE Engine Performance for Different Maximum Turbocharger Speeds – Volumetric Efficiency

The results shown in *Figure 4-6* are also evident by looking at the compressor maps of the two cases under analysis. A lower e-turbo speed will shift the operating points, represented in green in *Figure 4-7*, towards lower compression ratios that, however, are characterized by a higher efficiency.

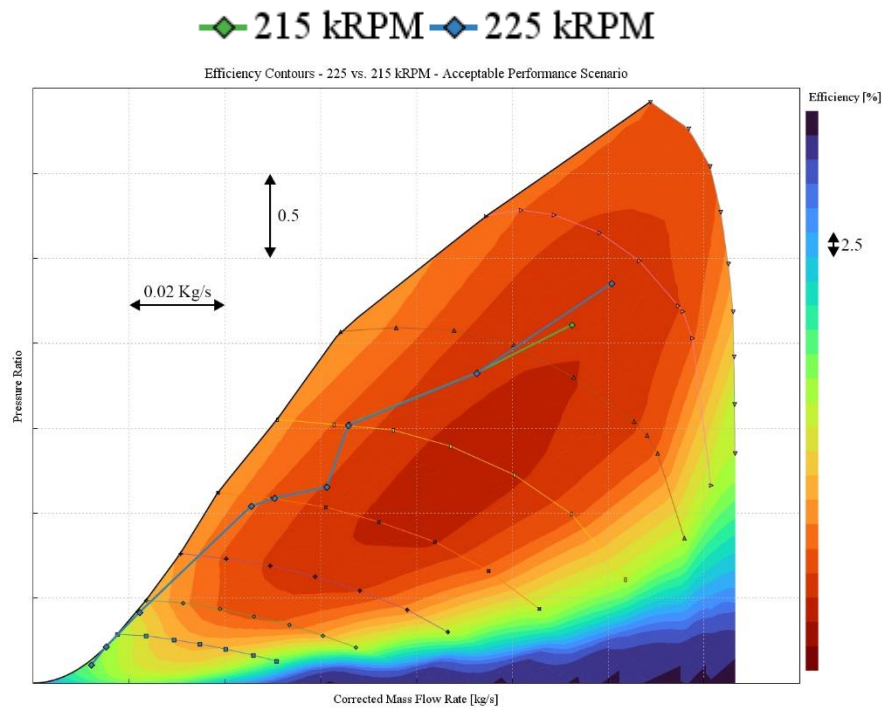


Figure 4-7 – PHOENICE Engine Performance for Different Maximum Turbocharger Speeds – Compressor Maps

### 4.2.2 Maximum Performance Scenario

The 20 bar BMEP limit was removed, and the engine could develop peak performance. However, this change did not affect the results much. As a matter of fact, the only difference between the unlimited and limited models is the fact that the BMEP reduction now also happens at 4000 RPM. The reason, once again, is due to the lower achievable boost. The BMEP reduction was 0.8 bar in this case too.

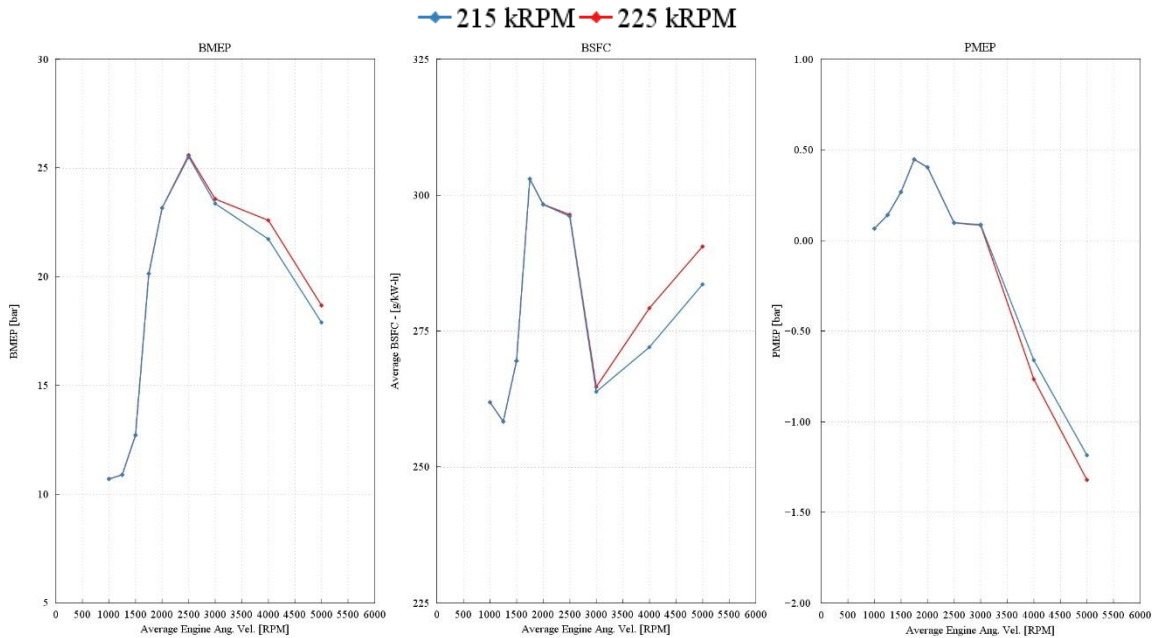


Figure 4-8 – PHOENICE Engine Performance for Different Maximum Turbocharger Speeds– uncapped BMEP MEP

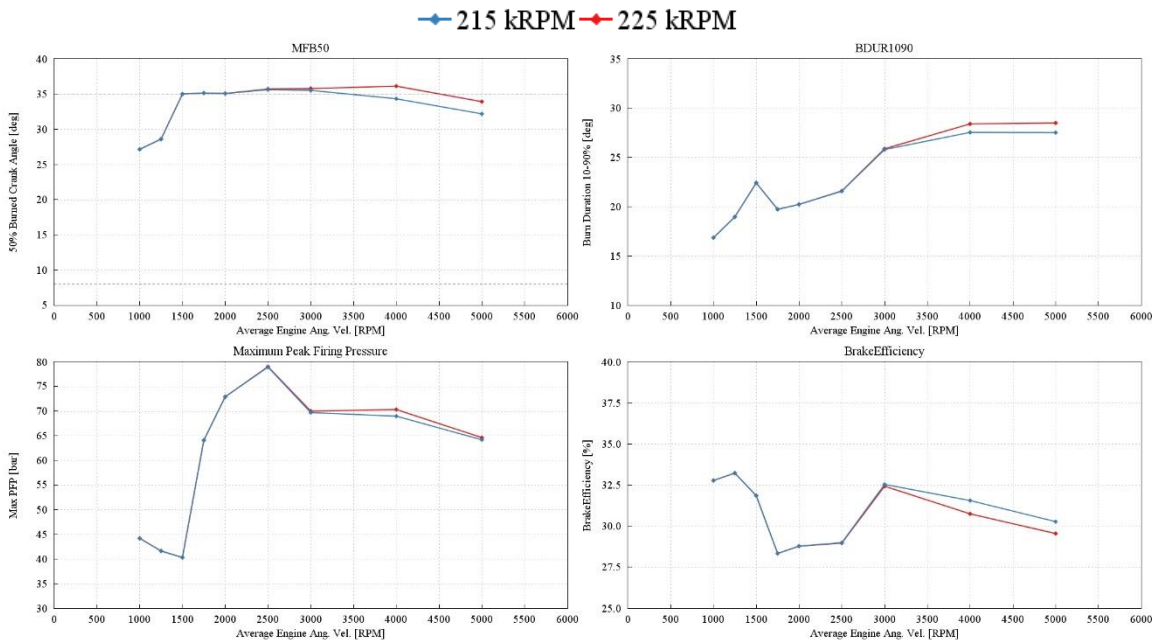


Figure 4-9 – PHOENICE Engine Performance for Different Maximum Turbocharger Speeds – uncapped BMEP Combustion Efficiency

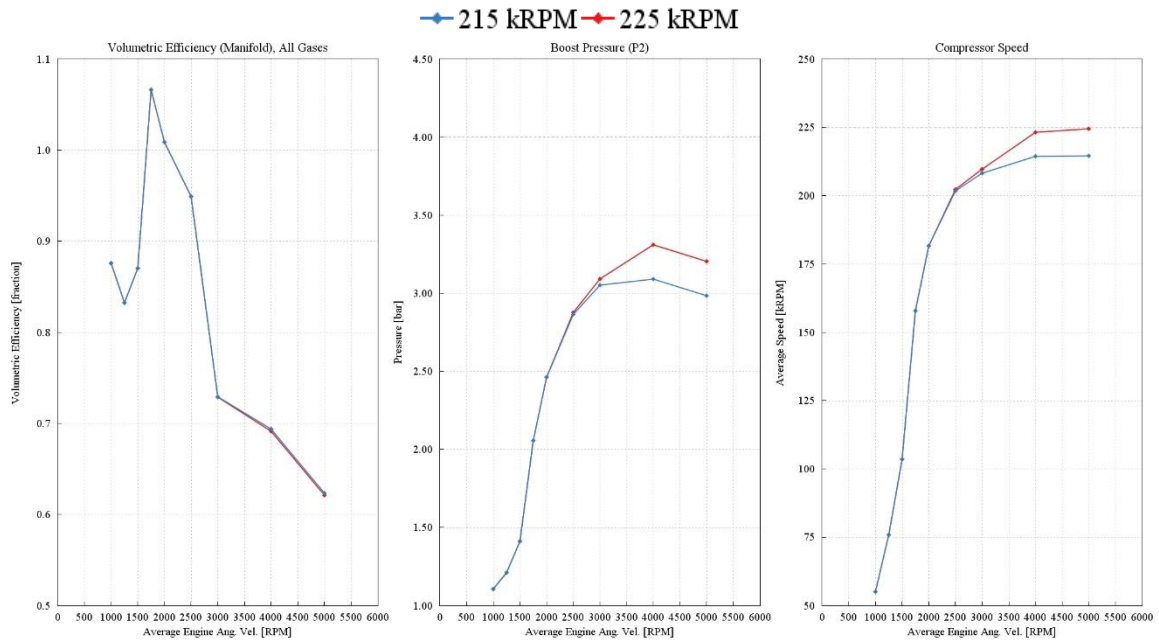


Figure 4-10 – PHOENICE Engine Performance for Different Maximum Turbocharger Speeds – uncapped BMEP Volumetric Efficiency

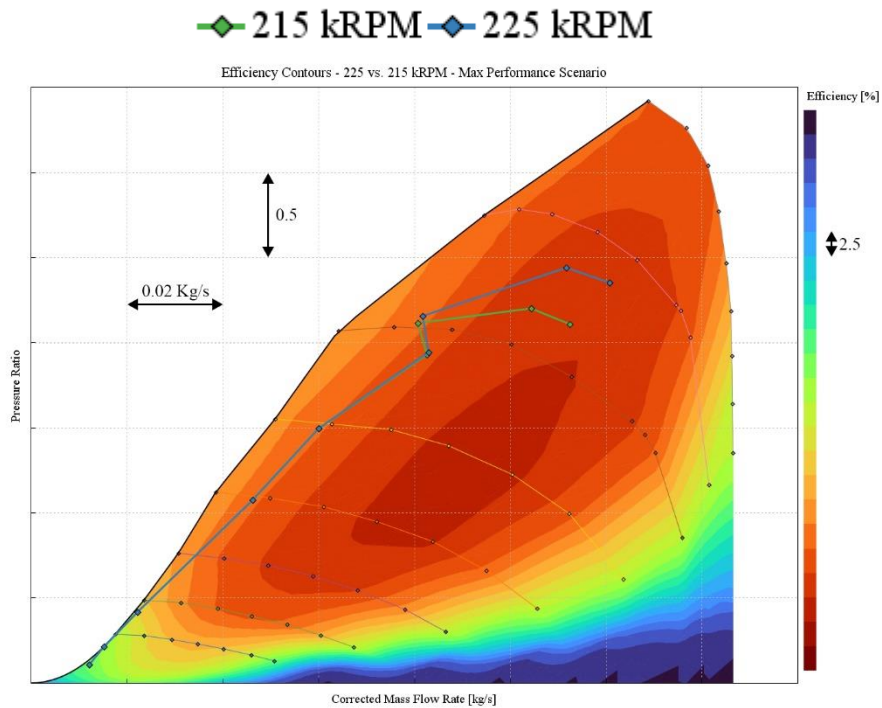


Figure 4-11 – PHOENICE Engine Performance for Different Maximum Turbocharger Speeds – max BMEP Compressor Maps

In conclusion, it is evident that, in both the limited and unlimited BMEP cases, the effect of a lower maximum turbocharger speed is negligible at low to medium loads, whereas it only has a minor influence at high RPMs.

### 4.3 Intake Valves Strategy Optimization

On top of the performance sensitivity analyses, IFPEN requested assistance to optimize the valve lifts of the MultiAir system. As a matter of fact, employing the VVA system, the PHOENICE engine can optimize the valve lifts at different operating conditions to minimize the BSFC.

The standard procedure to optimize the lifts involves testing many combinations of Intake Valve Opening (IVO) and Intake Valve Closure (IVC) for each operating point and selecting the most optimal combination. However, such an experimental campaign requires many hours in the testing facility, resulting in high costs.

Having at disposal a virtual tool, like the one created in this research activity, enables major time and cost savings as the majority of the tests can be simulated on a computer, and only the more relevant combinations have to be bench tested.

For these reasons, a full factorial Design of Experiment (DoE) was carried out on the digital twin to perform a sensitivity analysis on the intake valve phasing with the goal of minimizing the BSFC.

#### 4.3.1 Methodology and Boundary Conditions

The PHOENICE engine available at the IFPEN facility was not equipped with all the project features. As a matter of fact, both the exhaust line and the turbocharger were the baseline GSE-T4 ones. However, this is fine for the proposed virtual test bench, as the parametric engine model can quickly switch between different configurations.

The analysis was initially performed with the test bench configuration, which from now will be called the baseline, and subsequently repeated for the fully PHOENICE configuration, including the new exhaust line and turbo, and a so-called hybrid configuration, consisting of the baseline one with the PHOENICE turbo. The three configurations are graphically summarized in *Figure 4-12*.

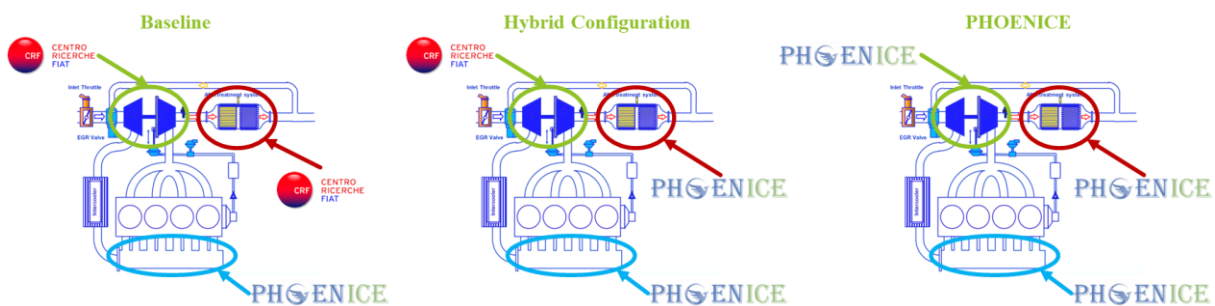


Figure 4-12 – VVA DoE Different Engine Configurations

Moreover, it is worth remembering the differences between the PHOENICE and the baseline components.

Intake System	Turbocharger	Exhaust Line
PHOENICE Swamble + LP EGR + WCAC	Wastegate Turbine	cc: TWC+GPF
	PHOENICE VNT E-Turbo	cc: EHC+2xTWC+GPF uE No -Ox+SCR+WHR

Figure 4-13 – VVA DoE Sub-assemblies' differences

It must be noted that, at the time of the analysis, the underfloor bricks of the PHOENICE exhaust line were yet to be discretized and tuned for pressure losses. Nonetheless, the two pressures are very similar at the mass flow rates achieved in the analysis.

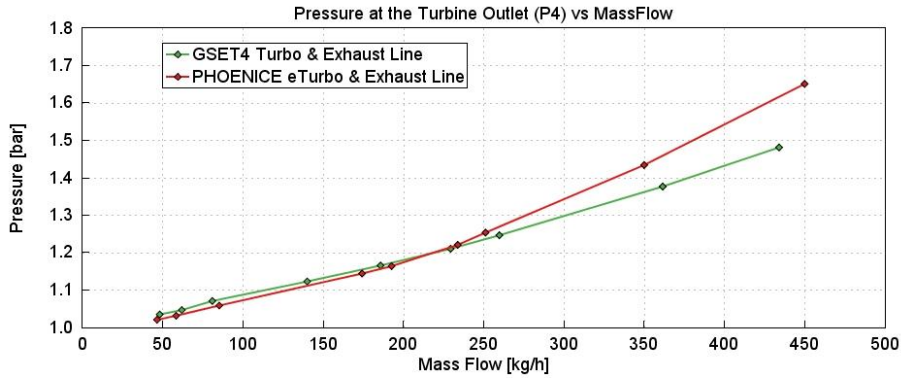


Figure 4-14 – Exhaust Back Pressure: GSE-T4 vs. PHOENICE

For each configuration, six operating points were considered. The key points were defined by FEV and IFPEN and are representative of both low and high-load conditions. All the operating points, displayed in *Table 4-1*, were to be run on a stoichiometric mixture with no EGR, as that is what was implemented on the actual engine test bench.

Key Points	Engine Speed [RPM]	Engine BMEP [bar]
1	1500	2
2	1500	5.5
3	2000	13.5
4	2600	15
5	3000	7
6	3000	13

Table 4-1 – VVA DoE Key Operating Points

To limit the simulation results file, a different GT-POWER model was made for each key operating point and each configuration. A DoE analysis results in a very large results file due to the many different configurations tested for each point. Indeed, with respect to the 720° cyclic engine scale, the allowed eIVO range was 305° to 395° with ten levels, whereas the eIVC range was 480° to 680° with 21 levels. Thus, for each key point, 210 different eIVC-eIVO combinations were considered.

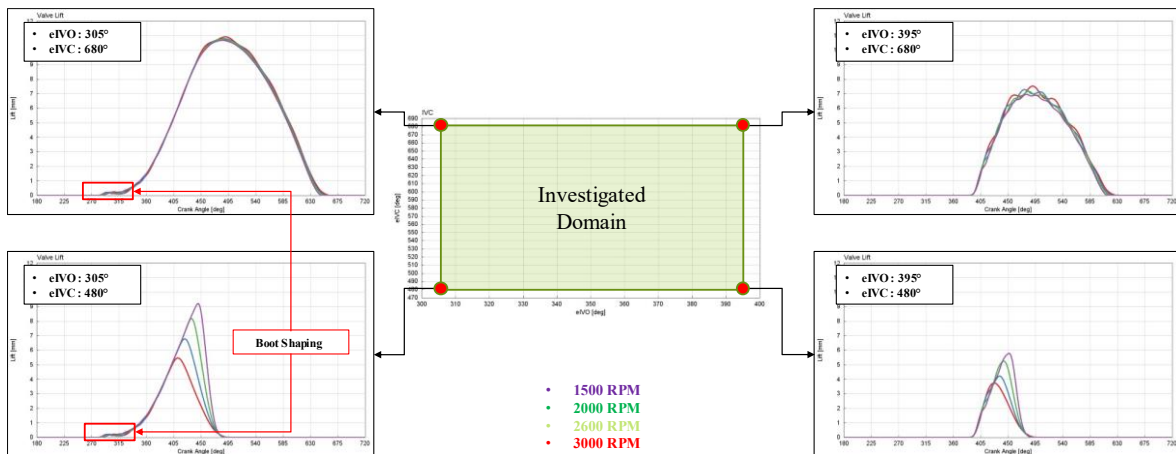


Figure 4-15 – Investigated eIVO – eIVC DoE Area

### 4.3.2 Results Analysis – Baseline Configuration

The results analysis will mainly focus on the 3000 RPM x 7 bar key point of the baseline configuration, however, similar considerations applied for the other ones too.

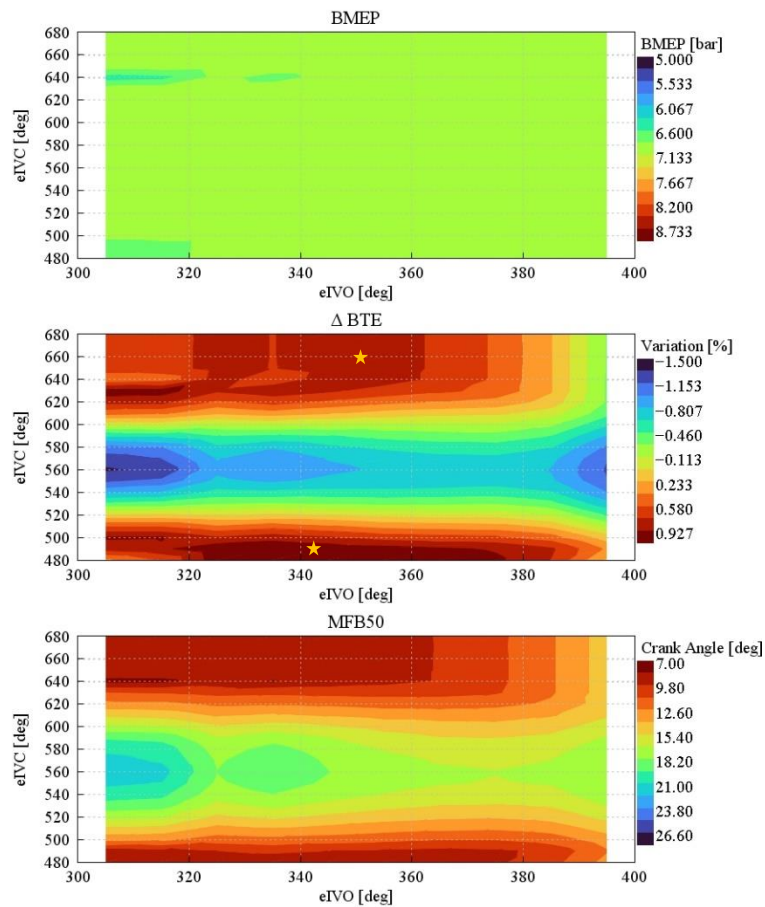


Figure 4-16 – VVA DoE 3000 RPM x 7 bar BMEP – BMEP, BTE and MFB50

Figure 4-16 shows how the engine can reach the target BMEP for any combination of IVO and IVC, however, looking at the anchor angle plots, it is evident that Late Intake Valve Closure (LIVC or late Miller) and Early Intake Valve Closure (EIVC or early Miller) offer a more optimally phased combustion. Recall that the ideal MFB50 is between 8 and 10°. The more optimally phased combustion for LIVC and EIVC is confirmed by the higher Brake Thermal Efficiency (BTE). As a matter of fact, a delta up to 1% higher BTE can be observed when exploiting Miller cycles. This happens for EIVC values close to 490°CA aTDCf and LIVC values between 640 to 680°CA aTDCf, respectively. While early Miller can reach higher efficiencies, late Miller can hold that high efficiency over a more significant portion of the map, allowing for some inaccuracy in the valve actuation. On the contrary, a zone of delayed combustion can be seen for IVC of around 560°CA.

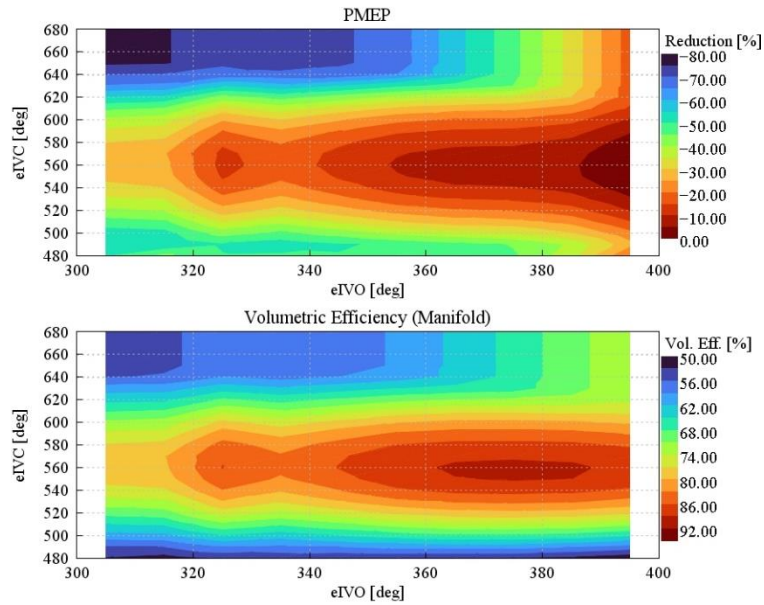


Figure 4-17 – VVA DoE 3000 RPM x 7 bar BMEP – PMEP and Volumetric Efficiency

A considerable reduction of the pumping losses can be observed, in *Figure 4-17*, due to the significant amount of de-throttling that happens for highly anticipated or retarded IVC in *Figure 4-18*.

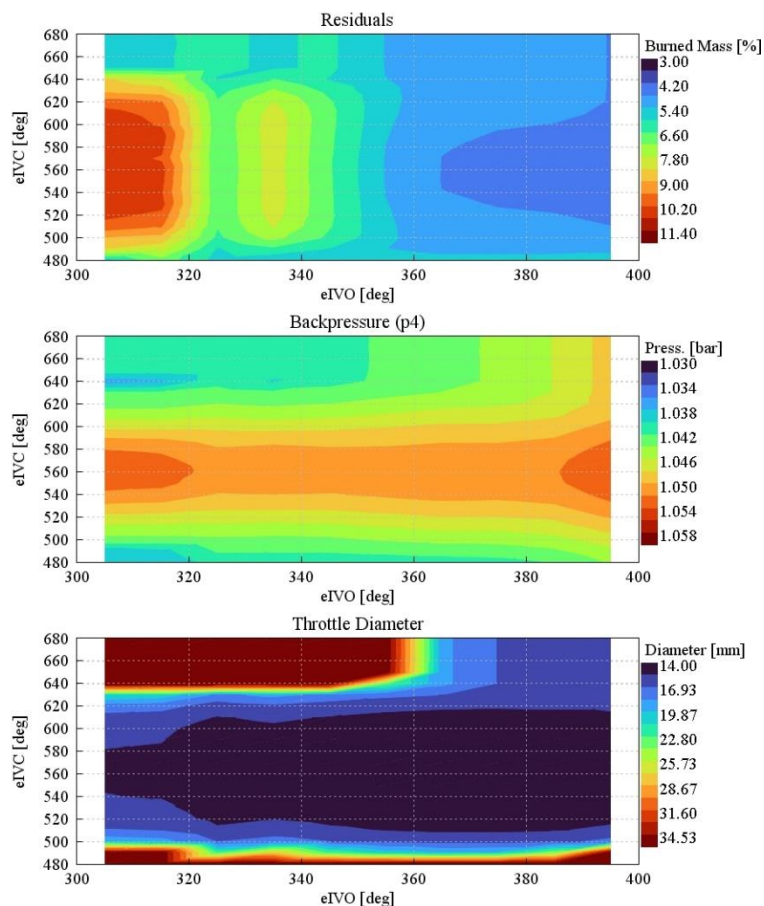


Figure 4-18 – VVA DoE 3000 RPM x 7 bar BMEP – Residuals, Backpressure and Throttling

Moreover, the high level of residuals for IVC values around 560°CA aTDCf explains the previously commented delayed combustion zone.

### 4.3.3 Experimental Validation

Figure 4-19 pictures the first engine prototype assembled and installed on the IFPEN test facility for preliminary experimental validations. As previously stated, the prototype did not include all the PHOENICE features and was run under stoichiometric conditions without EGR flow. This set-up is represented in the DoE model by the baseline configuration.



Figure 4-19 – PHOENICE Engine prototype at IFPEN test facility [22]

The prototype was run over the defined key points for different valve lift combinations. As can be seen from Figure 4-20, the correlation between experimental and simulation results is more than satisfactory. Both numerical and experimental findings provide consistent estimates of the BTE increases achieved by optimizing the valve lifts with either an EIVC or a LIVC strategy, with a slight edge for LIVC. Moreover, the experimental campaign also confirmed that the worst efficiency values are achieved in an area of IVC near 560°CA aTDCf.

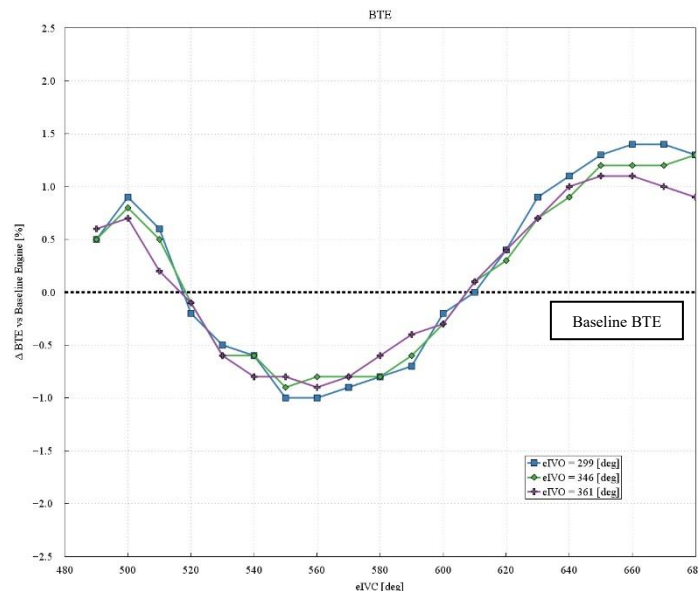


Figure 4-20 – 3000 RPM x 7 bar BMEP Experimental Results: BTE Improvements

This initial experiment is highly encouraging because, even in stoichiometric conditions without EGR, a significant boost in efficiency could be obtained. This emphasizes the benefits of the Swumble™ intake charge motion and the higher compression ratio.

### 4.3.4 Effects of Garrett E-Turbo – Hybrid Configuration

With the baseline configuration validated by the experimental campaign, the model was rerun in the hybrid and PHOENICE configuration, yielding a preliminary estimation of the efficiency values that could be achieved with the complete set-up. Unless specified, all results refer to the 3000 RPM x 7 bar BMEP key point.

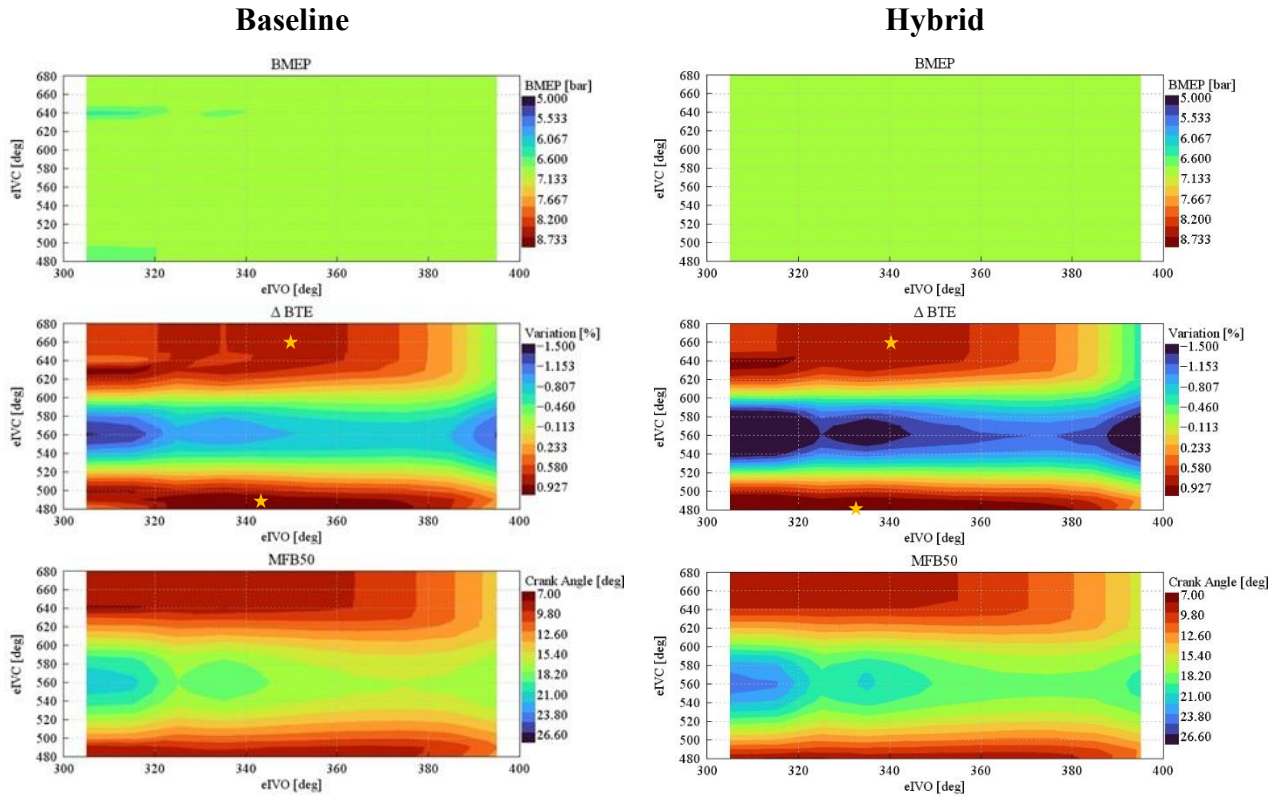


Figure 4-21 – VVA DoE 3000 RPM x 7 bar BMEP: E-Turbo Effect – BMEP, BTE and MFB50

Figure 4-21 shows how the PHOENICE E-Turbo increases the high-efficiency area. At the same time, the small areas where the target BMEP was not achieved are gone in the hybrid configuration. This is especially true in the higher load cases such as the 3000 RPM x 13 bar BMEP shown in Figure 4-22.

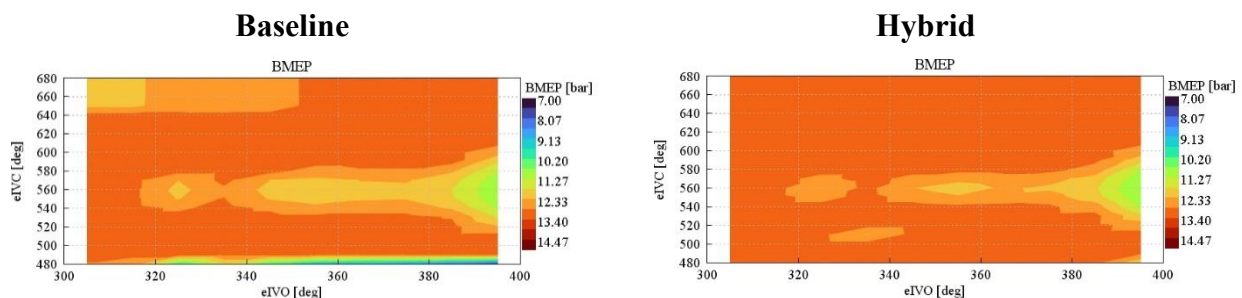


Figure 4-22 – VVA DoE 3000 RPM x 13 bar BMEP: E-Turbo Effect – BMEP

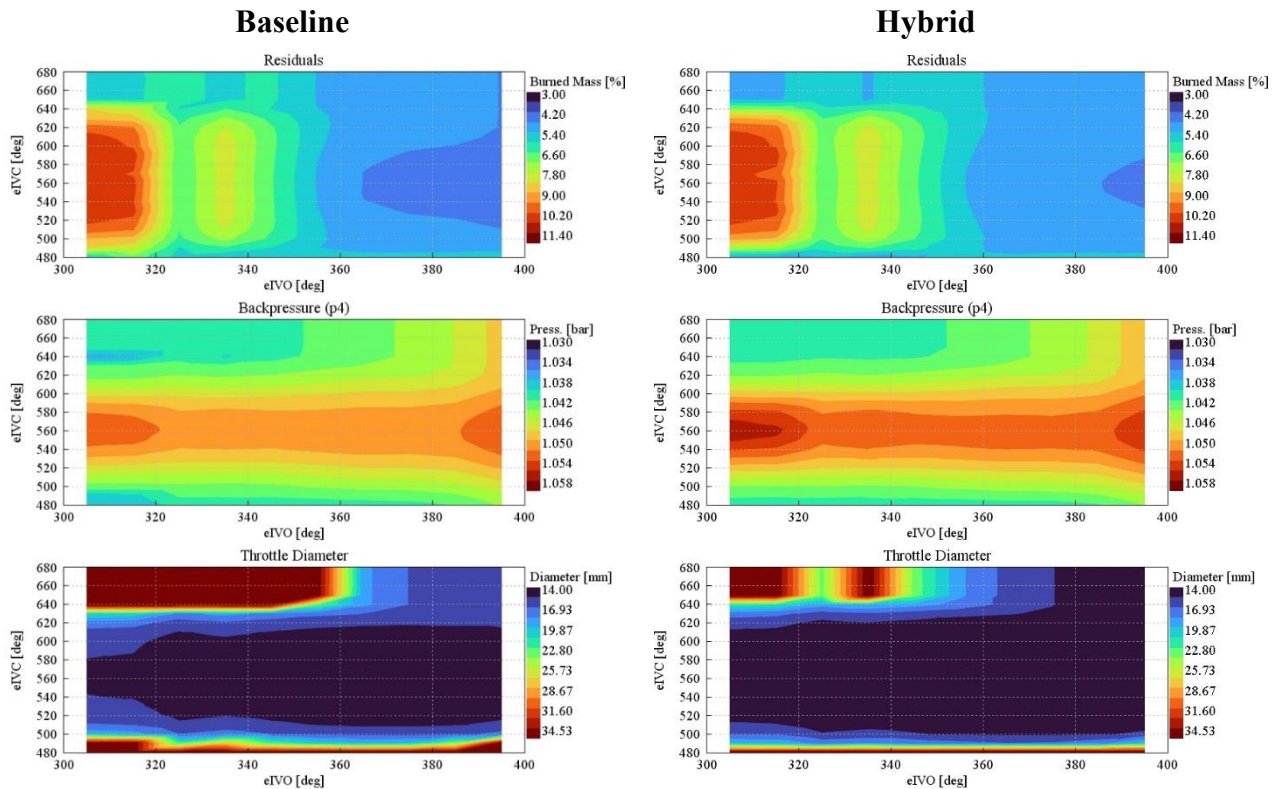


Figure 4-23 – VVA DoE 3000 RPM x 7 bar BMEP: E-Turbo Effect – Residuals, Backpressure and Throttling

While the PMEP and the residuals were not affected much, the backpressure, or pressure after the turbine outlet, is slightly increased. On top of that, it is worth highlighting how the new turbo forces more throttling. The reason behind this is that a larger minimum boost characterizes the Garret E-Turbo. Nevertheless, with the correct valve combination, throttling can be avoided.

### 4.3.5 Effects of PHOENICE Exhaust Line – PHOENICE Configuration

Finally, the PHOENICE exhaust line was also included in the model. It is worth remarking how, at the time of the simulation, the underfloor bricks of the PHOENICE exhaust line were yet to be discretized and tuned for pressure losses. Nevertheless, as seen in *Figure 4-14*, even at the key point with the highest load, the exhaust mass flow rate does not go over 180 Kg/h. Thus the backpressures will be very similar.

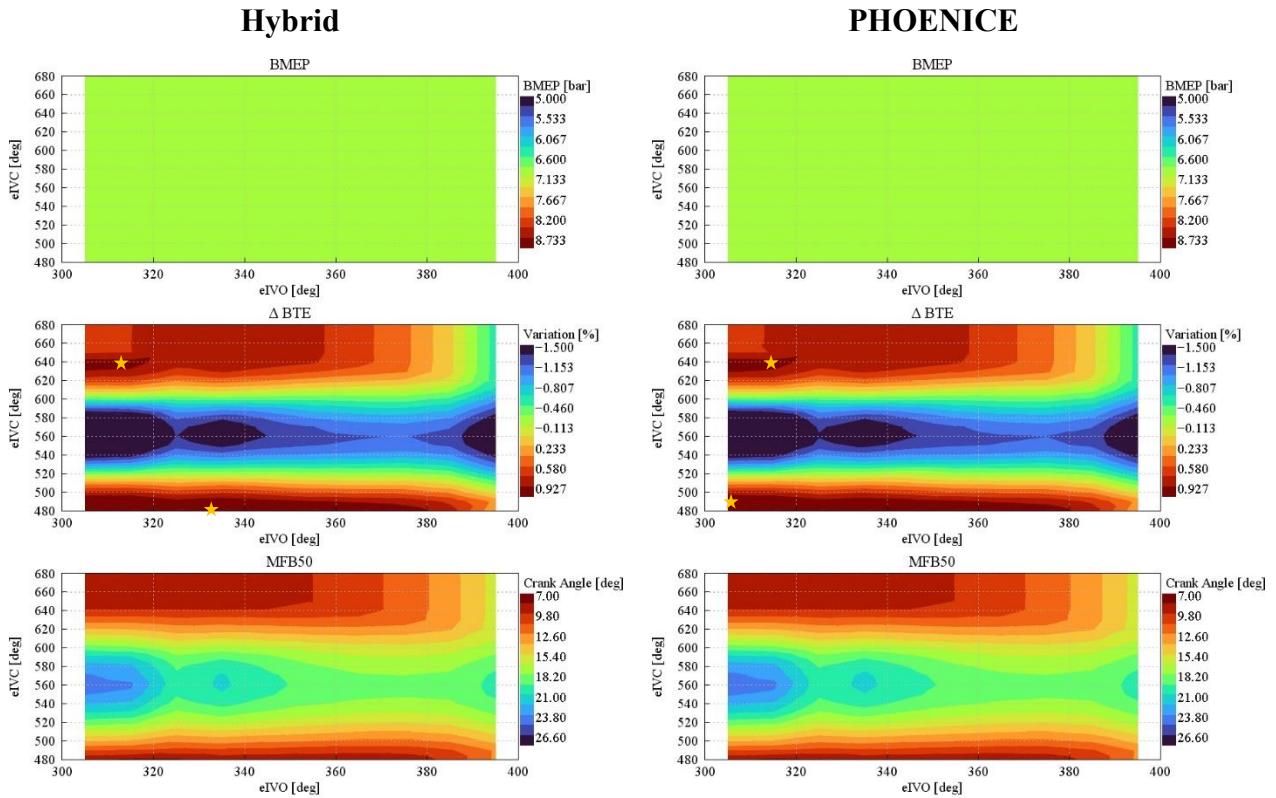


Figure 4-24 – VVA DoE 3000 RPM x 7 bar BMEP: Exhaust Line Effect – BMEP, BTE and MFB50

For the 3000 RPM x 7 bar BMEP key point, not much changes with the new exhaust line. A slight expansion of the high-efficiency area can be seen for eIVO below 320°CA aTDCf. However, switching to the higher load of 3000 RPM x 13 bar BMEP shows a further enlargement of the area where the target BMEP is reached, as shown in *Figure 4-25*.

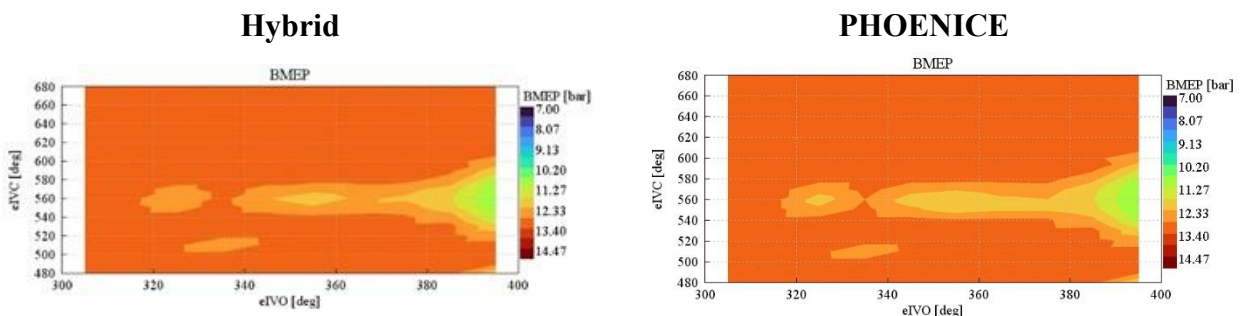


Figure 4-25 – VVA DoE 3000 RPM x 13 bar BMEP: Exhaust Line Effect – BMEP

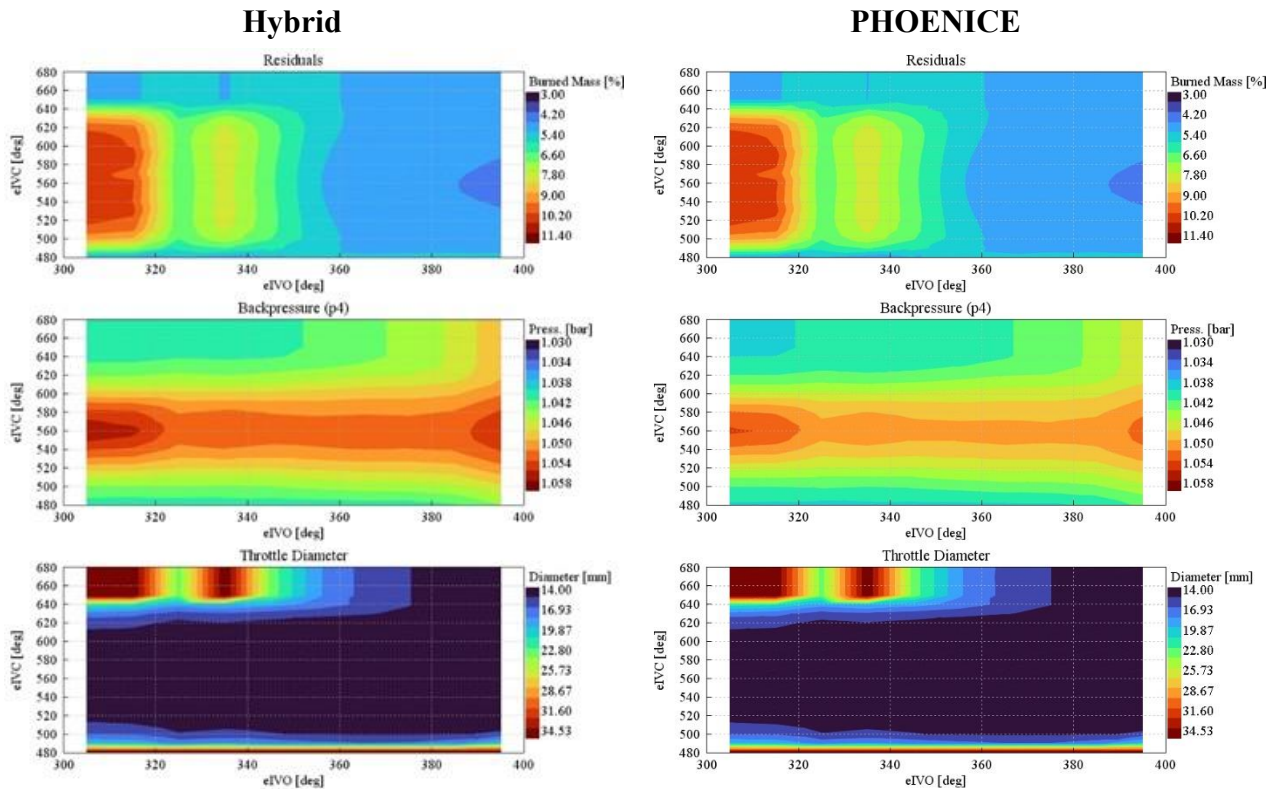


Figure 4-26 – VVA DoE 3000 RPM x 7 bar BMEP: Exhaust Line Effect – Residuals, Backpressure and Throttling

PMEP, residuals, and throttling were not affected much by the updated exhaust line. On the other hand, backpressures are slightly lower with respect to the original GSE-T4 line. However, the lack of underfloor bricks deeply affects this result

## 5 Model Correlation Against Experimental Data

The last topic covered in this research activity is the test bench validation of the virtual test rig flow lines as a function of different air-fuel ratios and EGR fractions. A Dual dilution combustion assessment was carried out in the IFPEN facility by means of an experimental campaign involving an EGR sweep for different AFR, spanning from stoichiometric to lean operation at lambda 1.43.

The experimental test measurements were used to check for consistency between the virtual test rig and the actual engine. At first, the experimental combustion was obtained from the pressure measurements and imposed in the correlation model to ensure the same initial conditions. Subsequently, the predictive combustion model was tuned to provide a preliminary steady-state evaluation of the digital twin's consistency.

### 5.1 Experimental Test Bench Description

The engine set-up used to carry out the experimental campaign is the same one described in *Chapter 4.3.3*, meaning that the PHOENICE exhaust line and the upgraded Garrett E-Turbo were unavailable. Nevertheless, to assess the capabilities of the Dual Dilution Combustion Approach (DDCA), the necessary feature is the new head design, which is responsible for the Swumble™ motion.

The Test bench set-up can be seen in *Figure 4-19* and summarized in *Figure 5-1*.

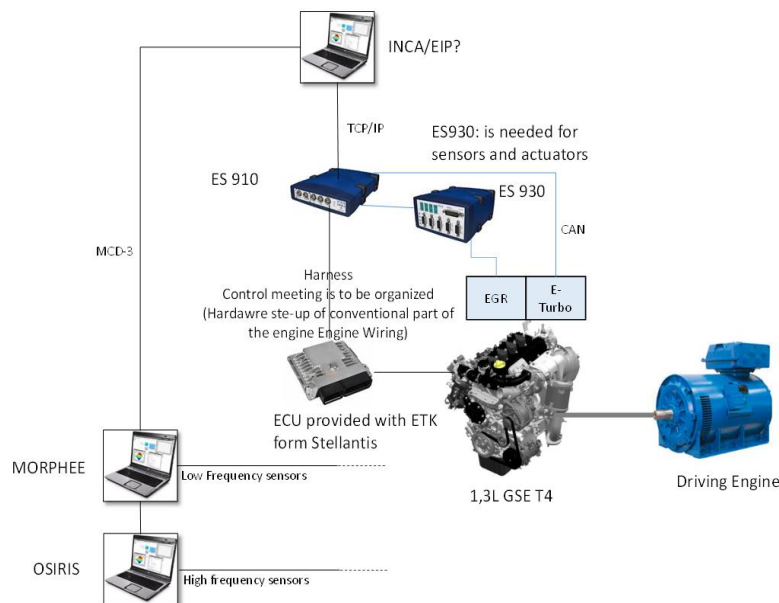


Figure 5-1 – Schematic of the PHOENICE Engine prototype at IFPEN test facility [22]

Throughout the experimental campaign, the engine is run at the fixed operating point of 3000 RPM x 7 bar BMEP by the engine brake, with fixed valve lifts  $e_{IVO} = 284.15^{\circ}\text{CA aTDCf}$ , and  $e_{IVC} = 630^{\circ}\text{CA aTDCf}$ . The EGR valve, the EGR flap, and the turbocharger were controlled accordingly to ensure the correct EGR fraction and air flow rate for engine dilution.

Indeed, 18 combinations were tested at the fixed operating point 3000 RPM x 7 bar BMEP as shown in *Table 5-1*.

#Test	$\lambda$	EGR Fraction [%]
1	1	0
2	1	5.2
3	1	10
4	1	15.2
5	1	20.6
6	1	21.5
7	1.11	0
8	1.11	5.3
9	1.11	9.8
10	1.11	15.1
11	1.11	20.1
12	1.25	0
13	1.25	5.1
14	1.25	10
15	1.25	14.4
16	1.43	0
17	1.43	5.2
18	1.43	7.2

Table 5-1 – IFPEN DDCA Assessment: EGR and Lambda Sweep Combinations

The PHOENICE engine was equipped with a vast set of sensors to measure all the relevant quantities, which can be split into two families: fast and slow measurements. Fast sensors are characterized by a very short sampling time, 0.1°C. They are mainly used to obtain the in-cylinder pressure evolution and the pressure evolution in the intake and exhaust manifold. Slow sensors, on the other hand, provide less accurate time-averaged results. They included pressure and temperature sensors and were located in the main areas of relevance in the flow lines, before and after the main components.

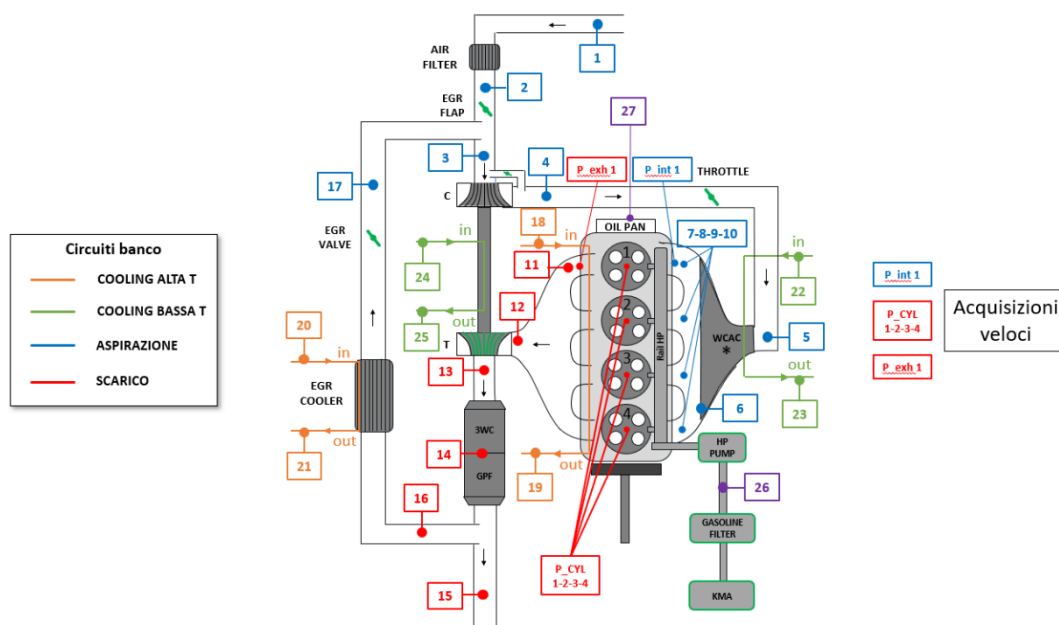


Figure 5-2 – IFPEN Test Bench Sensors Layout

## 5.2 Cylinder Pressure Only Analysis

For the model to be consistent with the existing prototype, it should be able to correctly predict the pressure and temperature values recorded by the slow sensors during the experimental campaign. However, for this condition to be met, it is crucial that the combustion closely resembles the experimental one. As a matter of fact, different combustion speeds and phasing will inherently alter the pressure and temperature evolution along the flow lines.

To ensure that the two combustions are equal, GT-POWER allows the user to perform the reverse run needed to calculate the burn rate from the measured cylinder pressure. This kind of simulation is called a reverse run as it proceeds in the opposite direction with respect to a standard engine simulation. As a matter of fact, in a typical engine simulation, the burn rate is the input from which cylinder pressures are derived. The opposite happens for a reverse run.

While GT-POWER offers more than one approach to this problem, the one employed in this thesis is called Cylinder Pressure Only Analysis (CPOA). CPOA is a standalone calculation that can be carried out in a separate simplified engine model with only a few input data. The model to be built for this analysis is trivial as it includes only two components: the Engine and Cylinder templates, as is shown in *Figure 5-3*. Valves, ports, and beyond are not necessary.

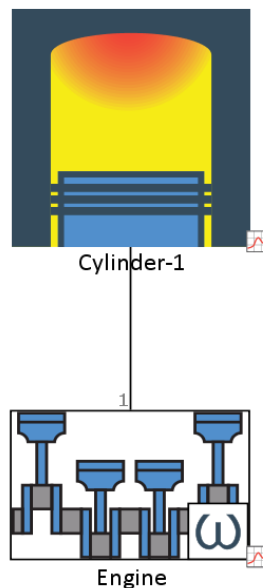


Figure 5-3 – GT-POWER 1D CFD Cylinder Pressure Only Analysis (CPOA) model

The input data required includes the engine geometry, cylinder wall temperatures, a heat transfer model, and general initial conditions. Particular attention should be used when evaluating such initial conditions as CPOA only simulates the closed volume portion of the cycle, thus, the information provided is representative of the trapped conditions for the combustion event. Such initial conditions include the volumetric efficiency, the air trapping ratio, the injected fuel mass, and the residual gas fraction. Moreover, the provided in-cylinder pressure cycle can be either a single cycle or an ensemble average of many cycles. This research activity used a single cycle, an average of the four individual cylinder cycles.

The methodology of a CPOA simulation is the following:

1. A preliminary evaluation of the burn rate is obtained from the cylinder pressure making some assumptions on the heat transfers.
2. This burn rate is then used to make a forward simulation to obtain the real heat transfers.
3. A final burn rate evaluation is made using the real heat transfers and the available results.
4. Lastly, the final burn rate is applied in a second forward run to compare measured and simulated values.

While CPOA is a relatively simple study that only requires a few input data, on the other hand, its main limitation is that some required parameters (i.e., trapping ratio and residual gas fraction) are difficult or impossible to measure in the test bench.

For the sake of this analysis, such information was initially derived from the VVA DoE analysis covered in *Chapter 4.3* and subsequently iterated with the complete engine model to obtain the definitive values.

The main parameters used to check the accuracy of the CPOA results are the consistency checks, the Lower Heating Value (LHV) multiplier, the compression heat release, and the overall matching between the simulated and measured pressure over volume evolution. *Figure 5-4* summarizes the obtained results. From the literature <sup>[21]</sup>, for a good combustion match, all the consistency checks should be within the acceptable ranges, the LHV multiplier should be as close as possible to one with a tolerance of 5%, and the compression heat release should be as close as possible to 0 with a 2% tolerance. The shown results satisfy all the above requirements and, looking at the log-P log-V plot, a good match between the experimentally measured and simulated evolutions can be seen.

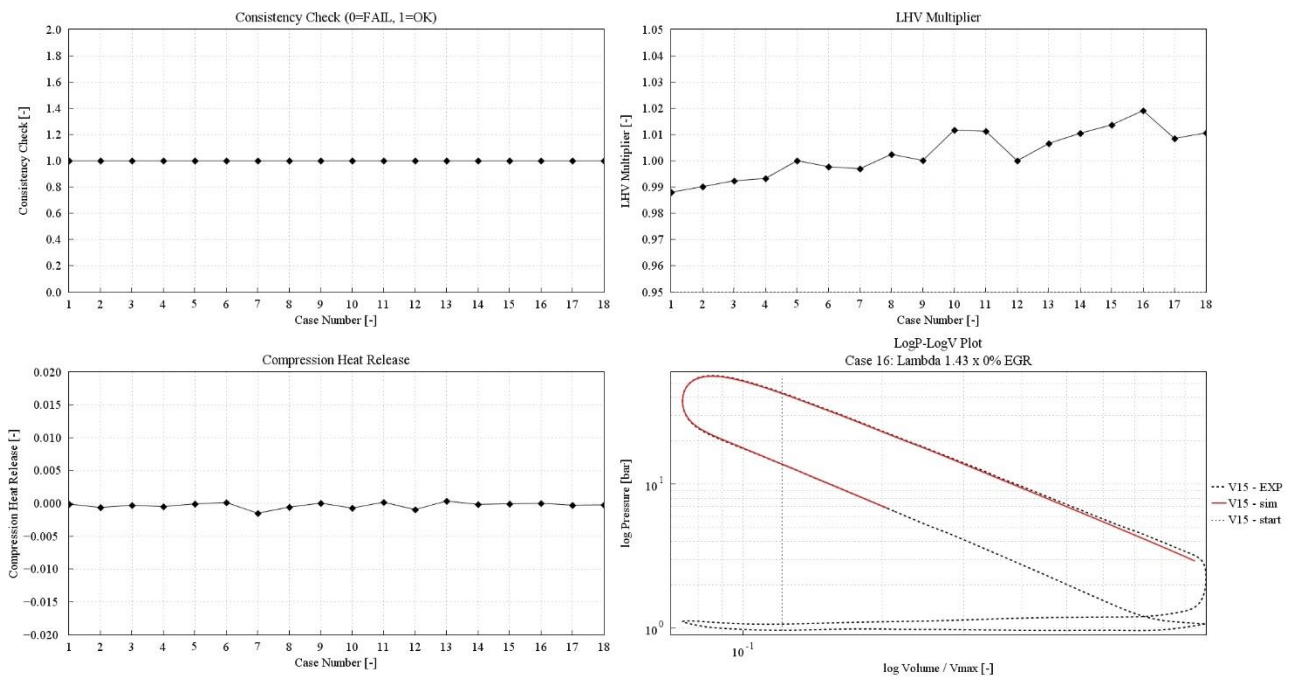


Figure 5-4 – CPOA Simulation Results

Finally, the simulated combustion was implemented in the complete model as a non-predictive fixed combustion with the EngCylCombProfile template. Non-predictive templates impose a burn rate as a function of the crank angle that will be followed regardless of the conditions in the cylinder if sufficient fuel is present.

As in this case study the main focus is to check the correlation between simulated and experimental pressures and temperatures, the combustion evolution should be the same. CPOA analysis automatically generates an EngCylCombProfile object to be copied into the model of interest.

The generated EngCylCombProfile follows the burn rate in *Figure 5-5*.

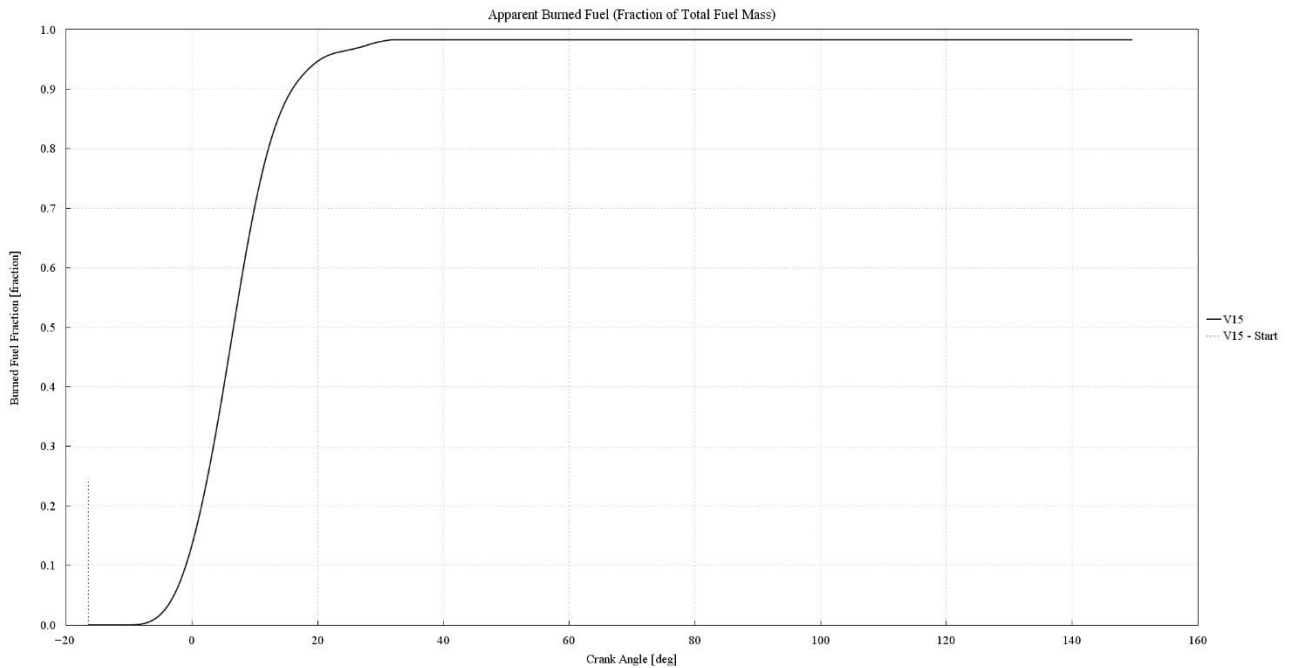


Figure 5-5 – CPOA generate burn profile

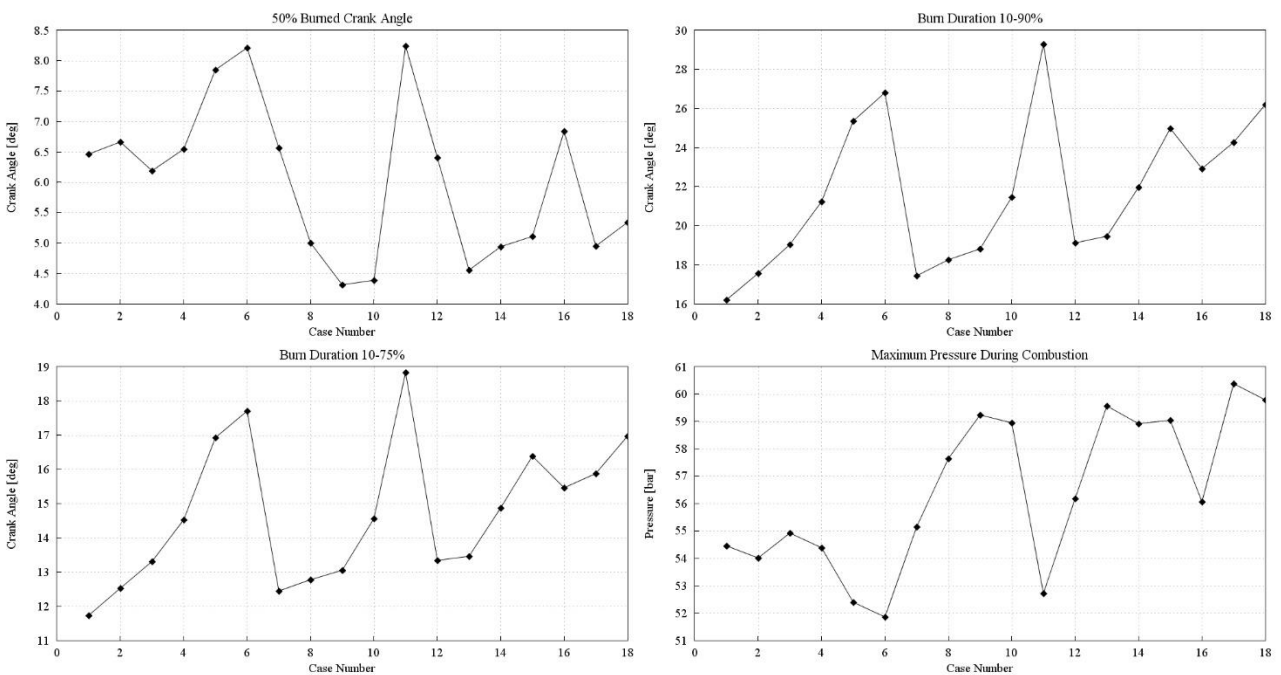


Figure 5-6 – CPOA Combustion main parameters

### 5.3 Correlation Model and Results

Having now fixed the combustion profile, more model tuning is necessary to match the experimental conditions. Indeed, to guarantee the same operating conditions, some test variables were imposed in the model. As a matter of fact, the turbocharger model should target the experimental boost pressure. Similarly, the EGR valve should be actuated to target the EGR fraction. Moreover, the WCAC outlet temperature and the ambient conditions should match the experimental condition. The engine coolant and oil temperature were also imposed.

Import_SPE_Data				
Parameter	Unit	Description	Case 1	
Case On/Off		Check Box to Turn Case On	<input checked="" type="checkbox"/>	
Case Label		Unique Text for Plot Legends	<3000x7_Polito_EGR_allR_GTP_Export.xlsx#Lambda_1#56#56#4#4>...	
Excel_File		Excel file name to import experimental bench data	3000x7_Polito_EGR_allR_GTP_Export.xlsx	
Sheet_Name		Sheet name containing the expe test data	Lambda_1	
Row_Start		Excel starting row	4	
Row_End		Excel last row	4	
Lambda_SPE		SPE AFR	<3000x7_Polito_EGR_allR_GTP_Export.xlsx#Lambda_1#56#56#4#4>	
EGR_SPE		SPE EGR Fraction	<3000x7_Polito_EGR_allR_GTP_Export.xlsx#Lambda_1#42#42#4#4>	
eIVO_SPE		SPE eIVO	<3000x7_Polito_EGR_allR_GTP_Export.xlsx#Lambda_1#37#37#4#4>	
eIVC_SPE		SPE eIVC	<3000x7_Polito_EGR_allR_GTP_Export.xlsx#Lambda_1#38#38#4#4>	
SA_SPE		SPE Spark Advance	<3000x7_Polito_EGR_allR_GTP_Export.xlsx#Lambda_1#41#41#4#4>	
SOI_SPE		SPE SOI	<3000x7_Polito_EGR_allR_GTP_Export.xlsx#Lambda_1#39#39#4#4>	
RailP_SPE		SPE Rail Pressure	<3000x7_Polito_EGR_allR_GTP_Export.xlsx#Lambda_1#40#40#4#4>	
P_amb_SPE		SPE Ambient Pressure	<3000x7_Polito_EGR_allR_GTP_Export.xlsx#Lambda_1#48#48#4#4>	
P_amb_EGR_Flap		SPE PO	<3000x7_Polito_EGR_allR_GTP_Export.xlsx#Lambda_1#49#49#4#4>	
T_amb_SPE		SPE Ambient Temperature	<3000x7_Polito_EGR_allR_GTP_Export.xlsx#Lambda_1#13#13#4#4>	
T_after_EGR_Flap		SPE T0	<3000x7_Polito_EGR_allR_GTP_Export.xlsx#Lambda_1#14#14#4#4>	
P2_SPE		SPE Boost Pressure	<3000x7_Polito_EGR_allR_GTP_Export.xlsx#Lambda_1#10#10#4#4>	
TS_SPE		SPE Intake Manifold Temperature	<3000x7_Polito_EGR_allR_GTP_Export.xlsx#Lambda_1#17#17#4#4>	
T_eGRC_SPE		SPE EGRC Outlet Temperature	<3000x7_Polito_EGR_allR_GTP_Export.xlsx#Lambda_1#27#27#4#4>	
T_Oil_SPE		SPE Engine Oil Temperature	<3000x7_Polito_EGR_allR_GTP_Export.xlsx#Lambda_1#43#43#4#4>	
T_Coolant_SPE		SPE Engine Coolant Temperature	<3000x7_Polito_EGR_allR_GTP_Export.xlsx#Lambda_1#44#44#4#4>	
FMEP_SPE	bar	SPE Friction Losses	<3000x7_Polito_EGR_allR_GTP_Export.xlsx#Lambda_1#54#54#4#4>...	

Figure 5-7 – Import of Experimental data from excel in GT-POWER case set-up

While the ambient conditions were directly implemented into the case set-up, the different temperatures required a HeatExchangerConn to force the experimental measurement. On the other hand, matching the BMEP, the boost pressure, and the EGR fraction is more complicated. As a matter of fact, during the test campaign, no measurements regarding the throttle, the turbocharger's wastegate, or even the EGR valve diameter were made. Consequently, to match these variables, PID controllers were used. The existing controllers' sub-assembly, shown in Figure 5-8, was simplified and implemented in the model.

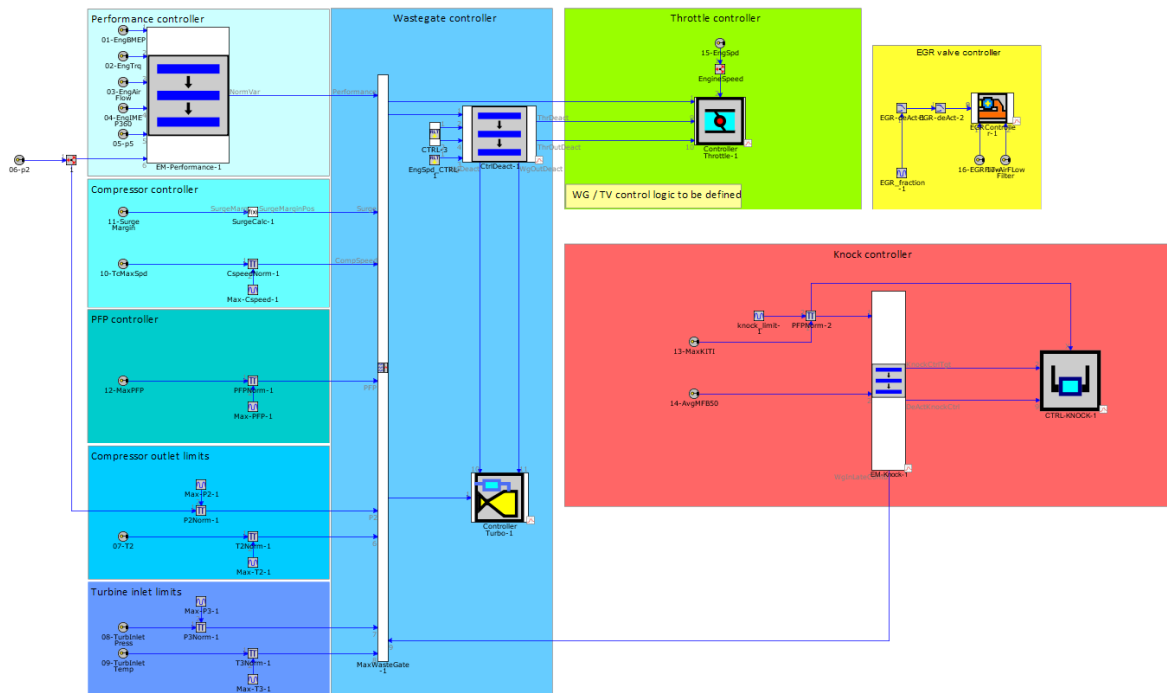


Figure 5-8 – Main model controllers' sub-assembly

The knock controller was used to impose the spark advance such that knock would not occur or would be limited. As the combustion was imposed, such a controller was no longer needed. Similarly, as 3000 RPM x 7 bar BMEP is a low-load operating point, the turbocharger operates far from the surge and operating limits. For this reason, the turbo controller was also simplified.

The final controllers' sub-assembly is shown in *Figure 5-9*.

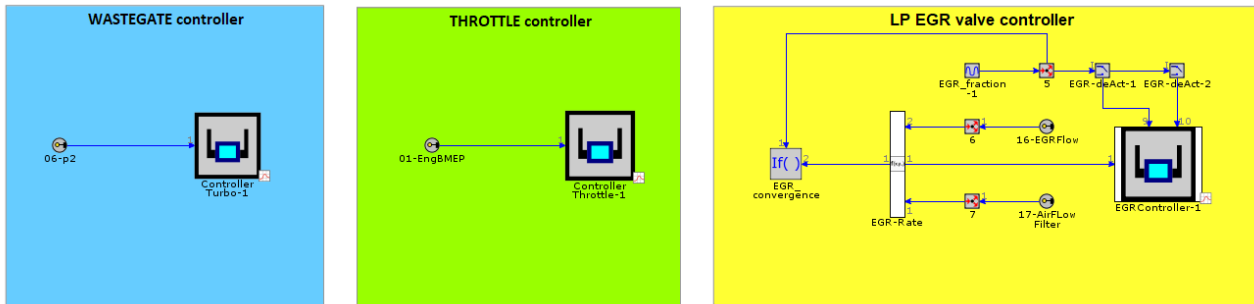


Figure 5-9 – Correlation model controllers' sub-assembly

It is worth noting that the main model used the GT-POWER-specific model-based controllers, whereas, in the correlation model, they were changed to PIDs. This is because while GT-POWER provides simple model-based controllers that do not require tuning for specific applications, they are not always the better performing. As a matter of fact, when simulating the correlation model with the model-based controllers, oscillations of results occurred.

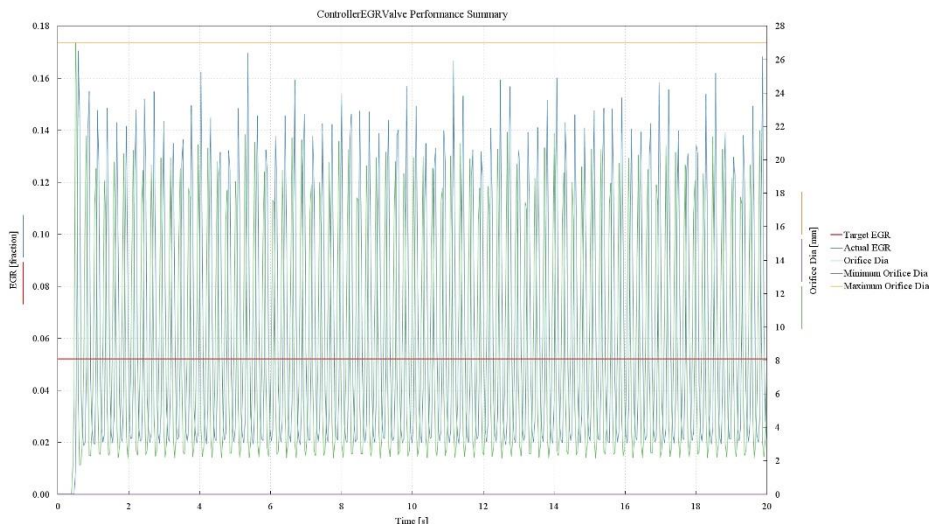


Figure 5-10 – Example of model-based EGR Valve Controller oscillating

The PID controllers used in the correlation model were designed and tuned by Powertech as part of a previously carried out run-in correlation activity.

Upon running the correlation simulations, a few things could be noticed.

1. The pressure evolution along the flow lines is well correlated with the experimental. Errors are in the order of a few millibars, 50 mbar at most.

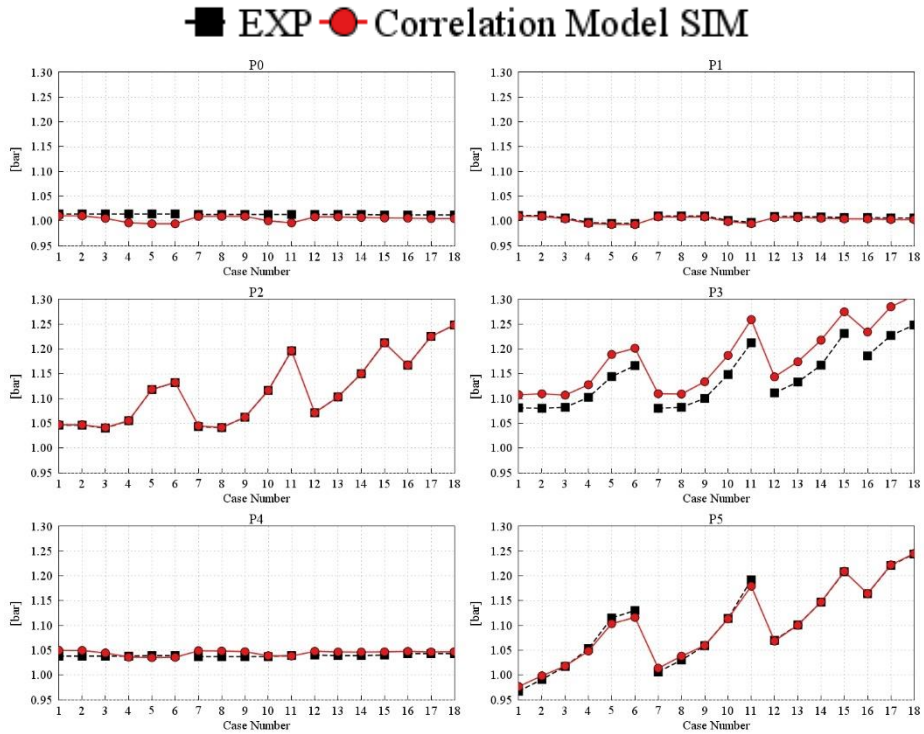


Figure 5-11 – Correlation Model pressure evolution vs. Experimental measurements

2. The temperature evolution along the flow lines is well correlated with the experimental. While errors are larger with respect to pressure, they do not affect the results as much.

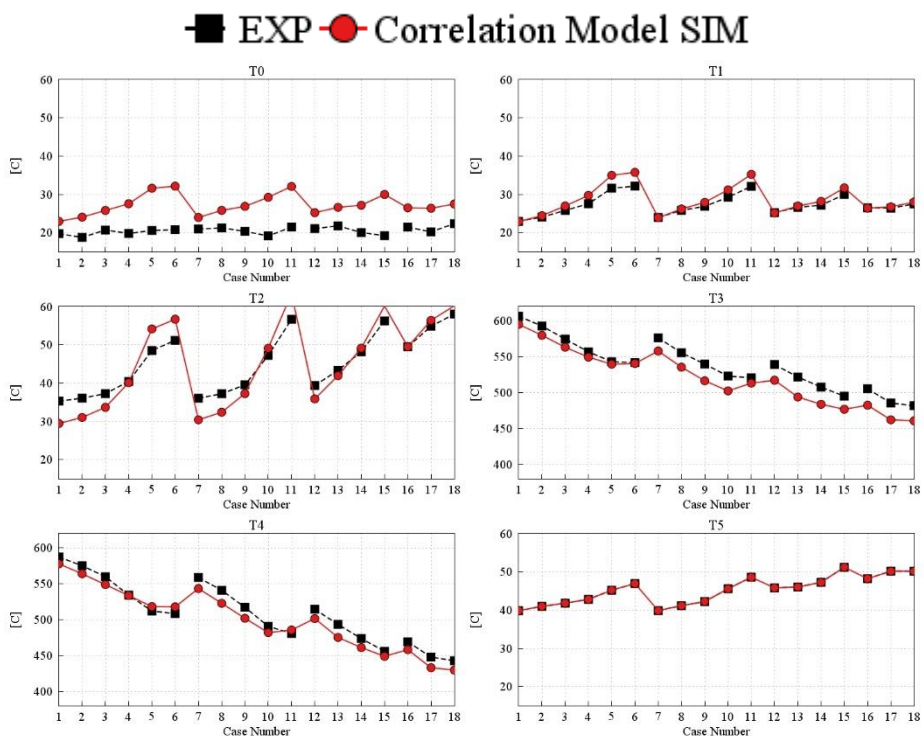


Figure 5-12 – Correlation Model temperature evolution vs. Experimental measurements

3. The operating parameters are well correlated with the experimental as they were imposed.

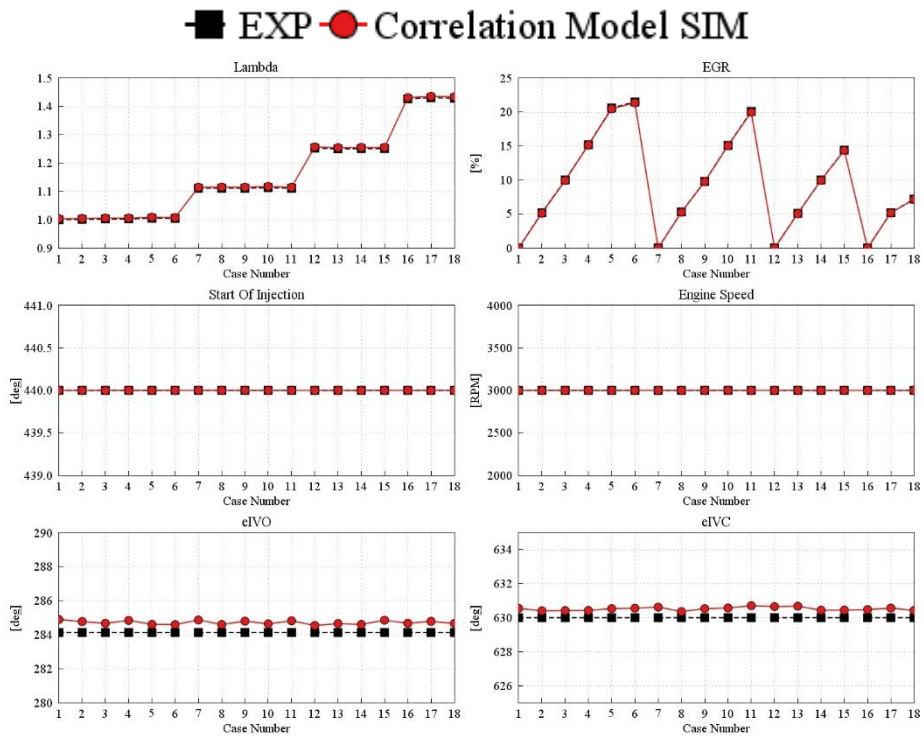


Figure 5-13 – Correlation Model operating parameters vs. Experimental measurements

4. As the combustion is imposed, the combustion parameters are also well correlated.

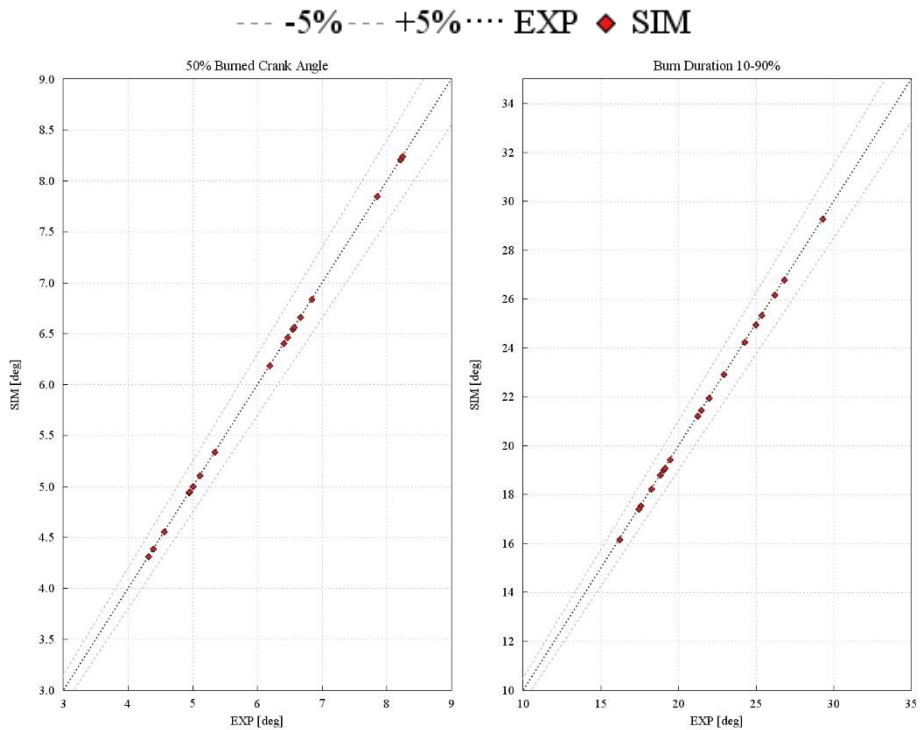


Figure 5-14 – Correlation Model combustion parameters vs. Experimental measurements

5. Moreover, the correlation model can achieve the same performance as the engine prototype.

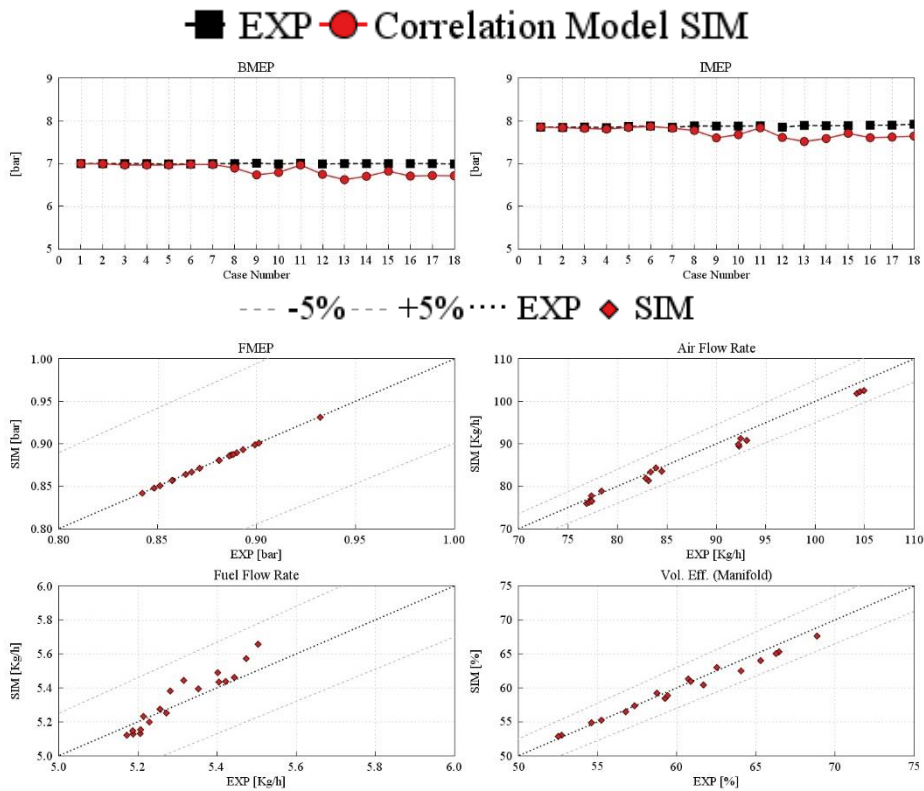


Figure 5-15 – Correlation Model performances vs. Experimental measurements

As a matter of fact, *Figure 5-15* shows how all performance parameters stay within the  $\pm 5\%$  bands in the regression plots.

This proves that, once the combustion is fixed and equal to the experimental one, the developed numerical tool can fully represent the engine prototype's results. This is an excellent result as it proves that the carried-out discretization and calibration activities were successful.

## 5.4 SITurb Combustion Model Tuning

With the engine model able to correctly predict the pressure and temperature evolutions, a more in-depth study can be made regarding the combustion model using the same data set.

If on the one hand fixed, non-predictive, combustion models can be used to quickly replicate experimental tests in an accurate way, on the other, whenever the operating conditions change, the burn rates must be updated. This solution is not acceptable in a framework where the created digital twin wants to be used as an alternative to conventional experimental campaigns.

For this reason, the complete virtual test rig model must utilize a predictive combustion model. Such models can predict the burn rate starting from the initial conditions (i.e., pressure, temperature, equivalence ratio, residuals, etc.). The GT-POWER template of choice for this application is the EngCylCombSITurb. The EngCylCombSITurb model, SITurb for short, predicts the burn rate for homogeneous charge spark-ignition engines taking into account the cylinder's geometry, the spark locations and timing, the air motion, and the fuel properties <sup>[21]</sup>. As a matter of fact, as seen in *Chapter 2.2.3*, SITurb also requires a detailed STL geometry of both the cylinder head and the piston cup. To properly calibrate a SITurb, a set of four variables must be optimized, over a range of operating conditions, to match a given experimental data set. The four variables are:

1. The Dilution Effect Multiplier (DEM)  $C_{DE}$ . Which measures the effect of the dilution.
2. The Turbulent Flame Speed Multiplier  $C_{TFS}$ . Which measures the effect of the turbulence intensity.
3. The Taylor Length Scale Multiplier  $C_{TLS}$ . Which measures the effect of the turbulence length scale.
4. And the Flame Kernel Growth Multiplier  $C_{FKG}$ . Which can be used to adjust the initial growth rate of the flame kernel.

Every SITurb combustion is run alongside an in-cylinder flow model. Recalling what was previously discussed in *Chapter 2.2.3*, the combustion, the knock, and the in-cylinder flow models were derived from a previous research activity carried out for a modified GSE-T3 engine with a similar compression ratio. In such a research activity, the predictive combustion was calibrated under stoichiometric conditions with no EGR flow. Consequently, despite the similar engines, the approximation of using the same models is no longer valid whenever different lambdas and EGR fractions come into play. Unfortunately, tuning  $C_{TFS}$  and  $C_{TLS}$  requires an engine-specific in-cylinder flow model to guarantee the correct Turbulence Kinetic Energy (TKE) level at the time of spark. Using the modified GSE-T3 flow model would not be ideal since it does not include the Swumble™ intake charge motion. Consequently, the combustion calibration procedure must be repeated once the updated flow model is available. At the same time, at the time of writing, the information needed to calibrate the flow model for the specific PHOENICE application is not yet available. Moreover, proper combustion calibration requires many experimental tests covering multiple operating conditions. However, at the time of writing, the available experimental results are all at the same operating condition (3000 RPM x 7 bar BMEP).

Thus, for the sake of this research activity, a preliminary SITurb tuning was performed, starting from the modified GSE-T3 combustion model, including only one of the four parameters: the DEM. This was the parameter of choice as it represents the primary difference between the modified GSE-T3 engine and the PHOENICE one. The obtained combustion model is by no means definitive and is intended to be used for preliminary evaluations until a proper calibration can be carried out.

While a single value of DEM is to be found in conventional SITurb calibration, the DEM was optimized for each case in this tuning activity. A manual sensitivity analysis over six CDE levels was carried out: 0.45, 0.75, 0.9, 1.0, 1.1, and 1.2. For each case, the selected DEM was the one yielding the lowest maximum cylinder pressure error with respect to the CPOA combustion.

		Considered DEM levels					
		0.45	0.75	0.9	1.0	1.1	1.2
Optimal DEM value for each case	1			x			
	2			x			
	3				x		
	4						
	5					x	
	6						x
	7				x		
	8				x		
	9				x		
	10					x	
	11						x
	12				x		
	13				x		
	14					x	
	15						x
	16						x
	17						x
	18						x

Table 5-2 – Optimal DEM for each of the 18 Cases

Consequently, to make the tuning more robust, the found results were imported into MATLAB® and, through the curve fitter tool, interpolated to obtain a polynomial equation of the DEM as a function of the chosen lambda and EGR fraction to be implemented in the GT-POWER model. This approach allows the combustion model to predict the burn rate for combinations of lambda and EGR fractions different from the ones tested by IFPEN.

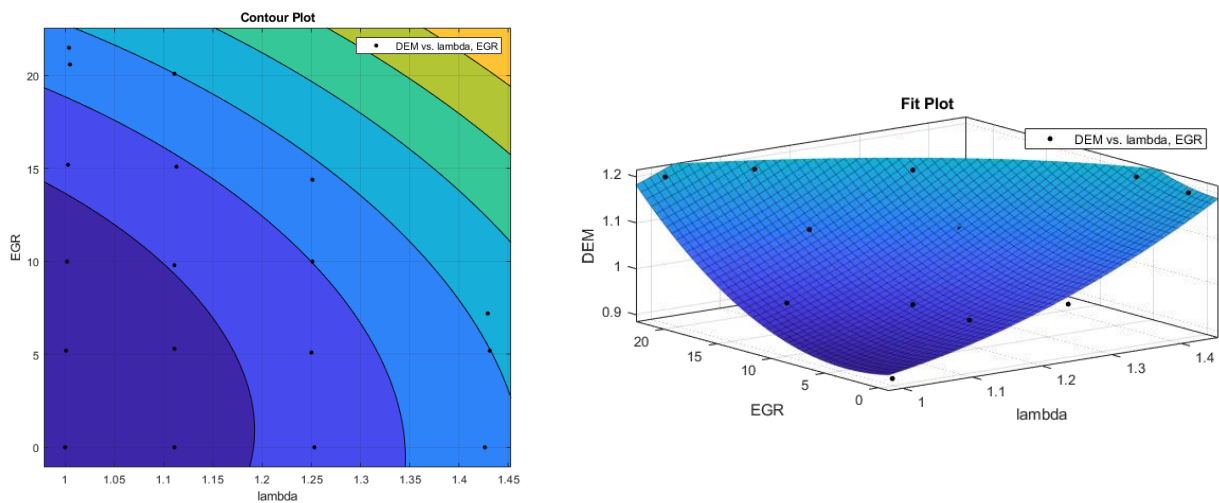


Figure 5-16 – Polynomial curve fit of the optimal DEM

The obtained fit equation is:

$$DEM(\lambda, EGR) = p_{00} + p_{10} \cdot \lambda + p_{01} \cdot EGR + p_{20} \cdot \lambda^2 + p_{11} \cdot \lambda \cdot EGR + p_{02} \cdot EGR^2$$

Where,

$$\begin{aligned} p_{00} &= 1.317 \\ p_{10} &= -1.078 \\ p_{01} &= -0.01749 \\ p_{20} &= 0.6813 \\ p_{11} &= 0.01357 \\ p_{02} &= 0.0007117 \end{aligned}$$

Finally, the model was run with the updated SITurb combustion instead of the imposed CPOA model presented in *Chapter 5.3*.

The following results were obtained:

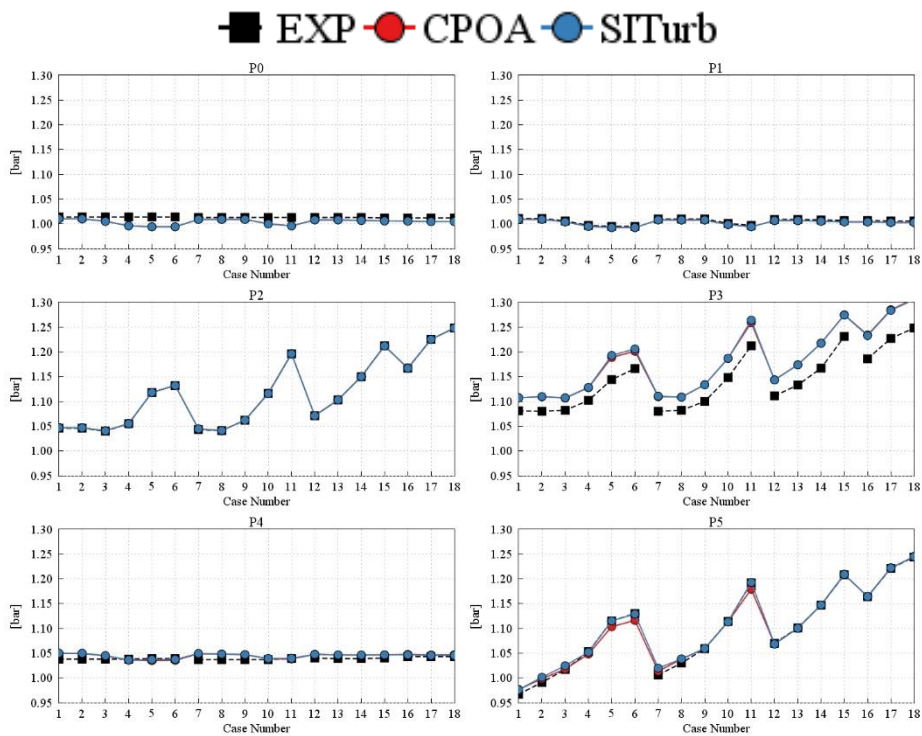


Figure 5-17 – SITurb pressure evolution vs. Experimental measurements and CPOA

The pressure evolution is still well correlated. Similar errors were found with respect to the model run with CPOA combustion.

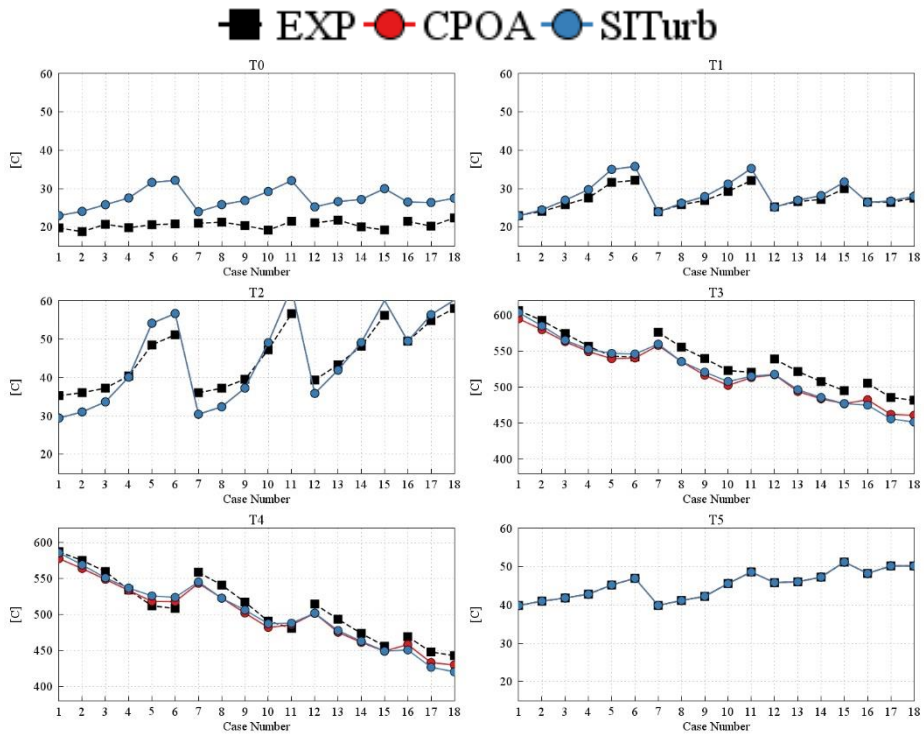


Figure 5-18 – SITurb temperature evolution vs. Experimental measurements and CPOA

The temperature evolution is still well correlated. Overall, the SITurb combustion can better reproduce the temperatures along the PHOENICE flow lines, and smaller errors with respect to CPOA can be seen.

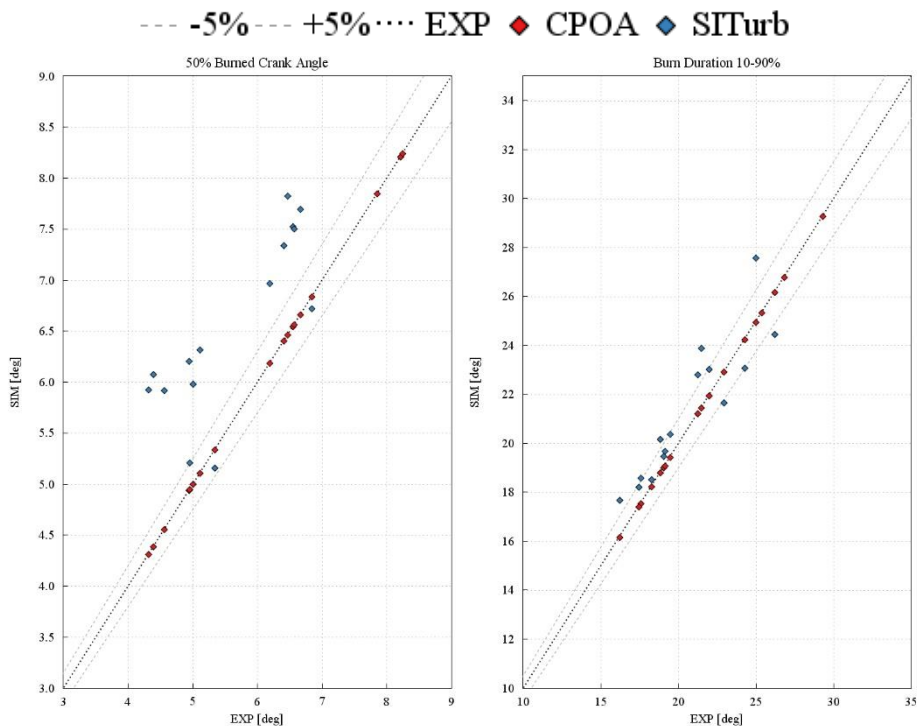


Figure 5-19 – SITurb combustion parameters vs. Experimental measurements and CPOA

On the other hand, the combustion parameters present significant errors with respect to the experimental values. While the burn duration is mostly OK, the MFB50 appears more retarded than the experimental one. The lower turbulence level of the GSE-T3 flow model explains this.

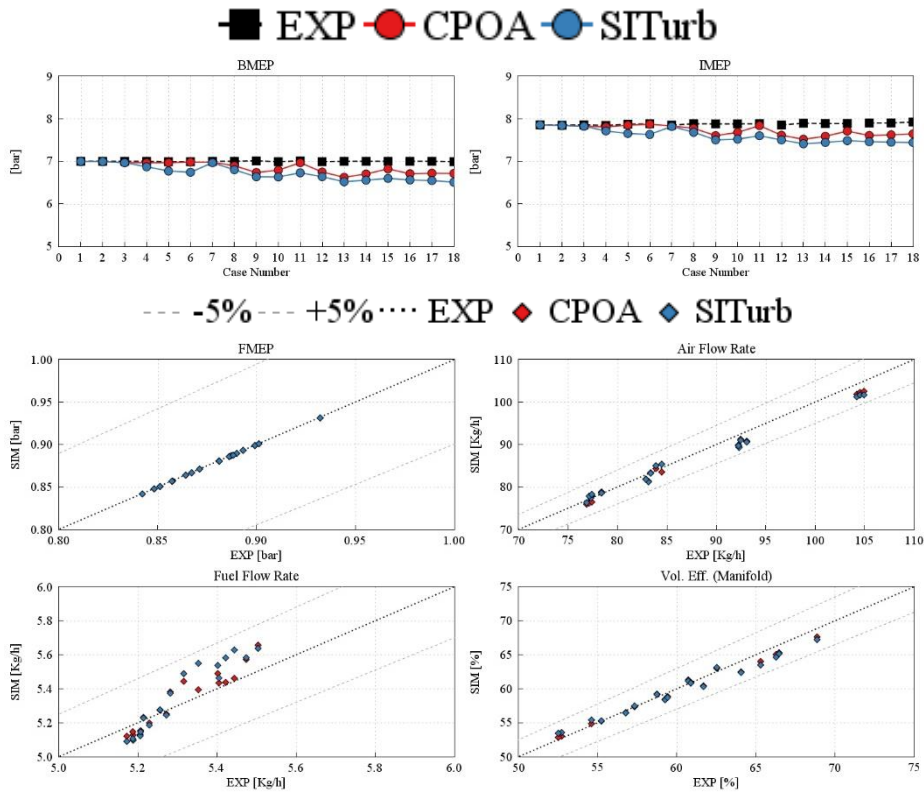


Figure 5-20 – SITurb performances vs. Experimental measurements and CPOA

Finally, *Figure 5-20* shows how the SITurb simulation can achieve similar results to the imposed combustion despite the not exact combustion. As a matter of fact, even in the most diluted conditions, the model can predict the correct airflow and volumetric efficiency thanks to the tuned DEM. Nevertheless, future steps will include a state-of-the-art combustion calibration once the data is available.

## 6 Conclusions

A complete digital twin of the PHOENICE high-efficiency spark ignition engine was developed. Making reference to the baseline GSE-T4 engine, the GT-POWER model was developed and calibrated: flow lines were discretized from their CAD geometries, tuned with experimental data in terms of pressure loss, and finally, imported into the 1D environment. A maximum brick pressure drop error after the calibration of 5.49 mbar was obtained. A similar procedure was then followed for the two heat exchangers with a maximum error of 1.81 mbar.

Subsequently, preliminary engine performance sensitivity analyses were conducted to understand the influence of various parameters and how they should be controlled. Indeed, the influence of a lower intake charge temperature and a lower maximum E-turbo speed were studied regarding achievable BMEP and BSFC. An increase of about 1% BTE was found when lowering the intake temperature from 50°C to 40°C, and a negligible effect on BMEP was noticed when lowering the maximum e-turbo speed. Moreover, a variable valve lift and timing optimization was carried-out to aid the experimental tests conducted in the IFPEN facility to achieve the lowest possible BSFC. An additional 1% BTE increase could be obtained by employing both an early or late miller strategy.

Finally, an assessment of the DDCA was simulated to ensure proper model correlation with its real-life equivalent. By imposing the experimental combustion by means of CPOA, the numerical tool proved to behave very similarly to the engine prototype tested in the IFPEN facility. All the important parameters were within a 5% tolerance with respect to the experimental measurements. Finally, the same data set was used to preliminary tune the predictive combustion model employing the dilution effect multiplier.

The numerical tool still requires some modifications to make the most out of it. Future steps will include a proper calibration of the combustion model by means of a Three Pressure Analysis (TPA) DoE optimization of all four parameters of the SITurb template; the modelization of waste heat recovery systems (TEG, EHRS, or both) whose utilization is yet to be confirmed; and finally, the dynamic calibration of the model to be performed once the engine testing procedure in the Politecnico di Torino facilities will be carried out.

Nevertheless, the developed numerical platform represents a solid base for the future of the PHOENICE project. The results obtained from the preliminary experimental investigations already look promising. Thanks to the engine's digital twin, it will now be possible to perform further system optimizations conveniently without conducting expensive test campaigns.

PHOENICE represents a big step for the automotive sector's future toward green mobility. Internal combustion engines still play a crucial role in transitioning to a net zero-emission transportation sector, especially in terms of customer acceptance and Total Cost of Ownership (TCO). The technology is not yet saturated, and the preliminary assessments demonstrated a large margin of improvement. In a framework where immediate action is needed to reduce greenhouse gas emissions, banning such an established and diffused technology without considering all the possible improvements is reckless. All available technologies should work together, side by side, to reach a common goal, there is no silver bullet to achieve green mobility.

## 7 References

- [1] - Ovaere, M. and Proost, S., “Cost-effective reduction of fossil energy use in the European transport sector: An assessment of the Fit for 55 Package” Energy Policy 168:113085, 2022, <https://doi.org/10.1016/j.enpol.2022.113085>.
- [2] - Samaras, Z., Kontses, A., Dimaratos, A., Kontses, D. et al., “A European Regulatory Perspective towards a Euro 7 Proposal” SAE Technical Paper 2022-37-0032, 2022, <https://doi.org/10.4271/2022-37-0032>.
- [3] - Claßen, J., Krysmo, S., Dorscheidt, F., Sterlepper, S. et al., “Real driving emission calibration – review of current validation methods against the background of future emission legislation”, Applied Sciences (Switzerland) 11(12), 2021, <https://doi.org/10.3390/app11125429>
- [4] - PHOENICE project website: <https://phoenice.eu/>
- [5] - <https://wayback.archive-it.org/12090/20190928010801/https://ec.europa.eu/inea/en/horizon-2020/projects/h2020-transport/green-vehicles/eagle>
- [6] - Bourhis, G., Laget, O., Kumar, R. and Gautrot, X., “Swumble In-Cylinder Fluid Motion: a Pathway to High Efficiency Gasoline SI Engines” in 27<sup>th</sup> Aachen Colloquium Automobile and Engine Technology, Aachen, 8-10 October 2018.
- [7] - Gautrot, X., Bardi, M., Leroy, T., Luca, P. et al., “Swumble™ In-Cylinder Fluid Motion of the second generation”, in *Proceedings of the SIA Powertrain and Electronics*, Rouen, 16-29 November 2020.
- [8] - Davies, P., Bontemps, N., Tietze, T. and Fausseit, E., “Electric Turbocharging – Key Technology for Hybridized Powertrains”, MTZ Worldw 80:30-37, 2019, <https://doi.org/10.1007/s38313-019-0096-y>.
- [9] - Li, T., Gao, Y., Wang, J. And Chen, Z., “The Miller cycle effects on improvement of fuel economy in a highly boosted, high compression ratio, direct-injection gasoline engine: EIVC vs. LIVC”, Energy Convers Manag 79:59-65, 2014, <https://doi.org/10.1016/j.enconman.2013.12.022>.
- [10] - Millo, F., Luisi, S., Borean, F. and Stroppiana A., “Numerical and experimental investigation on combustion characteristics of a spark ignition engine with an early intake valve closing load control”, Fuel 121:298-310, 2014, <https://doi.org/10.1016/j.fuel.2013.12.047>.
- [11] - <https://www.media.volvocars.com/global/en-gb/media/photos/7086>, accessed on 25.03.2023.
- [12] - Lumley, J. L., 1999. Engines, Cambridge University Press.
- [13] - Pulkrabek, W-W. (1998). Engineering fundamentals of the internal combustion engine, Prentice-Hall, Upper Saddle River, New Jersey.
- [14] - F. Millo, *Engine Emission Control Lecture Notes*, 2022
- [15] - <https://phoenice.eu/new/news-for/>, accessed on 25.03.2023.
- [16] - <https://www.maserati.com/global/en/news/mmxx/maserati-nettuno-engine>, accessed on 25.03.2023.
- [17] - PHOENICE Innovation Action
- [18] - <https://phoenice.eu/new/the-manufacturing-and-on-bench-characterization-of-waste-heat-recovery-systems-whrs-completed-by-marelli-europe/>, accessed on 25.03.2023.
- [19] - <https://instrumentationtools.com/seebeck-effect-theory/>, accessed on 25.03.2023.
- [20] - GT-POWER Flow Theory Manual
- [21] - GT-POWER Engine Performance Manual
- [22] - <https://phoenice.eu/new/the-first-engine-prototype-has-been-assembled-and-installed-at-the-ifpen-test-bench/>, accessed on 25.03.2023.